ABSTRACT

Hongxia Zhang

Blood Inflammatory Exosomes with Age Prime Microglia through Complement Signaling for Negative Stroke Outcomes

The systemic inflammatory milieu plays an important role in the age-related decline of functional integrity, but its contribution to age-related disease (e.g., stroke) remains largely unknown. Here, we found that activated complement molecules (C1q, C3a, C3b) in serum exosomes increased with age, whereas CD46, a C3b/C4b-inactivating factor, was higher in serum exosomes from young rats. These serum inflammatory exosomes passed the blood-brain barrier and primed the microglial response that led to exacerbation of synaptic loss and motor deficits after ischemic stroke via microglial C3a receptor (C3aR). When aged rats were exposed to serum exosomes from young rats, microglia-mediated synaptic loss was reduced and motor deficits after stroke were improved. Administration of C3aR inhibitor or microglial depletion attenuated synaptic loss associated with the treatment of serum exosome from aged rats, in parallel with improved post-stroke outcome. Our data suggest that peripheral circulating old exosomes act as inflammatory mediators and influence ischemic stroke outcome through a complement-microglia axis.

BLOOD INFLAMMATORY EXOSOMES WITH AGE PRIME MICROGLIA THROUGH COMPLEMENT SIGNALING FOR NEGATIVE STROKE OUTCOMES

Hongxia Zhang, MD, PhD

APPROVED:

Kunlin Jin, Major Professor

Doctoral Committee

Michael Forster, Committee Member

April 10, 2020

Shaohua Yang, Committee Member

Xiangrong Shi, Committee Member

Thomas Cunningham, University Member

David Siderovski, Chair, P&N

Michael Mathis, Dean, GSBS

BLOOD INFLAMMATORY EXOSOMES WITH AGE PRIME MICROGLIA THROUGH COMPLEMENT SIGNALING FOR NEGATIVE STROKE

DISSERTATION

Presented to the Graduate Council of the

Graduate School of Biomedical Sciences

University of North Texas

Health Science Center at Fort Worth

In partial fulfillment of the requirements

For the Degree of

DOCTOR OF PHILOSOPHY

By

Hongxia Zhang

Fort Worth, Texas

April 2020

ACKNOWLEDGMENTS

I would like to express my sincere gratitude to my mentor Dr. Kunlin Jin for his excellent mentorship and training in his laboratory during my graduate career. He provided selfless support, patience, and encouragement for my continued success in the completion of my research projects, as well as for my future professional career.

I would also like to thank the members of my committee: Dr. Michael Forster, Dr. Shaohua Yang, Dr. Xiangrong Shi for their valuable advices and constructive comments during my project. I also thank Dr. Thomas Cunningham for serving as the university member on my committee as well.

I also would like to thank the past and present members of Dr. Jin's laboratory: Brian Wang, Chris McElroy, Chenqi Yang and Menxiong Pan, for their support and guidance during my study. I would also thank training students in our lab: Chris Lo and Dana, for their help to the project.

Finally, I would like to thank my parents, siblings and families for their love and support during my doctoral studies.

TABLE OF CONTENTS

LIST OF FIGURES

LIST OF TABLES

LIST OF ABBREVIATIONS

AD	**Alzheimer's disease**
AMPK	**Adenosine monophosphate-activated protein kinase**
BDNF	**Brain-derived neurotrophic factor**
CAD	**Coronary artery disease**
CNS	**Central nervous system**
CR3, or C3aR	**Complement receptor 3**
C3aR	**C3a receptor**
C3aRI	**C3a receptor inhibitor**
CV	**Cresyl violet**
CSF1R	**Colony stimulating factor 1 receptor**
cAMP	**Cyclic adenosine monophosphate**
DAMPs	**Danger-associated molecular patterns**
dMCAO	**Distal middle cerebral artery occlusion**
DAPI	**4′,6-diamidine-2-phenylindole dihydrochloride**
DHA	**Docosahexaenoic acid**
EGFP	**Enhanced green fluorescent protein**

EVs	**Extracellular vesicles**
ECL	**Enhanced chemiluminescence**
EGFR	**Epidermal growth-factor receptor**
eNOS	**Endothelial nitric oxide synthase**
EIF4EBP1	**Eukaryotic translation initiation factor 4E binding protein 1**
FGF	**Fibroblast growth factor**
GFAP	**Glial fibrillary acidic protein**
GO	**Gene ontology**
KEGG	**Kyoto Encyclopedia of Genes and Genomes**
KOG	**Eukaryotic orthologous groups**
Iba1	**Ionized calcium binding adaptor molecule 1**
IPA	**Ingenuity pathway analysis**
INSR	**Insulin receptor**
IGF-1R	**Insulin-like growth factor 1 receptor**
IL-6	**Interleukin 6**
LRP	**Lipoprotein receptor-related protein**
lncRNAs	**Long noncoding RNAs**
LC-MS	**Liquid chromatography tandem mass spectrometry**

miRNA	**Micro RNA**
mRNA	**Messenger RNA**
MCA	**Middle cerebral artery**
Myelin PLP	**Myelin proteolipid protein**
MAPK	**Mitogen-activated protein kinase**
mTOR	**Mammalian target of rapamycin**
OPN	**Osteopontin**
O-exo	**serum exosomes from old rats**
PARP	**Poly (ADP-ribose) polymerase**
PBMC	**Peripheral blood mononuclear cell**
PBS	**Phosphate-buffered saline**
PFA	**Paraformaldehyde**
PVDF	**Polyvinylidene difluoride**
PTEN	**Phosphatase and tensin homolog 10**
PDK1	**Phosphoinositide dependent protein kinase 1**
PXN	**paxillin**
SVZ	**Subventricular zone**
tPA	**Tissue plasminogen activator**

TLRs	**Toll-like receptors**
TREM-2	**Triggering receptor expressed on myeloid cells 2**
TTC	**2,3,5-triphenyltetrazolium chloride**
TEM	**Transmission electron microscopy**
TREM1	**Triggering receptor expressed on myeloid cells 1**
TGFβ	**Transforming growth factor beta**
TNFα	**Tumor necrosis factor alpha**
NTA	**Nanoparticle-tracking analysis**
NeuN	**Neuronal nuclei**
vWF	**Von Willebrand factor**
Y-exo	**Serum exosomes from young rats**

INTRODUCTION

1. Ischemic Stroke and aging

Aging is characterized by the progressive loss of physiological integrity, which leads to an increased risk of functional damage and eventual death. As aging advances, structural and functional decline of the body can elevate the risk of major human diseases such as cancer, diabetes, cardiovascular and neurodegenerative diseases.

Stroke is one of the most common diseases in the older population. It remains the 5th leading cause of death and the leading cause of disability in the United States. Two types of brain stroke are hemorrhagic and ischemic. While ischemic stroke accounts for about 87 percent of all stroke (1). Systemic thrombolysis with intravenous tissue plasminogen activator (tPA) remains the only FDA proven drug for the treatment of patients with acute ischemic stroke (2, 3). Because of an increased risk of hemorrhage beyond 3-5 hours post stroke, only a small population of stroke patients (1-2%) can benefit from tPA. Several ischemic stroke models have been developed in a variety of species, including rodents, canines, rabbits, cats, as well as non-human primates to understand the physiopathology and outcome of ischemic stroke in humans (4-7). However, most animal models for experimental stroke *in vivo* are almost universally young-adult rodents used for the evaluation of the neuropathological, neurological, and neuro behavioral outcomes after

stroke. Younger animals are used due to their greater availability, lower cost, and fewer health problems (8). Ischemic stroke is a highly complex and heterogenous disorder, and the incidence, morbidity, and mortality of stroke has been increasing, especially in the aging human population (9). The persistent failure of human trials targeted at neuroprotective agents (10), which are effective in animal model of stroke, further indicates that the discrepancy between animal models and human diseases could have important clinical applications. One of the potential reasons is that ischemic stroke mainly occurs in the elderly but almost all experimental stroke research is focused on young-adult animals (11). Therefore, in this project, aged rats (22-month-old) were used to generate ischemic stroke model to mimic clinic conditions.

2. Correlation between age of laboratory rats and human

Biomedical researchers who use adult and aged animals as experimental tools often face the question: "At what age are laboratory rats and mice considered adult or aged"? Traditionally, biomedical scientists consider sexual maturity is the hallmark of adulthood. Sexual maturity in rats takes 49-60 days (12), but social maturity is reached several months later at about 5 to 6 months of age (13). Most researchers consider 60 days of age as an adult rat. Controversially, recent studies show that rat long bone metaphysis closed until 7 to 8 months after birth (14). The newest opinion is that closure of long bone metaphysis is a more accurate sign of maturity in rats. Female rats enter menopause between 15-18 months of age.

*"*What is the relationship between age in mice and rats and age in humans," is one of numerous questions raised by biomedical scientists. Compared to human's lifespan, a rodent lifespan is like a shooting star, fast and transient.

Rats in a laboratory setting live 2-3.5 years (average 3 years) (15), and only 5% live beyond 3 years of age. Current life expectancy in humans is 80 years (16). Therefore, we can translate a rat's age into "human years" based on the average life expectancy of human and rats. Such is that two rat weeks (13.8 rat days) almost equals one human year (15). Like all mammals, rats also have different developmental stages in their life, including infancy, puberty, adulthood, and old age (17). The duration of these stages is different between species, including between rats and humans. For example, the average weaning time for laboratory rats is about 3 weeks (14), while it is about 6 months in humans. In this weaning phase, a human year is roughly equivalent to 42.4 days in a rat's life. During puberty, one human year roughly equals 3.3 days in a rat's life (18). Compared to humans, 10.5 rat days equal to a human year in the adolescent phase (16, 18). In the adult phase, 11.8 rat days equal a human year (16, 18). In old age, 17.1 rat days equals a human year. Table 1 shows the comparability of human, rat, and mice years.

Table 1. Correlation between age of laboratory rats and human

Rat and mouse age in months	Rat age in human years	Mouse age in human years
1 months	9 years	14 years
3 months	15 years	23 years
6 months	18 years	34 years
9 months	24 years	46 years
12 months	30 years	58 years
24 months	60 years	70 years
30 months	75 years	85 years
36 months	90 years	100 years

3. Systemic Milieu, aging and lifespan

Aging is a fundamental biological process accompanied by a general decline in tissue function and increased risk for age-related disease. Risk for cardiovascular diseases, stroke, cancer, and neurodegenerative diseases is significantly increased with aging, especially in people of 60 years and older in the United States (19, 20). Systemic factors are shown to have potential intervention effects on the aging process and some age-related disease. Therefore, new and innovative approaches to identify specific pro-aging and rejuvenating factors may be very critical. Recent studies have demonstrated that these pro-aging and rejuvenating factors are present in young circulation systems and can reverse age-related impairments. For example, age-related decline in activity of muscle progenitor cells can be restored, while damaged muscle can be successfully repaired after exposure to the young systemic milieu through heterochronic parabiosis (an approach for exchanging systemic milieu of two organisms).

Evidence that the impact of the systemic milieu on lifespan is mainly from studies based on the heterochronic parabiosis model. Parabiosis is an experimental model where two animals joined together surgically to create shared circulation system through connection of the skin and muscle walls, which include joining of the scapula joints, body cavities, and skin (21). Heterochronic parabiosis is a process that joins the vascular systems (anastomosis) of young mice with old mice allowing for a joined blood circulation of two animals (22). This allows for interchanging of blood cells and soluble factors thereby altering the systemic milieu of a paired partner. The exchanging blood circulation between organism pairs could be confirmed by *in vivo* imaging, fluorescence microscopy, and flow cytometry (23). Using the parabiosis model established

between C57BL/6-TgN (ACTb-enhanced green fluorescent protein [EGFP]) transgenic mice and wild-type mice, GFP-positive blood cells were identified in the peripheral blood of the wild-type mice suggesting that a shared circulation manifest between the pairs (24). The advantage of the parabiosis model is that the attached animals are free of immune reaction (25).

The advantage of the parabiosis model is that the partnered animals share common circulating antigens, allowing cell migration and neovascularization without triggering an immunological reaction (25). In addition, parabiosis between male and female mice does not lead to formation of anti H-Y antibodies (26). Therefore, heterochronic parabiosis was not only helpful to discover and study detrimental and beneficial factors but also to assess the physiological or pathophysiological consequences in an organism as a whole upon exposure to the systemic milieu (27). On the other hand, although it is widely-used and beneficial to explore whether circulating factors in the blood can alter tissue function, methodology is technically difficult to perform, associates with high animal mortality and inflammation. The survival of parabiosis surgery is often limited due to some complications, like infection or cardiovascular diseases, which are apparently as a consequence of parabiosis (28). Besides technical challenge, kinetic is also one of the considerations for the parabiosis approach (29). Take parabiosis and lifespan extension for example, kinetics is a unique challenge as the young parabiont are aging and the "effector" parabiont age is not controlled during long-term experiment, which would be challenging to design experiments in which the animals would undergo sequential parabiotic pairing to a series of young animals so as to provide a more continual exposure to a youthful systemic milieu (29).

Several studies have reported the involvement of systematic milieu in lifespan. In 1957, McCay *et al,* found that little mates in youth combined could survive into old age including rats and Syrian hamsters. Pairs of heterochronic parabiosis could survive more than a year after parabiosis, indicating parabiosis seemed to be a promising technique for the study of aging to determine if the constant exchange of the blood between animals of two different ages may impact the chronic diseases of old age (30). In 1959, Hall *et al*. demonstrated that muscular dystrophy male mice have extended lifespans from 15 weeks to 24 weeks after being paired with a healthy partner using the parabiosis model (28). Notably, Ludwig and Elashoff first used the isochronic (old-old) and heterochronic parabiosis (young-old) model to systematically study the effects of heterochronic parabiosis on lifespan. They demonstrated that the old heterochronic parabiont had an extended lifespan compared to the isochronic old one (31), confirming the notion of the potential anti-aging or rejuvenating effects of the youthful systemic milieu. In the 20^{th} century, heterochronic parabiosis has been used to study the basic questions of aging regulation and lifespan (29). Though the molecular and cellular mechanisms underlying aging process remain largely unexplored, these studies established the idea that systemic milieu from healthy young animals may contribute to reversal in the aged organism (29).

Although convincing evidence of the effects of slowing aging or extending lifespan after administrating anti-aging remedies remains little, heterochronic parabiosis gives us a novel technique to elucidate the effects of the systemic milieu on increasing the lifespan in animals possessing fatal disease (29). The improved recovery in age-related diseases can be observed in studies focused on myogenesis, neurogenesis, memory and cognitive abilities, cardiac hypertrophy, and gastrointestinal related - disease.

In summary, parabiosis is a promised technique to study lifespan, namely, the possibility of reversing the pathological changes in an old animal by bathing its tissues in the blood of a young one. Despite its potential value, this model is complex and not "fine-tuned". More likely, mix of many factors in young blood plays "rejuvenation role" – cells and proteins. It will require many efforts to identify some of "enigmatic youth factors". Future direction may include to understand why systemic milieu can extend the lifespan in rodents. Identifying beneficial factors in young blood and detrimental molecules in old blood could provide a novel and effective mechanistic and therapeutic implication for aging and age-related disease.

While many of these age-related changes may be the consequences of cell intrinsic and tissue-localized mechanisms of aging, there is much interest in identifying whether changes in secreted signaling proteins contribute to tissue aging and functional impairment. It has been shown that circulating systemic environmental factors can be exchanged in a "heterochronic parabiosis" model, resulting in the mutual influence via blood-borne factors (32). Indeed, such changes in plasma or cerebrospinal fluid (CSF) proteomes are not only abundant with aging and disease (33, 34), but factors in young blood or plasma from mice or humans have been shown to be sufficient for rejuvenation e.g., to increase brain function in the hippocampus (33, 35, 36) and the subventricular zone (SVZ) (37). In addition to identifying pro-youthful factors in young blood that might boost rejuvenation, an emerging body of work has identified aged blood plasma and the factors within it, which may promote pro-aging processes in aging and age-related diseases (38). Of course, even though a single factor is identified as a specific rejuvenation or pro-aging factor, we also need to consider other circulating factors that it interacts with to cause the

supposed effect. Therefore, to mimic “heterochronic parabiosis” in the first part of this project, serum exosomes were isolated, injected by tail vein and investigated for the role in the treatment of ischemic stroke.

4. Extracellular vesicle and exosomes

Extracellular vesicle (EVs) are nano-sized (30–400 nm) membranous vesicles, which are thought to be released into the circulation and numerous biological fluids not only by one type of cell, but by cells of diverse origins, such as platelets, erythrocytes and endothelial cells (39), neurons, adipocytes and several other cells types (40, 41). There are at least three types of EVs in the blood: i) exosomes, which are small, 30–120 nm diameter membrane micro-vesicles, released by the fusion of multivesicular bodies with the plasma membrane; ii) microvesicles released by budding of small segments of the plasma membrane; iii) apoptotic bodies released from dying cells (42, 43). Due to overlap in the size, density, and cargo of these different types of EVs, it is difficult to determine the type of EVs isolated from cell cultures and body fluid samples (44).

Exosomes have the potential for directional homing to specific target cells, dependent on the physical properties of their membranes (45). It was confirmed that exosomes represent a specific subcellular compartment and are enriched with specific mRNA, miRNA and proteins that remain bioactive upon uptake by the recipient cell and thus play an important role in intercellular communication (46). Fortunately, the cargo is protected from degradation by proteases and RNases while the vesicle is in the interstitial space, and retains bioactivity once taken up by a recipient cell (47). In this way, exosomes facilitate the transfer of interactive signaling and enzymatic activities.

Exosomes contain a multitude of bioactive substances that play a critical role in physiological and pathological conditions such as immune responses, neurobiology, stem cell processes, vascularization, tumor biology, as well as a variety of age-related chronic diseases including neurodegenerative diseases (e.g., Alzheimer's disease, AD), metabolic diseases, and cardiovascular disease (48), which led us to examine whether the profile of exosomes are changed with age in humans and animals, and their role in ischemic stroke. In this project, we analyzed and compared the serum exosomes from young and old rats in terms of proteins alterations in the first part, and differentially expressed mRNA and miRNA and related aging signaling pathway in the second part of the project.

4.1 Protein changes in exosomes with age

The majority of research has focused on identifying differences in exosomes when comparing disease states and matched controls. Although increased concentration of exosomes has also been reported in cancer patients (49-51) and environmental stressors such as hypoxia (51) both *in vivo* and *in vitro*. Eitan et al. found that EV concentration decreases with advancing age due to enhanced EV internalization by both activated monocytes and B cells in humans (52).

Due to the transmission of bio-information through EVs between origin and target cells, EVs can be utilized for diagnostic purposes termed a 'liquid biopsy' (41), which gives rise to the hypothesis where vesicle proteins may account for the age-related differences in concentration based on internalization and activation. Eitan et al. further found significant changes in protein

levels both in EV surface and cytosolic proteins from lysed EVs (52). Levels of several apoptotic markers in EVs decrease with age, including p53, cleaved poly (ADP-ribose) polymerase (PARP) and cleaved Caspase-3. Three other proteins were significantly increased with age including CD151, a tetraspanin that enhances cellular processes involved in tumorigenesis and metastasis, MUCIN16 (also known as CA-125), a well-established circulating marker of ovarian cancer and possibly other types of cancers, and CD9, which also belongs to the tetraspanin family, commonly used as an exosomal biomarker that regulates cell adhesion, motility, activation and proliferation (53). CD14, MUC1 and NY-ESO1 are immune-related antigens, and levels of MUC1, MUCIN16, CD151 and NY-ESO1 are all reported to be higher in cancer cells (54-56). A recent study shows that MUC1 levels were decreased with age in plasma EVs in a small group of white males (57). This difference further highlights the need for large clinical studies of EV alterations with age. In addition, the reduction in EV concentration may result from the autonomous proteostasis malfunction which can impair clearance mechanism within aged cells (52). For example, the presence of many misfolded proteins in EVs were found in neurodegenerative diseases (58).

4.2 miRNAs profiles in exosomes with age

MicroRNAs (miRNAs) are small non-coding RNAs of ~25 nucleotides long that regulate gene expression post-transcriptionally by binding to complementary sequences in the 3′-UTR of multiple target mRNAs (59). Hunter et al. found that 104 and 75 miRNAs that were significantly expressed in micro-vesicle and peripheral blood mononuclear cell (PBMC) samples, respectively, in which 71 miRNAs were co-expressed among each sample group, suggesting

PBMCs could be one source of miRNAs that are present in the micro-vesicles or exosomes (60). In addition, different miRNAs may come from different sources. Circulating miRNAs in exosomes can also be released by glioblastomas (61) and mast cells (62). The recent studies show that cultured cell can release miRNAs into the media either as free miRNAs or encapsulated into exosomes (63). miRNAs were reported to involve in neurodegenerative diseases (64), age-related diseases (cardiovascular and neurodegenerative diseases) (65), and inflammatory disease (66) to mediate epigenetic exchange during aging (67). Therefore, miRNAs and/or exosomes may be part of circulating systemic environmental factors and regulate systemic milieu directly or indirectly.

Recent studies reported distinct miRNA expression patterns in the stroke pathogenic process, including hyperlipidemia, hypertension and plaque rupture [11], and atherosclerosis (68). Stroke-induced miRNA expression profiles have been reported in the blood and brain in both experimental models and stroke patients (69-71). Altered inflammation-related miRNA profiles following intracerebral hemorrhage have been reported in plasma (72). In addition, miRNA expression patterns have been used to predict the subtypes of stroke (71). Circulating miRNAs have been widely used as biomarkers for disease (73), especially in cardiovascular disease, where specific miRNA signatures have been shown to distinguish stable documented CAD (coronary artery disease) patients (74) or peripheral artery disease patients (75) from controls. Selvamani *et al.* investigated the effects of age and sex on miRNA expression patterns post-stroke, either using brain or circulating miRNA. Of the 168 circulating miRNAs examined 5 days post-stroke, 21 and 78 miRNAs were significantly upregulated at 2 days and 5 days post-stroke, respectively (76). Furthermore, a small cohort of five miRNAs (miR-15a, miR-19b, miR-

32, miR-136 and miR-199a-3p) were found to be highly expressed exclusively in adult females who exhibited significantly lesser cortical and striatal damage as well as the least amount of sensory-motor deficit, compared with middle-aged females, adult males and middle-aged males (76). These five miRNAs cohort needs to be investigated further as a collective biomarker for stroke outcome.

5. Neuroinflammation and stroke

Ischemic stroke immediately triggers an acute injury phase, which is characterized by excitotoxicity, the failure of ionic homeostasis, mitochondrial disruption, edema and oxidative stress (77). This primary brain injury is often irreversible. In ischemic stroke, the abrupt obstruction of blood supply in a vascular area results in the death of neural cells, forming an ischemic core which surrounded by a hypoperfused region termed penumbra. The compromised neural cells in penumbra can be repaired and blood supply can be restored. The results of therapeutic interventions aimed at blocking these early events 2 to 3 h after the onset of ischemia is encourage in animal models of ischemic stroke (78), which, however, fail in the clinical setting. Cells affected by primary or initial injury can trigger numerous cascades of secondary injury, which are mainly resulted from neuroinflammatory response, and continuous several hours to days after ischemic stroke (77, 79). Due to the clinic efficacy of blocking early events is limited by short therapeutic time window, preventing various steps in the inflammatory cascades may demonstrate clinic promise because of the wide window of protection (77). Inflammation response plays a vital role in the evolution of stoke pathophysiology and is closely related to the

prognosis after ischemic stroke, and thus blockade of inflammation significantly attenuates cerebral ischemic damage (80).

Ischemic stroke triggers a robust inflammatory response by releasing of danger-associated molecular patterns (DAMPs) from injured cells. DAMPs include nucleic acid and nucleotides, lipids, proteins and serum glucose (81). The immune cells are able to identify DAMPs via corresponding receptors, trigging intracellular signaling pathways (82). Among reactivated immune cells in the central nervous system (CNS), microglia rapidly respond to these danger signals (82). Cerebral inflammation amplifies vascular dysfunction, leading to neuronal cell death by releasing pro-inflammatory cytokines, chemokines and other cytotoxic mediators (83). For example, activation of endothelial cells (84) and invasion of peripheral myeloid cells and lymphocytes (85, 86) induce the progression of inflammation, which contributes to the damage of brain blood barrier (BBB) and vasculature (87). These events in turn ultimately worsen the outcome. However, the most intensive inflammatory response occurs in 7 days after ischemic stroke. During this phase, the number of infiltrating immune cells reduces significantly and the remaining immune cells in ischemic brain release anti-inflammatory or neurotrophic factors (83, 88, 89). For example, infiltrating macrophages become anti-inflammatory cells and clear death cell debris at the late stage of ischemia (81). Its mechanism of phenotype turning still mostly remains unclear. Here, we focused on microglia in this project to ask whether activated microglia affect the outcome of ischemic stroke after treatment of serum exosomes isolated from young and old rats.

5.1 Microglia

Microglia are resident immune cells of the CNS, and have important role in the normal adult brain, including neurogenesis and synapse remodeling by constantly monitor and respond to the functional status of synapses (90-92). Microglia also have macrophage function, such as phagocytosis and releasing of pro-inflammatory cytokines, and thus contribute to the most CNS pathologies by responding to many pathologic stimulations (79). After the ischemic stroke, resident microglia are activated shortly and accumulated at the lesion site and the penumbra (93). Upon activation, microglia undergo morphological changes to reduce complexity of cellular processes and transition from a ramified morphology to an amoeboid appearance (94), and functional changes (95, 96). Activated microglia can exhibit phenotypic and functional diversity based on the nature, strength and duration of the stimulus (96, 97). There are at least two activated phenotypes: pro-inflammatory microglia (also called classical or M1 cells) can release a number of pro-inflammatory cytokines (*e.g.*, IFNγ, TNFα) and thus considered to be neurotoxic. While, anti-inflammatory microglia (also called alternative or M2 cells) can release a number of anti-inflammatory cytokines (*e.g.*, TGF-β, IL-10) and neurotrophic factors and thus considered to be neuroprotective [92, 98].

In addition to releasing of both pro- and anti-inflammatory molecules, activated microglia are also characterized by high capacity for phagocytosis, which can remove of apoptotic cells and debris after injury in the brain. There is no obvious consistence with whether microglial phagocytosis is beneficial or detrimental in tissue repair (99). But it is true that microglia function as double sword after injury in the brain, as its phenotypic distribution changes from

pro- to anti- inflammatory microglia along with time. The microglial phagocytosis is activated via specific receptors expressed on the microglial surface (99). Complement receptors are one of them (100). Other receptors include Toll-like receptors (TLRs), triggering receptor expressed on myeloid cells 2 (TREM-2), Fc receptors, scavenger receptors (SR), pyrimidinergic receptor P2Y, G-protein coupled,6 (P2RY6), macrophage antigen complex 2 (MAC-2), mannose receptor, low-density lipoprotein receptor-related protein (LRP) receptor and osteopontin (OPN) (100-102). Ischemic stroke could induce peripheral neutrophils and monocytes/macrophages infiltration and activate resident microglia(83, 103). Whereas the resident microglia respond the injury in the early stage after ischemic stroke, followed peripheral macrophages infiltration in the ischemic core (99). Resident microglia can be rapidly activated and migrate to the infarction area and perform phagocytosis at 1 day after ischemic stroke (104), increasing tendency and reaching maximum at day 10 after ischemia (105). However, peripheral macrophages began to present in the infarction area at day 4 and reach the peak number in the following 3 days (105). Strikingly, among activated microglia, 25% of them have phagocytic function, which reach the maximum number as early as day 1 and remain the same level until the peripheral macrophages infiltration (105).

5.2 Complement cascade and microglia activation

Excepting clearance of cell debris, microglia could also execute phagocytosis of stressed-but-viable neurons and neurites, leading to neuron loss, which occurs not only during brain development but also in ischemic and neurodegenerative brains (106). Phagocytosis of dead and dying neurons and neuronal debris is beneficial, which could reduce neuroinflammation partly

(107). However, microglia can also phagocytose “healthy” neurons and neuronal progenitors (108-110) as well as synapse and neurites. Phagocytosis of neurons can be activated via binding microglial receptors. Specific signals on neurons include phosphatidylserine protein, de-sialylated glycoprotein calreticulin (106). In addition, the complement components C1q and C3 on neuronal surfaces may induce phagocytosis through binding to complement receptor 3 (CR3, or C3aR) on microglial surface. C1q can promote the conversion of C3 to C3a and C3b, and C3b can also be recognized by CR3 on microglia (106, 111, 112). There is also inhibitory signal presented on neuronal cells which can modulate microglial phagocytosis of neurons, such as CD47 (106). In the infarction area in the brain after ischemia, phagocytosis may be beneficial as it eliminates harmful cell debris and reduces inflammation. However, neurons in peri-infarct area may be stressed but viable and could be reversed by changed in microenvironment. Overreaction of activated microglial phagocytosis in this region may be detrimental. Therefore, we investigated whether microglia-complement play a role in the outcome of ischemic stroke after treatment of serum exosomes from rats in this project.

6. Neuroplasticity and brain function, stoke outcome

Stroke patients exhibit continued functional recovery for many years after onset of stroke (113). Similarly, neurobehavioral function recovery can be observed in animal models of stroke, but with less time. Even recovery occurs, re-emergent post-stroke behavior is unlikely to be the same with pre-stroke patterns due to the loss of neurons that have highly specific functions (114). When the cortical region is destroyed after focal ischemic stroke, the only way to accomplish true recovery might be to restore the destroyed circuits which mapped inputs signal from sensory neurons to motor neurons. Circuit remapping after ischemic stroke damage may involve different

cellular and molecular mechanisms (115). Beneficial factors that induced in the peri-infarct region, such as brain-derived neurotrophic factor (BDNF), could improve functional recovery after ischemic stroke (116). These factors may encourage the sprouting of new axons (117) and support the increased elaboration of dendrites and spines (118). In addition, many of the genes and proteins are indicated to be important for neuronal growth, synaptogenesis and proliferation of dendritic spines (119). However, increased expression of these genes only occurs in a short time after stroke (120), suggesting a critical period of heightened neuroplasticity may exist after stroke (114). Consistently, it was observed that low frequency spontaneous activity in surviving neurons appeared, which contributed to a permissive environment for axonal sprouting, only 1-3 days after focal ischemic stroke in rat (121). Regulation of synaptic activity is part of homeostatic mechanisms after stroke. Besides that, homeostatic mechanism could also trigger the formation of new synapses that would compensate for lost structural circuits (114). Thus, axonal sprouting (122) and increased in dendritic spines production (117) after stroke are the important processes to return post-stroke synaptic activity to normal levels. Although the molecular determinants of homeostatic synaptic plasticity are not fully known, inflammatory cytokines and neurotrophic factors are involved (114).

CHAPTER 1

Blood Inflammatory Exosomes with Age Prime Microglia through Complement Signaling for Negative Stroke Outcomes

1. Introduction

Aging is a fundamental biological process accompanied by a general decline in tissue function and increased risk for many diseases. With the aging of the U.S. population, age-related decline, such as cognitive decline in the elderly, is quickly becoming a health care priority (123). Thus, it is important to identify a way to maintain functional integrity by protecting against the aging process. Although the underlying mechanisms remain elusive, age-related changes in the systemic milieu are likely to play an important role. Compelling evidence indicates that systemic administration of young blood plasma into aged mice reverses age-related cognitive decline (35), whereas exposing young mice to plasma from aged mice impairs their cognitive function (33). Similarly, age-related decline in myogenesis and neurogenesis can be restored after exposure to a ‘‘youthful’’ systemic environment through heterochronic parabiosis (32, 124). Importantly, age-related cardiac hypertrophy can also be reversed by exposure to a young systemic environment, in parallel with reduced cardiomyocyte size (23). Currently, there is little evidence showing whether age-related changes in blood can contribute to age-related diseases such as ischemic

stroke, which remains the fifth leading cause of death and the leading cause of long-term disability in the U.S. with limited effective treatment.

Exosomes are extracellular microvesicles that contain specific proteins, RNA, microRNAs (miRNAs) and long noncoding RNAs (lncRNAs) (125). Although exosomes were discovered several decades ago (126), only recently have they been shown to be vital in cell communication by transferring their cargo between source and target cells, through which they can affect the rate of aging(127), the development and progression of cardiovascular disease (128) and cancer (129). Pusic *et al.*(130) found that the youthful systemic milieu enhances remyelination in aged animals and that environmental enrichment of aged animals produces exosomes that mimic this promyelinating effect(47). Consistently, recent studies have shown that administration of exosomes released from mesenchymal stromal cells promotes neuroplasticity and functional recovery after ischemic stroke(131, 132). Based on these findings, we hypothesized that peripheral circulating exosomes derived from young or aged animals may serve as vehicles to deliver beneficial or detrimental signals**,** respectively, from the periphery to the brain and may thus influence functional outcome after ischemic stroke.

In this study, we found that systemic administration of serum exosomes from aged rats (O-exo) into aged ischemic rats worsened motor deficits, increased infarct volume, primed the microglial response and increased synaptic loss. Conversely, exposing aged rats to serum exosomes from young rats (Y-exo) improved neuroplasticity and functional recovery after ischemic stroke. Through proteomic analysis, we found that activated complement proteins (C1q, C3a, C3b) in

peripheral circulating exosomes increased with age, whereas levels of CD46, a *C3b*/C4b-*inactivating* factor, were higher in Y-exo. Either inhibiting C3a receptor (C3aR) or depleting microglia attenuated synaptic loss and motor deficits associated with O-exo treatment. Our data suggest that peripheral circulating exosomes act as inflammatory mediators and influence ischemic stroke outcome (Figure 1).

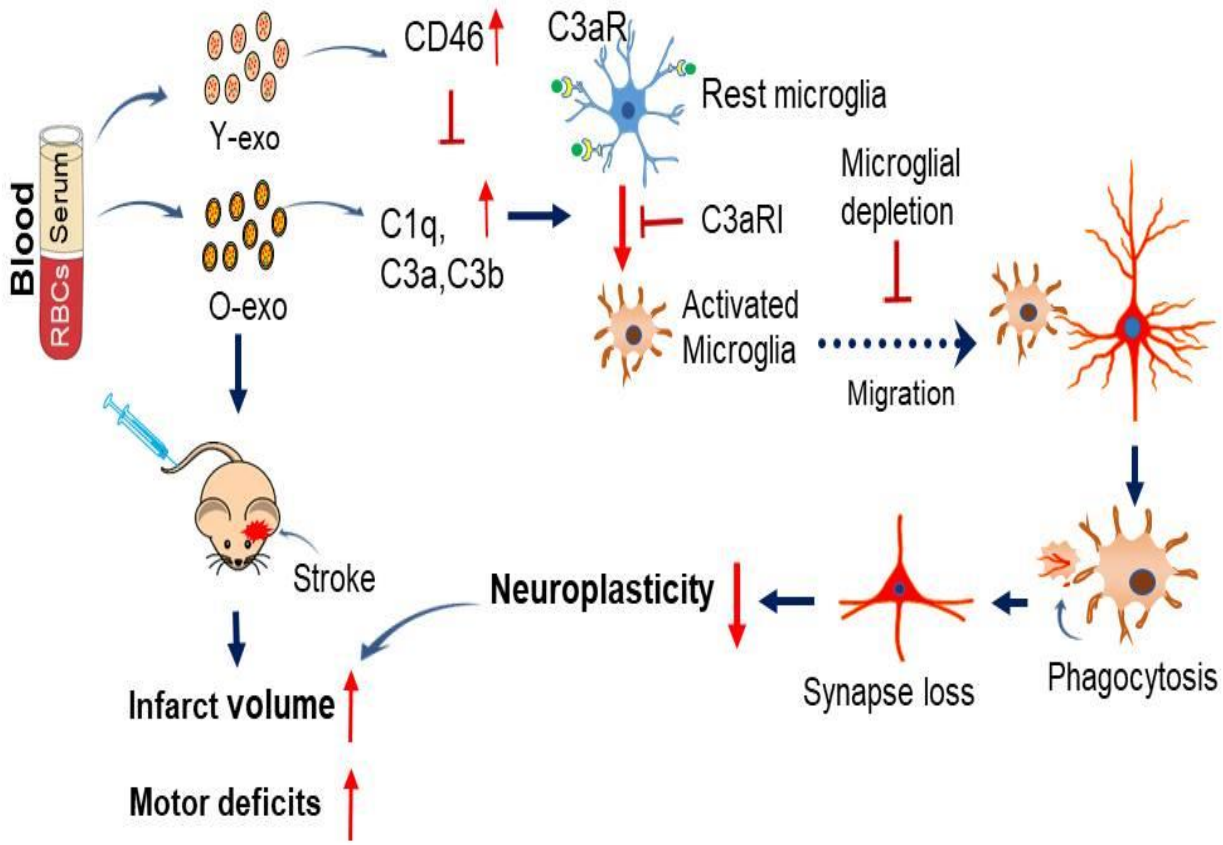

Figure 1. Illustration of blood inflammatory exosomes with age contributing to stroke outcome via a complement–microglia axis.

Complement opsonins and anaphylatoxins that accumulate in blood exosomes with age can prime microglia to make them prone to overreactions that exacerbate *synaptic loss* and motor deficits after ischemic stroke via microglial C3aR. In Y-exo, there is an increased level of CD46, which blocks complement activation, and thus microglia, to attenuate detrimental ischemic outcomes. Y-exo, serum exosomes from young rats; O-exo, serum exosomes from aged rats; C3aRI, C3aR inhibitor.

2. Materials and methods

2.1 Focal ischemic stroke

Young (3-month-old) and aged (21- to 23-month-old) male Fisher 344 rats were obtained from the National Institute of Aging (NIA) aged rodent colonies and anesthetized with 2.0% isoflurane in 70% N_2O/30% O_2 using a mask. Permanent distal middle cerebral artery occlusion (dMCAO) was performed as described previously(133). Briefly, a 2-cm incision was made between the left eye orbit and tragus under the surgical microscope. The temporal muscle was retracted laterally, and a 3-mm diameter craniotomy was made rostral to the foramen ovale. The dura was incised with a 26–gauge needle and the distal middle cerebral artery (MCA) was exposed. The left MCA was occluded by electrocoagulation (Fine Science Tools, Cat # 18000-00) without damaging the brain surface. Interruption of blood flow was confirmed visually under the microscope, the temporal muscle was repositioned, and the skin was closed. Rectal temperature was measured and maintained at 37 ± 0.2°C with a heating blanket (Harvard Apparatus, Cat # 507220F). In sham-operated controls the distal MCA was visualized but not occluded. All animal procedures were approved by Institutional Animal Care and Use Committee (IACUC) of University of North Texas Health Science Center and conducted according to the National Institutes of Health (NIH) Guide for the Care and Use of Laboratory Animals. Every effort was made to minimize suffering and to reduce the number of animals used.

2.2 Isolation of serum exosomes

Whole blood was collected from young or aged rats *via* cardiac puncture into a BD Vacutainer® Plus Glass Serum blood collection tubes (BD, Cat # 366430). After collection, the whole blood samples were allowed to clot by standing at room temperature for 30 min. The clots were

removed by centrifugation for 10 min at 1,000 x *g* using a refrigerated centrifuge. The isolated serum was aliquoted and stored at -80°C.

Exosomes from young or aged rat serum were isolated using the ExoQuick Exosome precipitation kit (System Biosciences, Cat # EXOQ20A-1) according to the manufacturer's instructions. In brief, serum (500 µl) was centrifuged at 3000 x *g* for 15 min to eliminate cells and cell debris. The supernatant was transferred to a sterile microtube and an appropriate volume of exosome precipitation solution was added for 30 min at 4°C. The mixture was then centrifuged at 1500 x *g* for 30 min, and the exosome pellet was resuspended in sterile 1X phosphate-buffered saline (PBS).

2.3 Injection of serum exosomes

To investigate the effect of serum exosomes on outcomes in ischemic rats, serum exosomes (300 µg) from young or aged male Fisher 344 rats (N = 5 each group) or vehicle (PBS) were injected intravenously in aged male rats at 3 h after dMCAO, twice per day for 3 days. The dose was determined based on our previous studies and other studies using stem cells-derived exosomes for stroke treatmentthe modification from previous studies (131, 134). At 72 h after injection, animals were euthanized, and the brains were sampled.

To monitor peripheral circulating exosomes trafficking in the brain, the exosomes were labeled with the ExoGlow-Vivo dye, a unique dye developed for *in vivo* studies, using the ExoGlow-Vivo EV Labeling Kit (System Biosciences, Cat # EXOGV900A-1). The labeled exosomes or

vehicle were administered intravenously via the tail vein into sham-operated or ischemic rats 3 h after dMCAO. The rats were then euthanized 72 h after injection.

2.4 Characterization of serum exosomes

Concentration and size distribution profile of the isolated exosomes were determined by nanoparticle-tracking analysis (NTA) using SBI's Exosome Nanosight Analysis Service (System Biosciences, Palo Alto, CA). The serum exosomes were also observed using transmission electron microscopy (TEM, *FEI Tecnai G2 Spirit BioTwin*) to identify the morphology and the extent of dispersion, which was performed at the Electron Microscopy Core Facility, University of Texas Southwestern Medical Center, Texas, USA. The enrichment of exosomes was further confirmed by western blotting using antibodies against exosomes, such as CD63, CD9, and CD81.

2.5 Infarct volume measurement

Infarct volume was determined as described previously(135). Rats were anesthetized with 4% isoflurane in 70% N_2O and 30% O_2 and decapitated after treatment. The brains were removed quickly and cut into 2-mm sections. The sections were stained with 2% 2,3,5-triphenyltetrazolium chloride (TTC; Sigma-Aldrich, St. Louis, MO, USA. Cat # T8877) solution for 20 min at 37°C and then fixed in 4% paraformaldehyde (PFA) solution overnight. In some cases, rat brains were embedded in paraffin, cut into 5-μm coronal sections (100-μm apart), and stained with 0.1% Cresyl violet (CV; Sigma-Aldrich, St. Louis, MO, USA. Cat # C5042). Both stained sections were photographed using a Nikon E 950 digital camera attached to a dissecting microscope, and infarct area was measured using NIH's Image J (version 1.62). The ischemic

lesion area was calculated as the difference between the intact area of contralateral hemisphere and the intact area of the ischemic hemisphere. Infarct volume was calculated by multiplying the infarct area by the thickness of the section and expressed as a percentage of the intact contralateral hemispheric volume (136).

2.6 Golgi-Cox staining

Golgi-Cox staining was performed to visualize dendritic spine structure in superficial and deep cortical layer neurons using the FD Rapid GolgiStain kit (FD Neuro-technologies, Inc, Cat # PK401/401A) according to the manufacturer's instruction (137, 138). In brief, rats were deeply anesthetized and intracardially perfused with PBS, followed by 4% PFA. The brain sections were immersed in the Golgi-Cox solution for 12 days in the dark at room temperature and then transferred to 30% sucrose solution. Coronal sections were cut at 60-μm and stained according to FD Rapid GolgiStain's protocol. The slides were subsequently washed with distilled water followed by dehydration in ascending alcohol concentrations, cleared in xylene, and then mounted with Per-mount (Vector, H-5000).

2.7 Dendritic spine quantification

Dendrites and dendritic spines were analyzed from cortical layers II/III or V of the peri-infarct primary motor cortex (M1) between 0 and 0.5 mm anterior to the bregma, corresponding to the approximate center of the cortical infarct, with the aid of an atlas (139). M1 regions were chosen as previous study showed that focal ischemic stroke induced significant structural plasticity in the peri-infarct motor cortex but not in the more distant ipsilateral cortical regions (118). In addition, dendrite and dendritic spine structure was also examined in the M1 region of the

contralateral cortex (a within-animal control). Criteria for inclusion in the analyses were that the neuron had to be well impregnated with Golgi-Cox stain, unobstructed by other dendrites, blood vessels or glia, and that the dendritic arborization was intact and visible in the plane of the section.

Three images of the peri-infarct area in the M1 region of the ischemic brain per section or the corresponding region on the contralateral cortex were captured by using an Olympus confocal scanning system mounted on Olympus microscope (BX 61, Olympus) with an HSD channel and FV 10-ASW software (Olympus Fluoview, Version 4.02), with x 600 magnification. Dendrites and dendritic spines were analyzed from at least 9 pyramidal cells per animal (N = 3-5 per group). For quantification of dendrites and spines of pyramidal neurons, NIH's image J (version 1.62) was used to invert image signals to RGB. Imaris software (version 8.0, Bitplane,) was used to track neurites with the FilamentTracer module by means of a semiautomatic autopath method. Fifty images were collected as high-resolution image z-stacks with a step size of 0.66 µm. On the automatically tracked dendrites, Golgi stains were manually indicated under interactive 3D visualization using the built-in Spot detection module. Staining in each dendritic segment underwent manual thresholding such that all visually discernible protuberances in 3D were identified according to the range values of the length of spines in the cortical M1 region. Both apical and basilar dendritic trees were analyzed for total length and total number of spine segments (140). Dendritic spine length and diameter was automanually marked in each individual dendritic spine from the center of the dendritic shaft to the distal tip of the spine based on threshold. Dendritic length and branches were determined by a measure of the total length of each basal or apical dendrite and the number of dendritic spines refers to all dendritic spines

contained within the total length of each dendrite. All neurons were measured with the same parameters in terms of threshold and limitations.

2.8 Immunofluorescence staining

Immunofluorescence staining and double or triple immunostaining were performed on brain sections as previously described (141, 142). The primary antibodies used were as follows: rabbit anti-ionized calcium binding adaptor moleculae 1 (anti-Iba1, 1:1000, WAKO, Cat # 019-19741), chicken anti-Homer1 (1:500, Synaptic Systems, Cat # 160006), mouse anti-CD68 (1:100, Serotec, Cat # MCA341R), goat anti-CD86 (1:200, R&D, Ca t# AF1340), rat anti-CD206 (1:100, Serotec, Cat # MCA2235GA), rabbit anti Neuronal nuclei (anti-NeuN, 1: 100, Millipore, Cat # ABN78) and rabbit anti-glial fibrillary acidic protein (anti-GFAP, 1: 500, DAKO, Cat # Z0334), rabbit anti myelin proteolipid protein (anti-myelin PLP, 1: 1000, Novus Biologicals, Cat # NBP1-87781), mouse anti-C3aR (1: 50, Santa Cruz, Cat # sc-133172), rabbit anti-vWF (1: 100, Millipore, Cat # AB7356). The secondary antibodies used were as follows: Alexa Fluor 350-, 488-, 594-, or 647-conjugated donkey anti-rat, anti-rabbit, anti-mouse, or anti-goat IgG (ThermoFisher Scientific, 1:1000). DAPI (4′,6-diamidine-2-phenylindole dihydrochloride; Vector Laboratories) was used to counterstain nuclei, and fluorescence signals were detected with Olympus Confocal Scanning System mounted on Olympus microscope (BX 61, Olympus), which interfaced with FV 10-ASW software (Olympus Fluoview, version 4.02).

For co-localization analysis, double or triple immunostained-positive cells in the peri-infarct region of sections were imaged with X60 Zeiss Neofluar oil-immersion objective (numerical

aperture=1.3) using sequential scanning mode, with a final X120 magnification of images. Corresponding images were taken in the contralateral hemisphere. Three standard sections with 9 fields per animal in 200-µm intervals were analyzed. All sections were scanned with the same acquisition parameters.

2.9 Western blotting

The brains were removed and placed in a coronal brain matrix and cut into 2-mm sequential sections. The specimens were collected in PBS and the different brain regions were dissected. Brain tissue was lysed in RIPA buffer (1% Triton-X100, 0.5% sodium deoxycholate, 0.1% SDS in 1X PBS, pH 7.4) with 1X protease and phosphatase inhibitor cocktail (ThermoFisher Scientific, Cat # 78440). The protein concentration was determined using Quick Start Bradford protein assay (Pierce™ BCA Protein Assay kit, Thermo Fisher Scientific) and normalized for protein content. The lysates (30 µg) were loaded on 8-12% SDS-PAGE gels and subsequently transferred onto a polyvinylidene difluoride (PVDF) membrane (Merck Millipore, Cat # IPVH00010). The blot was incubated in blocking buffer (5% milk in Tris-buffered saline with Tween) and then incubated with the primary antibody solution overnight at 4°C. Protein signals were detected with horseradish peroxidase–conjugated secondary antibodies and Pierce enhanced chemiluminescence (ECL) substrate (ThermoScientific, Cat # 32106). The data were recorded and analyzed using the ChemiDoc Imaging System (Bio-Rad). β-actin bands were used for normalization.

Primary antibodies include mouse anti-CD63 (1:1000, BD Pharmingen, Cat # 551458), mouse anti-CD9 (1:1000, BD Pharmingen, Cat # 551808) and mouse anti-CD81 (1:1000, Santa Cruz,

Cat # sc-7637), rabbit anti-Iba1 (1:2000, WAKO, Cat# 019-19741), mouse anti-CD68 (1:1000, Serotec, Cat # MCA341R), mouse anti-C3 (1:1000, Santa Cruz, Cat # sc-28294), rat anti-CD46(1:100, Abcam Cat # ab180625), mouse anti-C1q (1:100, Abcam, Cat# ab71940), mouse anti-beta-action (1:2000, Cell Signaling Tech, Cat # 3700s), goat anti-CD86 (1:200, R&D, Cat# AF1340), mouse anti-CD11b (1:100, Serotec; Cat# MCA275R), rat anti-CD206 (1:100, Serotec, Cat# MCA2235GA). Secondary antibodies include horseradish peroxidase (HRP)-conjugated anti-rabbit, anti-mouse, anti-rat, anti-goat IgG secondary antibodies (Cell Signaling Tech).

2.10 Proteomic analysis of serum exosomes

Exosomes from young and aged rat blood were processed for proteomic analysis by SBI's Exosome Proteomics Services (System Biosciences, USA). The protein concentration of each exosome was determined by Qubit fluorometry (Invitrogen) and each sample (10 μg) was processed by 10% SDS-PAGE. The band was excised, and in-gel digestion was performed using a ProGest robot (DigiLab). The different proteomic contents of young-Exo and old-Exo were analyzed using nano liquid chromatography tandem mass spectrometry (LC-MS/MS) with a Waters NanoAcquity HPLC system interfaced to a ThermoFisher Q Exactive. The resulting LC-MS/MS raw data were processed using Mascot (Matrix Science) and searched against the UniProt Rat database. The Mascot DAT files were parsed into Scaffold (Proteome Software) for validation, filtering and to create a non-redundant list per sample. Data were filtered using 1% protein and peptide false discovery rate (FDR) and requiring at least two unique peptides per protein. The criteria for protein identifications were accepted if a minimum of two peptides were detected or a unique peptide was detected with an FDR <1%.

2.11 Biological functions and pathway analysis

Biological function annotation of the proteins was analyzed by Blastp (Blast2GO version 4) using whole database, and mapped, annotated with gene ontology (GO) database (http://geneontology.org/). All of the rat proteins were used as the basis for calculating enrichment values. Statistically altered functions of different expressed exosome proteins were calculated by Fisher's exact test in Blast2GO. A cutoff of absolute fold change ≥1.5 was used for differentially expressed proteins and a corrected *p*-value <0.05 was considered significant. To further understand the biological significance of differentially expressed exosome proteins, pathway analysis was analyzed by *KOBAS* (KEGG Orthology Based Annotation System; http://kobas.cbi.pku.edu.cn). The association of the genes with different pathways was computed using the Kyoto Encyclopedia of Genes and Genomes (KEGG) database (http://www.genome.jp/kegg). One-way ANOVA was applied to calculate peptide and protein abundance expression. A Z score ≥ 2 or ≤ -2 indicated significant activation or significant inhibition, respectively.

2.12 Complement 3a receptor antagonist treatment

SB290157 (Cat # 559410, Merck Millipore), a C3a receptor inhibitor (C3aR) (143), was diluted in sterile PBS/0.5% DMSO to a concentration of 1 nM, as previously described (144). Rats were randomized to receive intraperitoneal injections of either SB290157 (1 mg/kg) or an equal volume of vehicle (PBS/DMSO) 1 h prior to exosome administration. Outcome was determined 3 days after treatment.

2.13 Microglial depletion

To deplete microglia *in vivo*, rats were fed with the colony stimulating factor 1 receptor (CSF1R) inhibitor PLX3397 (MedChemExpress Inc.) formulated in standard chow (Lab Diet 5LG4, Lab Supply Inc.) at 290 mg/kg as previously described (145). Respective controls received standard chow. Rats were fed for at least 28 days prior to dMCAO to ensure maximum microglia depletion, and this lasted until the end of the experiment.

2.14 Behavioral testing

Rats (N=8-16 per group) underwent neurobehavioral tests to evaluate motor function. Animals were trained prior to ischemic stroke and motor deficits were assessed at different durations thereafter. The investigator performing the tests was blinded to the experimental condition.

2.14.1 Ladder rung walking test

The skilled ladder rung walking test is used to evaluate placing, stepping and inter-limb coordination (146) and the procedure was performed as described previously (147). Animals were video recorded as they walked across the runway five times per session. Foot fault was generally scored on a rating scales according to the quality of limb placement on the rungs. There were 6 rating scales: 0 total miss, 1 deep slip, 2 slight slip, 3 replacements, 4 corrections, 5 partial placements, 6 correct placements. The number of errors was defined as each limb placement that received a score of 0, 1 or 2 points and then was counted. The percentage of errors in total steps was calculated and averaged for five trials for each rat.

2.14.2 Cylinder test

The cylinder test was designed to evaluate locomotor asymmetry in rodent models of stroke. Forelimb use bias was analyzed by observing the rat's movements over 3-minute intervals in a transparent, 18-cm-wide, 30-cm-high Plexiglas cylinder. A mirror behind the cylinder made it possible to observe and record forelimb movements when the rat was facing away from the examiner. After an episode of rearing and wall exploration, a landing was scored for the first limb to contact the wall or for both limbs if they made simultaneous contact. The cylinder score was calculated using the following equation: (Ipsilateral forelimb contacts – contralateral forelimb contacts)/total contacts.

2.15 Statistical analysis

All values were expressed as mean ± SEM. All experiments were randomized and performed by a blinded independent researcher. Statistical significance of differences between means was evaluated using Student *t*-test between two groups and one-way ANOVA followed by *Turkey* test for three groups. Values of $p < 0.05$ were considered statistically significant. All statistical analyses are conducted using GraphPad Prism software (version 5.0).

3. Results

3.1 Age-related changes in serum exosome characteristics

To investigate whether age-dependent peripheral circulating exosomes could act as inflammatory mediators to influence functional outcome after ischemic stroke, we isolated serum exosomes from 3-month-old (young) and 21- to 23-month-old (aged) rats, which correlate to ~20 and

56–69 years of age in humans, respectively. We first performed western blotting with antibodies against exosome-specific markers to confirm the enrichment of exosomes. All exosome protein markers including CD63, CD9 and CD81 were enriched in the O-exo (Figure 2A) and Y-exo samples. We also verified serum exosome morphology and size using transmission electron microscopy (TEM), which showed clear circular membrane vesicles with a diameter of ~40 nm (Figure 2B). We further quantified the number and size distribution of Y-exo and O-exo by NTA. The NTA showed a strong enrichment in particles in the range of 40–120 nm (Figure 2C), consistent with the presence of a multimodal size distribution of exosomes with a diameter of ~70–120 nm as shown in previous studies (148, 149). Interestingly, O-exo had a larger diameter (107 ± 0.8 nm, mean ± SE) relative to Y-exo (85 ± 0.7 nm) but were present at a lower concentration (14.84×10^{12} particles/mL) as compared with Y-exo (8.75×10^{12} particles/mL; Figure 2D), suggesting that the concentration and size of serum exosomes change with age.

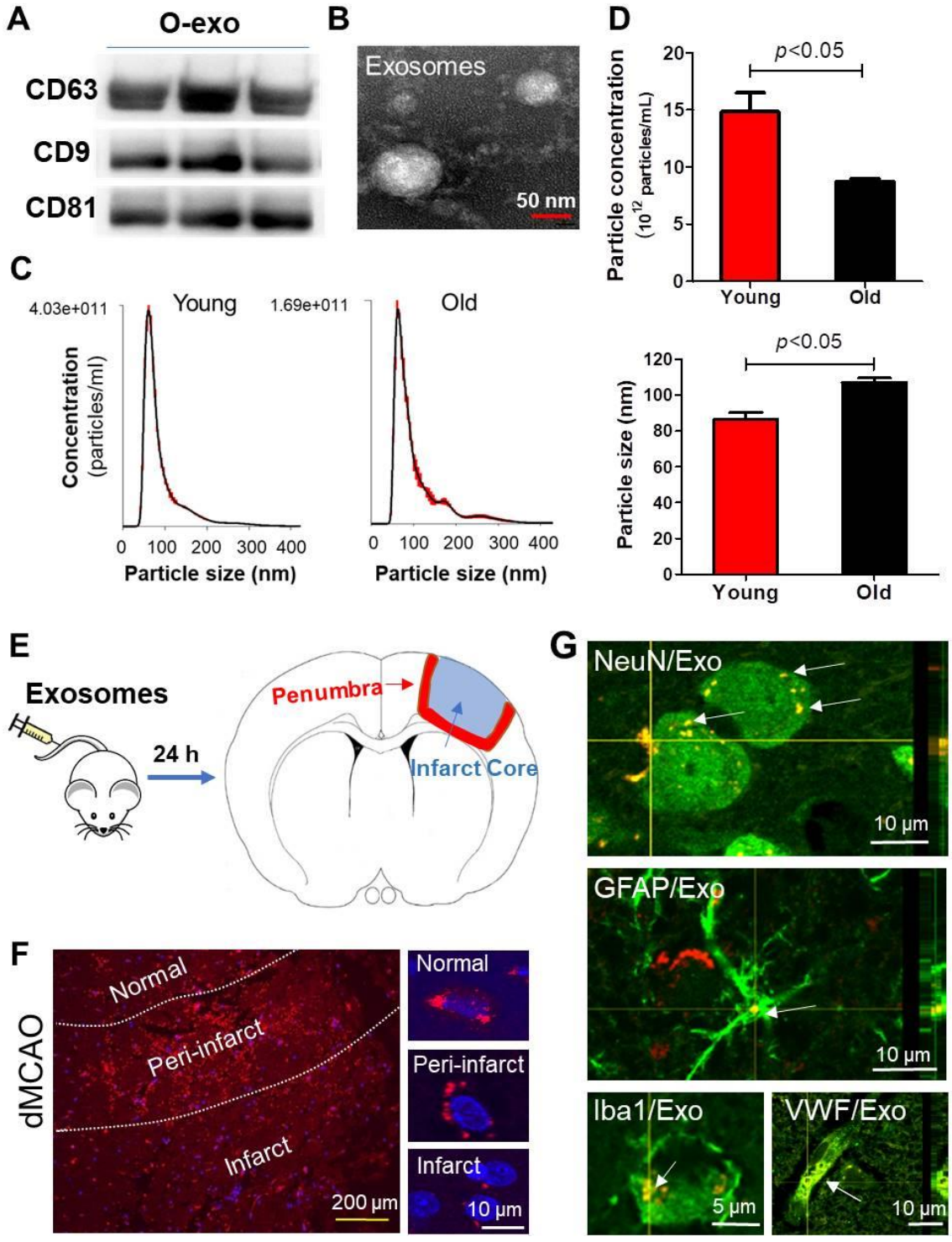
A
O-exo
CD63
CD9
CD81
B
Exosomes
50 nm
C
Young
Old
4.03e+011
1.69e+011
Concentration (particles/ml)
0 100 200 300 400
Particle size (nm)
D
p<0.05
Particle concentration (10^{12} particles/mL)
Young
Old
p<0.05
Particle size (nm)
E
Exosomes
24 h
Penumbra
Infarct Core
F
dMCAO
Normal
Peri-infarct
Infarct
200 μm
Normal
Peri-infarct
Infarct
10 μm
G
NeuN/Exo
10 μm
GFAP/Exo
10 μm
Iba1/Exo
5 μm
VWF/Exo
10 μm

Figure 2. Characterization and crossing the BBB of serum exosomes.

(**A**) Serum exosome samples from three aged rats were analyzed by western blotting with antibodies against the exosome-specific markers CD63, CD9 and CD81. The experiment was repeated three times (N = 3 per group each experiment). (**B**) Representative electron micrograph showing typical morphology and size range of O-exo. (**C**) NTA was used to determine the concentration and size distribution of Y-exo and O-exo. (**D**) Quantification of the concentration (top graph) and size (bottom graph) of serum exosomes determined by NTA. **(E)** Schematic illustrating intravenous injection of fluorescently labeled serum exosomes into sham-operated and ischemic rats 3 h after ischemia onset; rats were euthanized 24 h after injection. Topographic location of ischemic regions including penumbra (a rim of tissue surrounding the severely ischemic core (in red) and infarct core (in blue) are indicated. **(F)** A representative image (left panel; low-magnification view) shows the distribution of fluorescently labeled exosomes (red) in the ipsilateral cortex. The labeled exosomes were predominantly located in the cytoplasm of the brain cells in the normal and peri-infarct (penumbra) regions and infarct core (right panel; high-magnification view). **(G)** Representative confocal microscopic images indicate that fluorescently labeled exosome-positive cells were positive for NeuN, GFAP, Iba1 and VWF expression in the ischemic cortex of aged rat brains. Error bars denote SEM. N = 3–6 rats per group. Exo, exosomes; Y-exo, serum exosomes from young rats; O-exo, serum exosomes from aged rats.

3.2 Intravenously injected exosomes pass the BBB and home mainly to the peri-infarct regions after stroke

The brain is traditionally considered an "immune-privileged" site due to the isolating effect of the blood-brain barrier (BBB) (150), which is, however, damaged after ischemic stroke. To determine whether exosomes can transfer molecular signals from the blood to the brain, we labeled O-exo with a new proprietary, non-lipophilic dye for tracking exosome biodistribution *in vivo*. We intravenously administered these labeled exosomes into sham-operated and ischemic aged rats 3 h after ischemic stroke (Figure 2E). Fluorescently labeled exosomes were observed throughout the normal and ischemic regions of the brain, including the striatum, hippocampus and cerebellum, at 24 h after the injection but were rarely detected in the subventricular zone (SVZ) (data not shown). Interestingly, the labeled exosomes accumulated mainly in the peri-infarct region (penumbra) of the cortex after focal ischemia (Figure 2F). To determine the phenotypes of the labeled exosome-positive cells, immunofluorescence staining was performed on the brain sections using antibodies against GFAP (for astrocytes), NeuN (for neurons), Iba1 (for microglia) and von Willebrand factor (VWF) (for endothelial cells). As shown in Figure 2G, the labeled exosome-positive cells co-localized with NeuN, GFAP, Iba1 and VWF. These findings suggest that the intravenously injected serum exosomes can pass through the BBB and be internalized by brain cells including neurons.

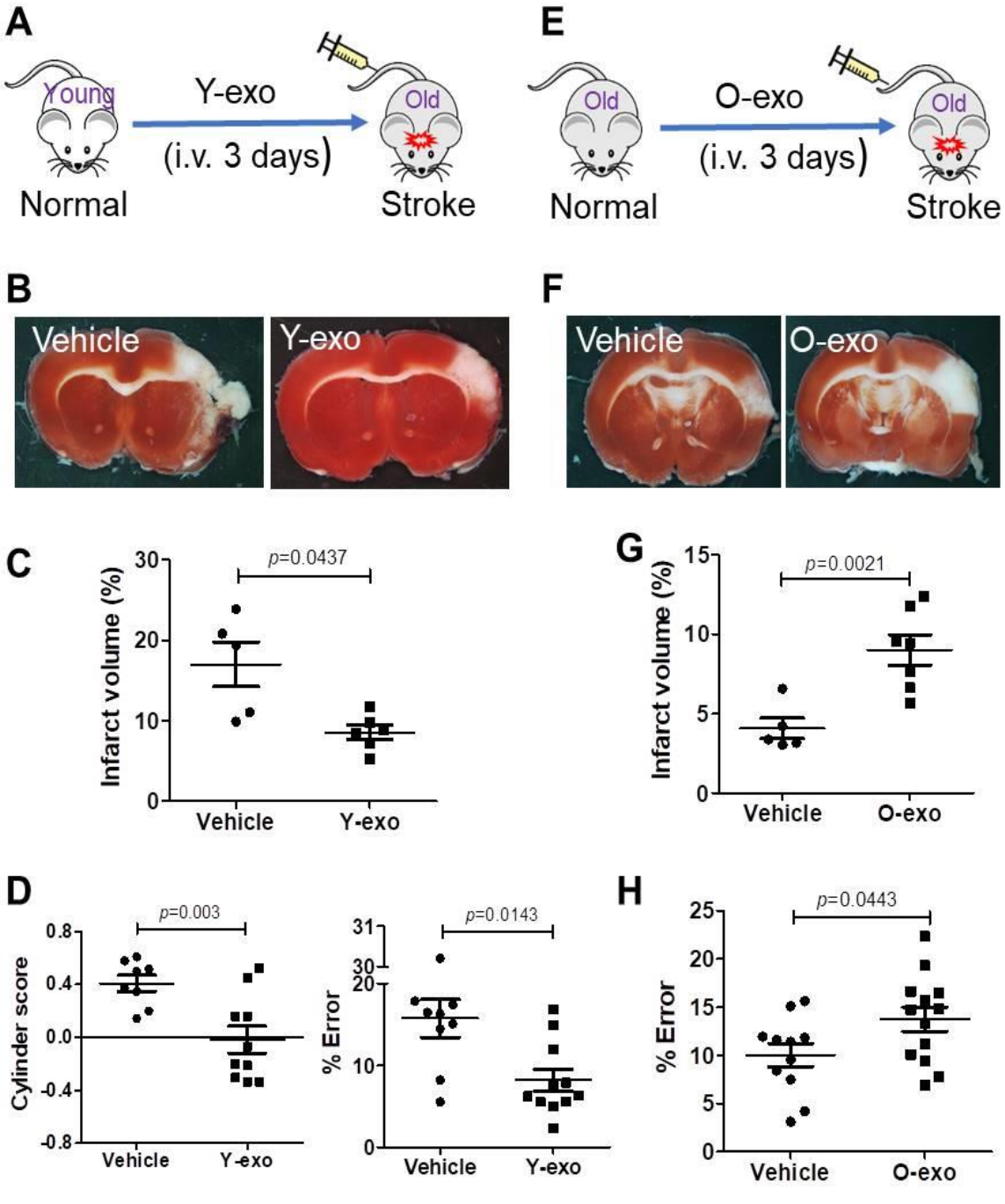
A
Young
Y-exo
(i.v. 3 days)
Old
Normal
Stroke
E
Old
O-exo
(i.v. 3 days)
Old
Normal
Stroke
B
Vehicle
Y-exo
F
Vehicle
O-exo
C
Infarct volume (%)
p=0.0437
Vehicle
Y-exo
G
Infarct volume (%)
p=0.0021
Vehicle
O-exo
D
Cylinder score
p=0.003
Vehicle
Y-exo
% Error
p=0.0143
Vehicle
Y-exo
H
% Error
p=0.0443
Vehicle
O-exo

Figure 3. The effect of serum exosomes on stroke outcome is age dependent.

(A) Schematic illustrating intravenous injection of Y-exo into aged ischemic rats 3 h after ischemic stroke, twice per day for 3 days. **(B)** Infarct areas (white) in triphenyltetrazolium chloride (TTC)-stained (red) coronal brain sections from vehicle– and Y-exo–treated rats 3 days after stroke. **(C)** Quantitative analysis of infarct volume in vehicle– and Y-exo–treated rats 3 days after ischemic stroke. **(D)** Motor deficits of aged ischemic rats were assessed by the cylinder test (left graph) and ladder rung walking test (right graph) on the fourth day after administration of vehicle or Y-exo. **(E)** Schematic illustrating the protocol of O-exo injection into aged ischemic rats. **(F)** Representative images of TTC-stained brain sections at 72 h after focal ischemia in vehicle-treated and O-exo–treated rats. **(G)** Administration of O-exo significantly increased the infarct volume, as compared with the vehicle-treated group. **(H)** Rats treated with O-exo after stroke show significant improvement in motor deficits as compared with vehicle-treated rats. Data are presented as the mean ± SEM. N = 7–12 rats per group. Y-exo, serum exosomes from young rats; O-exo, serum exosomes from aged rats.

3.3 Y-exo attenuate, but O-exo deteriorate stroke outcome

Despite more than 1000 neuroprotective agents showing promise in experimental models of ischemic stroke, not one has been successfully translated to clinical practice as a treatment for acute ischemic stroke (151), which has created some doubt regarding the validity of current stroke animal models as predictive tools (152). Indeed, young animal models of stroke have been used to predict the clinical efficacy of neuroprotective agents due to their wide availability, lower cost and fewer health problems (8). However, aged animals show significant differences relative to young animals in their response mechanisms, ischemic consequences, and histological changes (153). In addition, stroke occurs most often in the elderly population, and stroke patient outcomes are highly influenced by age (154). Thus, we used aged rats as a stroke model in this study.

To determine whether peripheral circulating exosomes contributed to functional outcomes after ischemic stroke, we first injected Y-exo intravenously into aged rats with 23-month-old 3 h after focal ischemia, twice per day for 3 days (Figure 3A). The infarct volume was significantly reduced in the group treated with Y-exo at 72 h after injection, as compared with the vehicle group (Figure 3B and C). Consistently, the motor deficits as assessed by a cylinder test and ladder rung walking test were significantly improved in the Y-exo-treated group as compared with the vehicle group (Figure 3D), suggesting that Y-exo attenuate stroke outcome. We then asked whether O-exo treatment worsens stroke outcome. O-exo were intravenously injected into aged rats with 21-month-old at 3 h after ischemic stroke, twice per day for 3 days (Figure 3E). The brain tissue damage in the O-exo-treated group was significantly greater than that in the vehicle group after treatment (Figure 3F). Quantification showed that the infarct volume was

significantly larger in the O-exo-treated group than that in the vehicle group (Figure 3G). Consistent with histological data, neurobehavioral testing also showed that motor deficits worsened 72 h after O-exo treatment as compared with vehicle (Figure 3H), indicating that O-exo treatment deteriorated the functional outcome in aged ischemic rats.

3.4 Serum exosomal priming of the microglial response after ischemic stroke is age dependent

Mounting evidence indicates that *the microglia-mediated* inflammatory response plays a fundamental role in the pathophysiology and prognosis of ischemic stroke. Activated *microglia* release both pro- and anti-inflammatory mediators**,** which can have both beneficial and detrimental effects on neurons. In ischemic stroke, the secondary damage occurs mainly in the penumbra, the area surrounding the core of infarction (peri-infarct region), where neuronal cells are reversibly affected by ischemia (155). Therefore, the penumbra is a target for neurorepair and neuroprotective therapies (156). Indeed, we found that the number of $Iba1^+$ microglia was substantially increased in the penumbra after ischemic stroke (Figure 4A). These microglia retracted their ramifications, displayed an amoeboid morphology (amoeboid microglia) and were immunopositive for CD68 (a lysosomal protein expressed at high levels by activated *microglia* and at low levels by resting microglia). These activated microglia were observed most frequently in the penumbra and to a minor extent in the infarction core 2 days after stroke. Quantitative data showed that much lower expression of microglia and activated microglia in the penumbra compared with contralateral side of brain cortex of aged ischemia rats (Figure 4B). Western blotting confirmed that Iba1 and CD68 were significantly increased in the penumbra after focal

ischemia (Figure 4C-F). Taken together, these findings suggest that activated microglia were induced and accumulated in the penumbra after ischemic stroke.

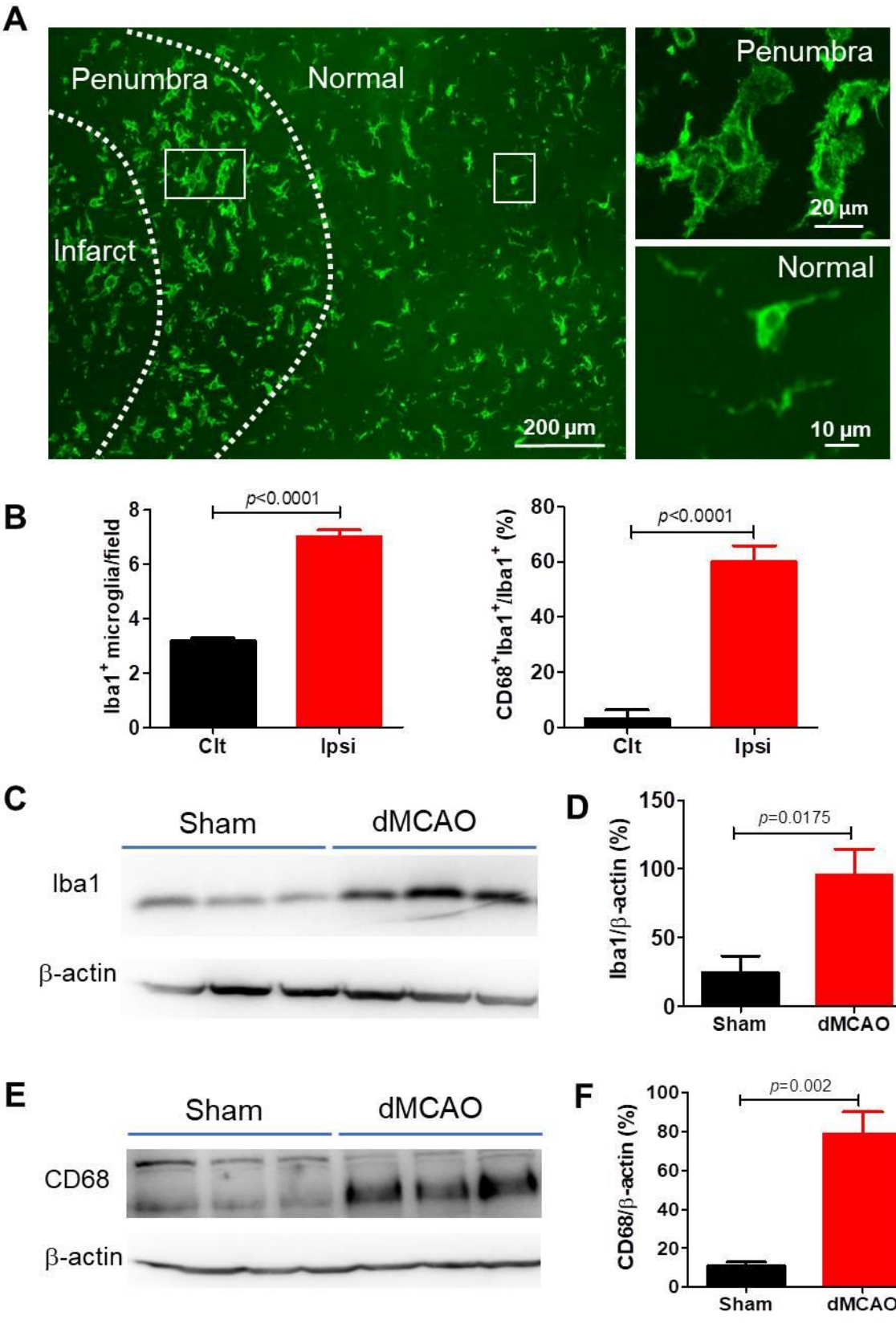
A
Penumbra
Normal
Infarct
200 μm
Penumbra
20 μm
Normal
10 μm
B
p<0.0001
Iba1+ microglia/field
Clt
Ipsi
p<0.0001
CD68+Iba1+/Iba1+ (%)
Clt
Ipsi
C
Sham
dMCAO
Iba1
β-actin
D
p=0.0175
Iba1/β-actin (%)
Sham
dMCAO
E
Sham
dMCAO
CD68
β-actin
F
p=0.002
CD68/β-actin (%)
Sham
dMCAO

Figure 4. Focal ischemic stroke induces a microglial response in the penumbra.

(A) Immunocytochemistry shows the distribution pattern of $Iba1^+$ cells in the ischemic cortex, suggesting that activated microglia are located mainly in the penumbra. Left panel: low-magnification view of $Iba1^+$ cells in the infarct core, penumbra and adjacent normal area. Top right panel: morphology of activated microglia in the penumbra. Bottom right panel: morphology of microglia in the normal area. **(B)** Immunostaining showed increased expression of Iba1-positive microglia and $Iba1^+CD68^+$ double positive activated microglia in ischemic cortex. **(C-D)** Relative quantification of Iba1 protein detected by western blots in sham-operated and ipsilateral cortex after focal ischemia. **(E-F)** Relative quantification of CD68 protein detected by western blots in sham-operated and ipsilateral cortex after ischemic stroke. dMCAO, distal middle cerebral artery occlusion. β-actin was used as a protein loading control. Data represent the mean ± SEM (N = 4–6). Clt, contralateral; Ipsi, ipsilateral.

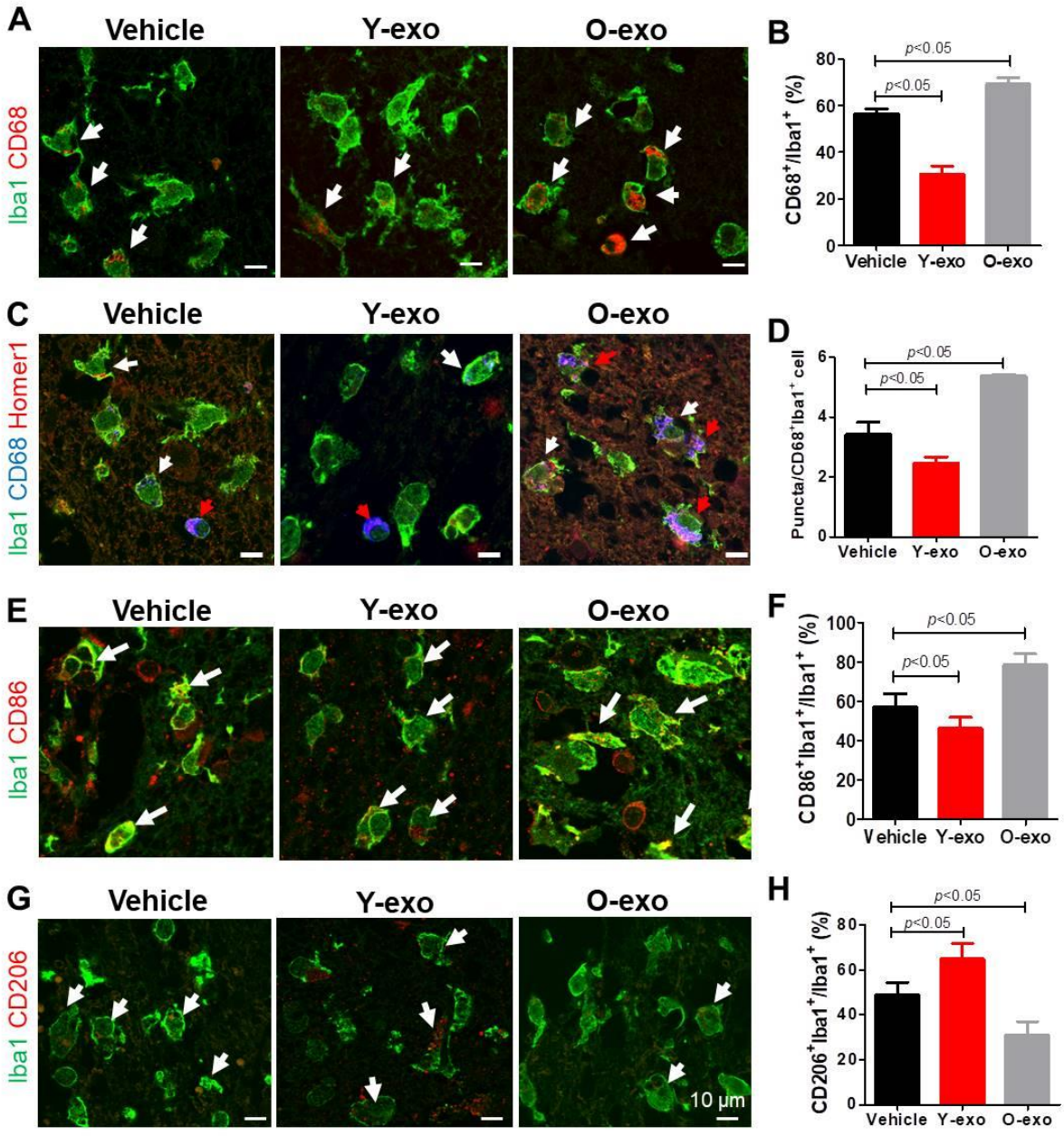
A
Vehicle
Y-exo
O-exo
Iba1 CD68
B
p<0.05
p<0.05
CD68+/Iba1+ (%)
Vehicle Y-exo O-exo
C
Vehicle
Y-exo
O-exo
Iba1 CD68 Homer1
D
p<0.05
p<0.05
Puncta/CD68+Iba1+ cell
Vehicle Y-exo O-exo
E
Vehicle
Y-exo
O-exo
Iba1 CD86
F
p<0.05
p<0.05
CD86+Iba1+/Iba1+ (%)
Vehicle Y-exo O-exo
G
Vehicle
Y-exo
O-exo
Iba1 CD206
10 μm
H
p<0.05
p<0.05
CD206+Iba1+/Iba1+ (%)
Vehicle Y-exo O-exo

Figure 5. Serum exosomes prime the microglia response after ischemic stroke.

(A) Representative confocal images of $Iba1^+$(green) $CD68^+$(red) microglia in the M1 region of the penumbra in aged ischemic rats treated with vehicle, Y-exo or O-exo. White arrows indicate $Iba1^+CD68^+$ microglia. **(B)** Quantitative analysis of $Iba1^+CD68^+$ microglia in the penumbra in vehicle-, Y-exo– and O-exo–treated aged rats 72 h after ischemia. **(C)** Representative confocal images of $Iba1^+$ (green), $CD68^+$ (blue) and $Homer1^+$ (red) microglia in the penumbra after vehicle, Y-exo or O-exo. White arrows indicate $Iba1^+CD68^+$ microglia. Red arrows indicate $Iba1^+CD68^+$ $Homer1^+$ microglia. **(D)** Quantification of the phagocytic response of microglia in the M1 region of the penumbra in aged ischemic rats after vehicle, Y-exo or O-exo treatment. **(E)** Representative confocal images from the penumbra (M1 region) showing expression of Iba1 (green) and CD86 (red) after serum exosome treatment. White arrows indicate $Iba1^+CD86^+$ microglia. **(F)** Quantification of $Iba1^+CD86^+$ microglia in vehicle-, Y-exo or O-exo-treated ischemic rats. **(G)** Representative confocal images of Iba1 (green) and CD206 (red) in the penumbra of the aged ischemic brain after serum exosome treatment. White arrows indicate $Iba1^+CD206^+$ microglia. **(H)** The number of $CD206^+$ microglia in the penumbra after vehicle, Y-exo or O-exo treatment. Data are presented as the mean ± SEM. N = 3–6 rats per group. Y-exo, serum exosomes from young rats; O-exo, serum exosomes from aged rats.

Intravenous injection of O-exo into aged rats 3 h after focal ischemia resulted in a significant increase in Iba1-positive ($Iba1^+$) and CD68-positive ($CD68^+$) cells (activated microglia) at 72 h after treatment as compared with vehicle (Figure 5A and B). The majority of these cells were distributed in the penumbral M1 region of the cerebral cortex (also called primary motor cortex), but only a few $Iba1^+CD68^+$ cells were found in the ischemic core. At 72 h after ischemic stroke, aged ischemic rats treated with Y-exo exhibited significantly fewer $Iba1^+CD68^+$ cells in the penumbral M1 region of the parietal cortex than those treated with vehicle (Figure 5A and B). Few to no $Iba1^+CD68^+$ cells were found in the contralateral cortical area (Figure 9B).

To investigate the impact of activated microglia in phagocytosis, we performed triple-label immunofluorescence staining for Iba1, CD68 and Homer1, a postsynaptic density protein and thus a marker for the synapse. The triple-immunopositive ($Iba1^+CD68^+Homer1^+$) microglia were observed in the penumbral M1 region of the cerebral cortex. Confocal images show that $Homer1^+$ puncta were localized inside the lysosome of $Iba1^+CD68^+$ microglia (Figure 5C). An increased frequency and higher density of $Homer1^+$ puncta in single microglia were found in the O-exo-treated aged ischemic brains (Figure 5C). Quantification of colocalized postsynaptic puncta revealed a significant loss of synapses in aged ischemic rats treated with O-exo, as compared with the vehicle group (Figure 5D). In contrast, ischemia-mediated loss of synapses in aged rats was significantly attenuated after intravenous injection of Y-exo 72 h after stroke (Figure 5D). These data indicate that O-exo significantly amplified the phagocytic activity of microglia in the penumbra after ischemic stroke.

After ischemic stroke, activated microglia polarize to the classic pro-inflammatory type (M1) or alternative protective type (M2). M1 microglia secrete pro-inflammatory cytokines and exacerbate ischemic injury, whereas the M2 microglia promotes anti-inflammatory responses. Therefore, the beneficial or detrimental effects of activated microglia on neurons may be accounted for by their polarization state and functional responses after stroke. To examine the polarization of activated microglia in the ischemic brain after serum exosome treatment, immunofluorescence staining was performed using antibodies against M1-associated (CD86) and M2-associated (CD206) proteins. Both $Iba1^{+}CD86^{+}$ microglia (M1) and $Iba1^{+}CD206^{+}$ microglia (M2) were observed in the penumbra after stroke (Figure 5E and G). Quantitative analysis showed that $Iba1^{+}CD86^{+}$ microglia were significantly increased but $Iba1^{+}CD206^{+}$ cells were reduced in the penumbral M1 regions in aged ischemic rats treated with O-exo as compared with vehicle (Figure 5F and H). In contrast, the number of M1 microglia was reduced and the number of M2 microglia was increased in the M1 regions in the aged ischemic rats 72 h after Y-exo treatment as compared with vehicle (Figure 5F and H). The data suggest that the Y-exo and O-exo influence the *polarization* of microglia to the M1 and M2 phenotypes in the ischemic brain.

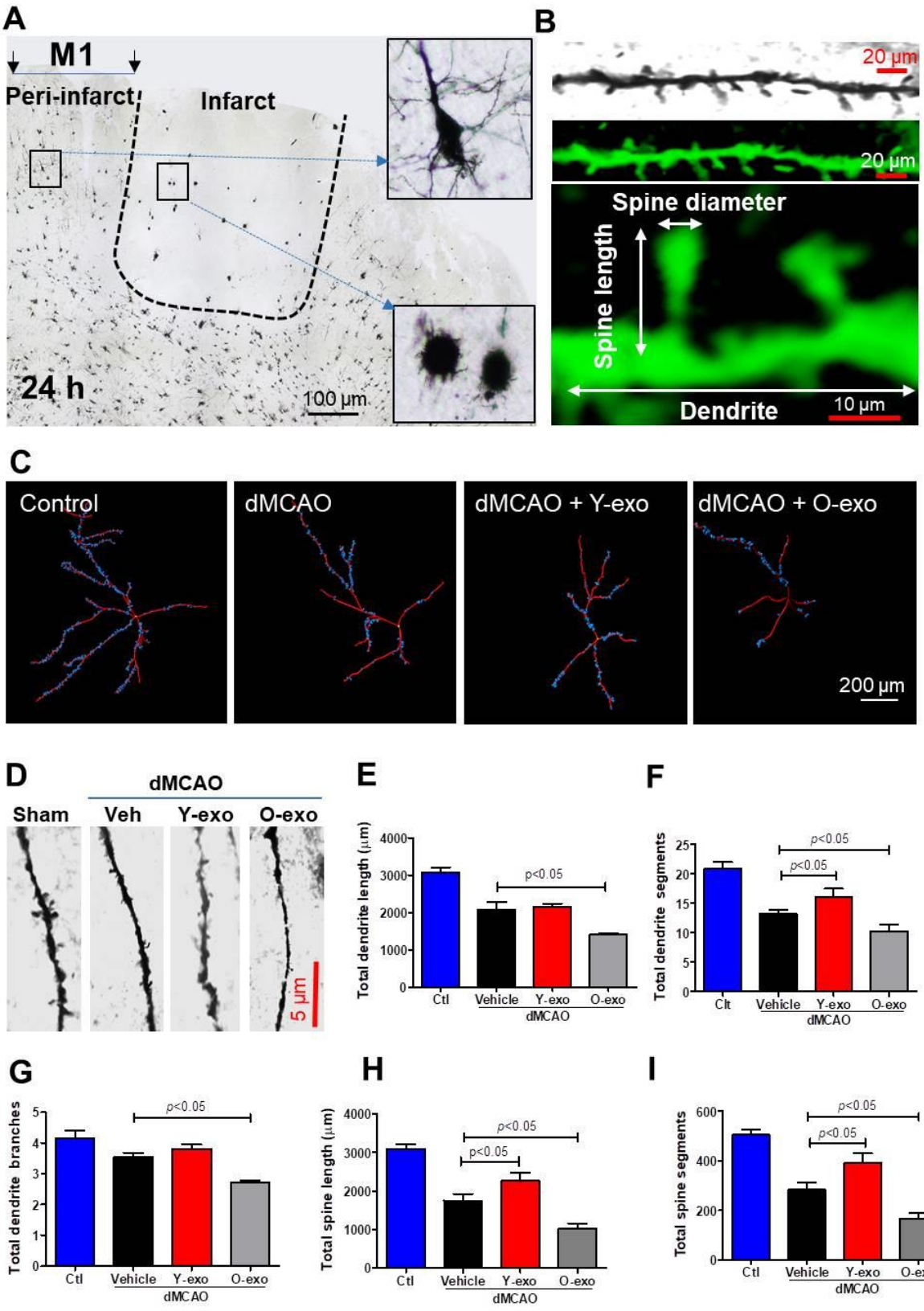
A
M1
Peri-infarct
Infarct
24 h
100 μm
B
20 μm
20 μm
Spine diameter
Spine length
Dendrite
10 μm
C
Control
dMCAO
dMCAO + Y-exo
dMCAO + O-exo
200 μm
D
dMCAO
Sham
Veh
Y-exo
O-exo
5 μm
E
Total dendrite length (μm)
p<0.05
Ctl
Vehicle
Y-exo
O-exo
dMCAO
F
Total dendrite segments
p<0.05
p<0.05
Clt
Vehicle
Y-exo
O-exo
dMCAO
G
Total dendrite branches
p<0.05
Ctl
Vehicle
Y-exo
O-exo
dMCAO
H
Total spine length (μm)
p<0.05
p<0.05
Ctl
Vehicle
Y-exo
O-exo
dMCAO
I
Total spine segments
p<0.05
p<0.05
Ctl
Vehicle
Y-exo
O-exo
dMCAO

Figure 6. Serum exosomes contribute to neuronal dendritic plasticity in the aged ischemic brain.

(A) Representative micrograph showing the pattern of Golgi-stained neurons from an aged ischemic brain. Insets show higher-magnification images of dendritic morphology of Golgi-Cox–stained cortical layer V pyramidal neuron**s** from the peri-infarct and infarct regions in the aged rat. **(B)** Confocal image of a pyramidal neuron dendrite covered with spine segments. Top panel: cropped and enlarged image of the Golgi-Cox–stained dendrite and spine segment. Middle panel: computer rendering of the dendritic segment with spines using Imaris software. Bottom panel: illustration of the structure of a neuronal dendrite and its spines. **(C)** A representative three-dimensional reconstruction of a Golgi-Cox–stained pyramidal neuron and the semi-automated trace generated by Filament Tracer in each group. **(D)** Representative high-magnification images of dendrite and spine segments of each group. **(E–I)** Quantitative analyses of the effects of vehicle or serum exosomes on (E) dendritic length, (F) number of dendritic segments, (G) number of dendritic branches, (H) total spine lenght and (I) number of spine segments acquired from layers II/III and V pyramidal neurons in the peri-infarct cortex and in the corresponding contralateral cortex (Ctl) and viewed at 60× magnification. The data are shown as the mean ± SEM. N = 3–5 rats per group. Y-exo, serum exosomes from young rats; O-exo, serum exosomes from aged rats.

3.5 The effect of serum exosomes on neuroplasticity is age dependent

Based on the findings that O-exo exacerbated but Y-exo attenuated microglial phagocytosis of the synapse as described above, we postulated that the effect of serum exosomes on synaptic plasticity in the ischemic brain is age dependent. The dendritic spines of neurons are the postsynaptic terminals that receive excitatory synaptic input and are implicated in mediating synaptic plasticity (157). Excitotoxicity is a key pathophysiologic mechanism of neuronal injury in the ischemic brain and associated with motor deficits. We therefore investigated the effects of Y-exo and O-exo on ischemia-induced structural alterations of neuronal dendrites and dendritic spines in aged ischemic brain using Golgi-Cox staining (Figure 6A).

The dendritic plasticity of cortical layers II/III and V pyramidal neurons was analyzed in the penumbral M1 region and the corresponding contralateral cortex in each group. We reconstructed the morphology of pyramidal neurons in three dimensions and analyzed dendritic spines and dendrites using Imaris software (Figure 6B and C). We found that total dendritic length and segments and total spine length and numbers in cortical layers II/III and V pyramidal neurons were significantly reduced with age. We further confirmed that focal ischemia significantly decreased the total process length and dendritic spine segments of neurons that survived. The level of spine density also dropped in the penumbral M1 region 72 h after focal ischemia as compared with the corresponding contralateral cortex.

Ischemic stroke–induced loss of primary dendritic spines in the cortical penumbra was exacerbated after intravenous injection of O-exo as compared with vehicle. Conversely, Y-exo treatment ameliorated the destructive effects of focal ischemia on dendritic spine damage (Figure

6D). Quantification showed that focal ischemia−induced loss of neurons in terms of the length, numbers and branches of dendrites and spines was exacerbated after O-exo treatment in the aged ischemic brain, an effect that was, however, reversed after Y-exo treatment (Figure 6E−I).

3.6 Microglial depletion reverses O-exo-mediated impairments in dendritic plasticity and motor function after stroke

To further investigate whether O-exo amplified microglial phagocytosis of synapses, leading to worsened dendritic plasticity, we first depleted the microglia in the brain using PLX3397, a small-molecule CSF-1R inhibitor. Microglia are the only type of immune cells in the CNS that express CSF-1 under physiological conditions (158), and the development and survival of microglia critically depend on CSF-1R signaling(159, 160). Administration of CSF-1R inhibitor can thus effectively wipe out microglia without harmful effects on animals(159, 161). The aged rats were provided with PLX3397-containing chow or standard chow for 28 days. The efficacy of microglial elimination by PLX3397 was determined based on immunofluorescence staining using anti-Iba1 (Figure 7A). The number of $Iba1^+$ cells in the cortex and striatum was significantly reduced in the aged rats fed the PLX3397 chow as compared with those on a standard diet (Figure 7B). These rats continued to receive PLX3397 or standard chow diet after focal ischemia until the end of experiments to avoid the subsequent repopulation of microglia in the brain.

Next, we determined microglial *phagocytosis* in these microglia-depleted aged ischemic brains 72 h after O-exo treatment. We found that after depletion of microglia, the fluorescent signal corresponding to Homer1 expression in the lysosome of $Iba1^+CD68^+$ cells were significantly

reduced in aged ischemic rats (Figure 7C). Quantitative analysis showed that the number of $Iba1^{+}CD68^{+}$ cells in the peri-infarct M1 region was significantly reduced compared with vehicle (Figure 7D), which is consistent with the reduction of $triple^{+}$ puncta in each cell (Figure 7D). We also analyzed dendrites and dendritic spines using the Imaris software after microglial depletion. Aged ischemic rats with microglial depletion that were treated with O-exo showed significant increases in total dendritic length, branches and segments (Figure 7E) and total spine segments and length (Figure 7F), as compared with those treated with O-exo alone. These data indicate that the effect of O-exo on dendritic plasticity resulted from amplified microglial phagocytosis in the ischemic brain.

We then examined the effect of O-exo treatment on functional outcomes in aged ischemic rats fed a PLX3397-containing diet or a standard diet. The infarct area was attenuated in aged rats treated with O-exo + PLX3397 as compared with the group treated with O-exo only (Figure 7G). As expected, the infarct volume was similarly affected, along with improvement in motor deficits (Figure 7H). Taken together, our results suggest that O-exo reduced neuroplasticity and ischemic outcome by amplifying microglial phagocytosis.

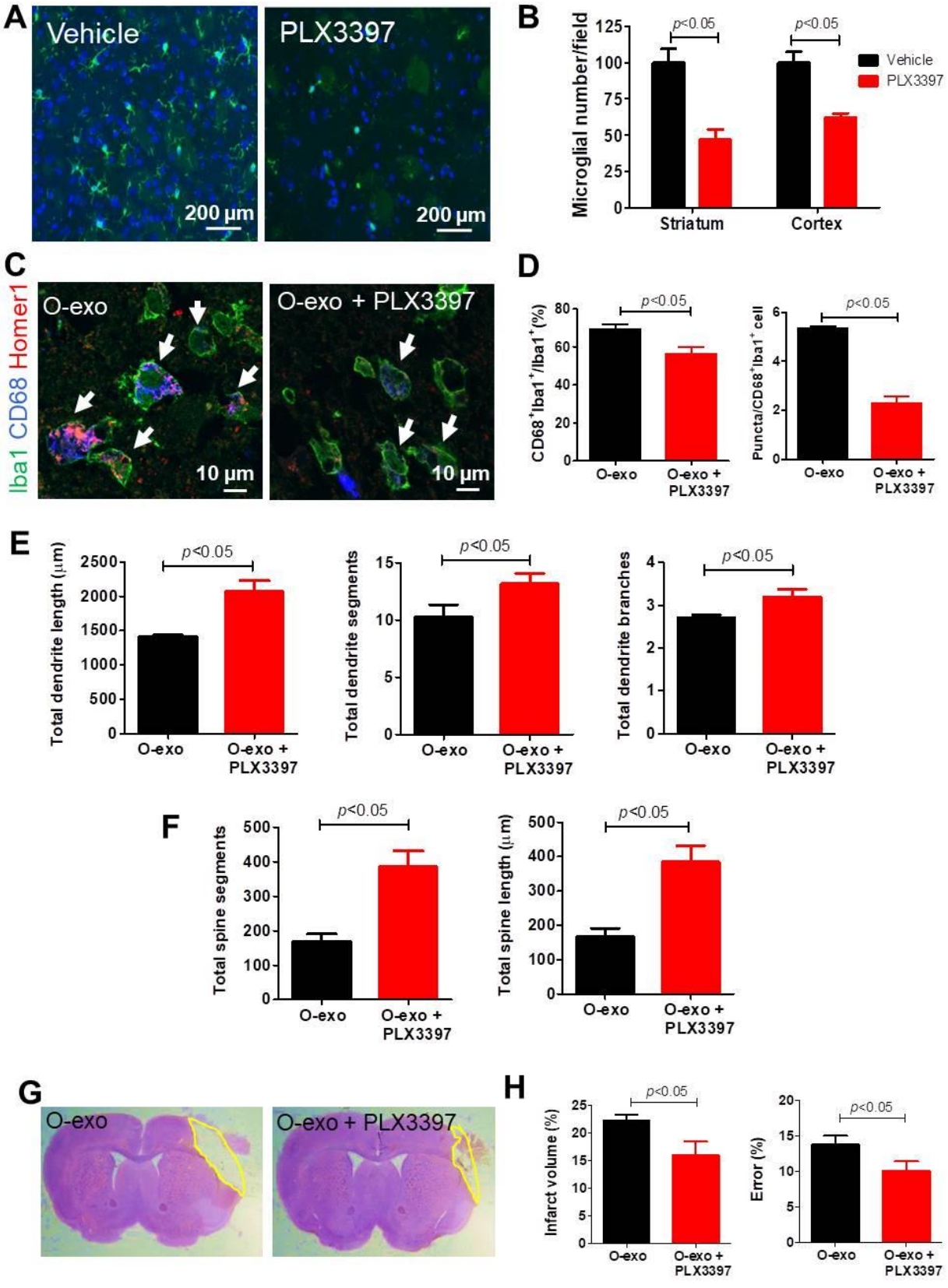
A
Vehicle
PLX3397
200 μm
200 μm
B
Microglial number/field
p<0.05
p<0.05
Vehicle
PLX3397
Striatum
Cortex
C
Iba1 CD68 Homer1
O-exo
O-exo + PLX3397
10 μm
10 μm
D
CD68+Iba1+/Iba1+(%)
Puncta/CD68+Iba1+ cell
p<0.05
O-exo
O-exo + PLX3397
E
Total dendrite length (μm)
Total dendrite segments
Total dendrite branches
p<0.05
O-exo
O-exo + PLX3397
F
Total spine segments
Total spine length (μm)
p<0.05
O-exo
O-exo + PLX3397
G
O-exo
O-exo + PLX3397
H
Infarct volume (%)
Error (%)
p<0.05
O-exo
O-exo + PLX3397

Figure 7. Microglial depletion reverses O-exo–mediated detrimental impairments in dendritic plasticity and motor function.

(A) Representative images of brain sections from aged rats immunostained for Iba1 (green) after being fed a PLX3397-containing or standard diet OR PLX3397 or vehicle treatment for 28 days. DAPI was used as a nuclear counterstain (blue). **(B)** Quantitative analysis of $Iba1^+$ cells in the striatum and cortex of sham-operated aged rats treated with PLX3397 or vehicle. **(C)** Representative confocal images of cells in the peri-infarct M1 region immunostained for Iba1 (green), CD68 (blue) and Homer1 (red) after treatment with O-exo alone or O-exo + PLX3397 for 3 days. White arrows indicate $Iba1^+CD68^+$ $Homer1^+$ microglia. **(D)** Quantitative analysis of $Iba1^+CD68^+$ cells (left graph) and the number of puncta in each microglia (right graph) in the penumbra of aged rats treated with O-exo with and without microglial depletion. **(E, F)** Quantitative analyses of the effects of O-exo on **(E)** total dendritic length, branches and segments and **(F)** total spine segments and length in aged ischemic rats fed a PLX3397-containing diet or a standard diet. **(G) Representative images of** *Cresyl violet–stained* brain sections from aged ischemic rats treated with O-exo alone or O-exo + PLX3397 for 3 days. **(H)** Quantification of infarct volume (left graph) and ladder rung walking test (right graph) in aged ischemic rats fed a PLX3397-containing or standard diet at 3 days after treatment with O-exo. The data are shown as the mean ± SEM. N = 7–12 rats per group. O-exo, serum exosomes from aged rats.

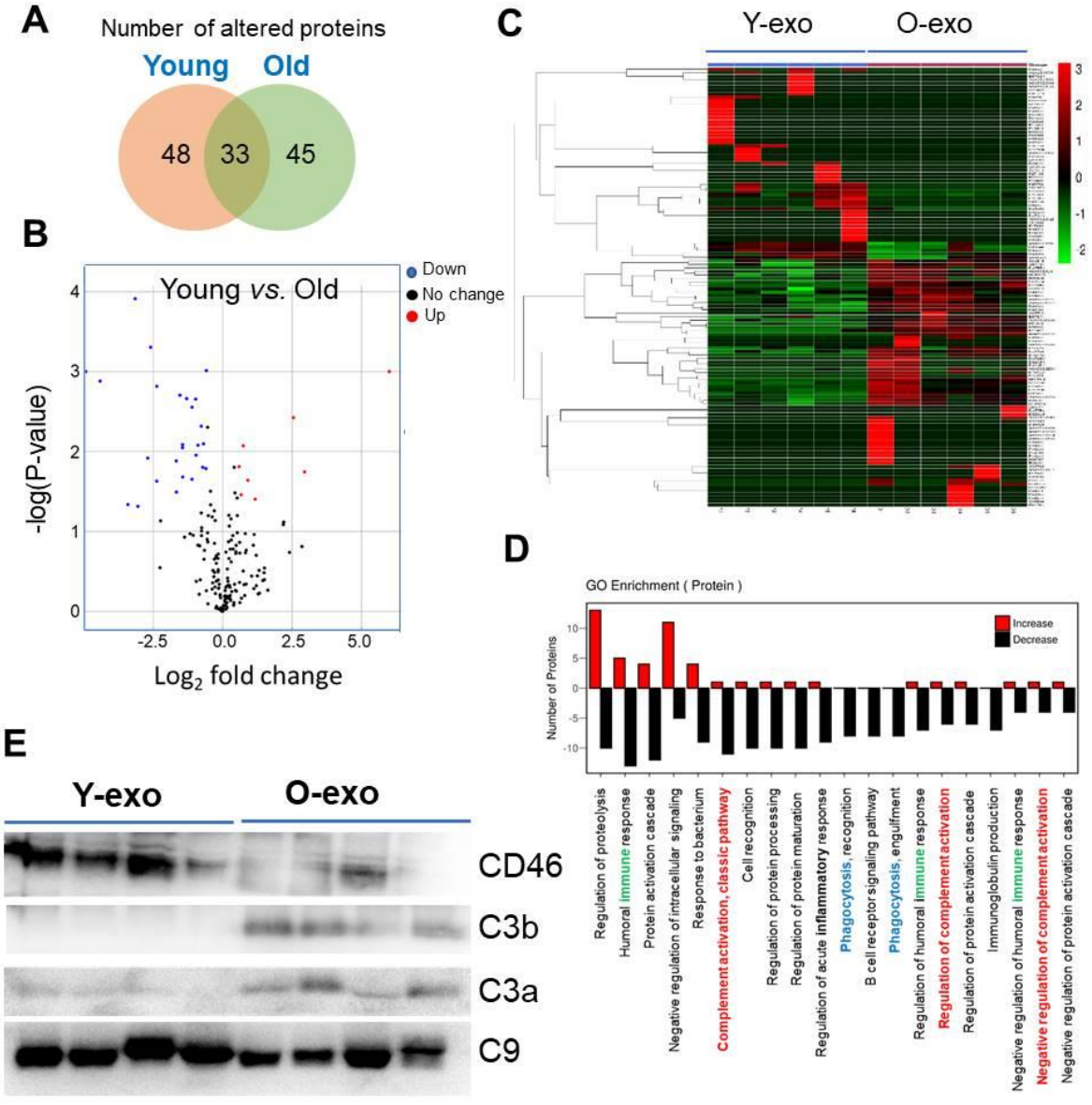
A
Number of altered proteins
Young
Old
48
33
45
B
Young vs. Old
Down
No change
Up
-log(P-value)
Log2 fold change
C
Y-exo
O-exo
D
GO Enrichment (Protein)
Increase
Decrease
Number of Proteins
Regulation of proteolysis
Humoral immune response
Protein activation cascade
Negative regulation of intracellular signaling
Response to bacterium
Complement activation, classic pathway
Cell recognition
Regulation of protein processing
Regulation of protein maturation
Regulation of acute inflammatory response
Phagocytosis, recognition
B cell receptor signaling pathway
Phagocytosis, engulfment
Regulation of humoral immune response
Regulation of complement activation
Regulation of protein activation cascade
Immunoglobulin production
Negative regulation of humoral immune response
Negative regulation of complement activation
Negative regulation of protein activation cascade
E
Y-exo
O-exo
CD46
C3b
C3a
C9
F
CD46
C3b
C3a
p<0.05
Relative intensity
Y-exo
O-exo

Figure 8. Proteomic profiles of Y-exo and O-exo.

(**A**) Venn diagram depicts the overlap of the altered serum exosome proteins between young and old rats as determined by proteomics. A total of 277 proteins were identified, of which 55 (19.86%) and 71 (25.63%) proteins were increased in Y-exo and O-exo, respectively. **(B)** Volcano plot displaying the distribution of identified serum exosome protein changes with age and significance. **(C)** Heatmap representation of significantly changed proteins. Fold change values > 1.5 and a P-value <0.05 were set as the filter criteria. **(D)** GO enrichment analysis for biological processes of up-regulated (red) and down-regulated (black) proteins in Y-exo was performed. Immune, complement cascade and phagocytosis in the GO categories are indicated by green, red and blue respectively. **(E)** Western blot analysis of selected proteins from Y-exo and O-exo. Data represent the mean ± SEM (N = 6). C9 was used to protein loading control. **(F)** Relative quantification of selected proteins detected by western blotting. Data represent the mean ± SEM (N = 6 biological replicates for the Y-exo and O-exo groups) using unpaired two-tailed Student's t-test. Each experiment was repeated three times with similar results. The data are shown as the mean ± SEM. N = 3–6 rats per group. Y-exo, serum exosomes from young rats; O-exo, serum exosomes from aged rats.

3.7 Proteomic analysis reveals different profiles of complement signaling in Y-exo and O-exo

To further determine the underlying molecular mechanism behind the deteriorating effects of O-exo on ischemic stroke, we analyzed the protein profiles of Y-exo and O-exo using proteomics. Proteins were considered significantly changed between Y-exo and O-exo using the parameters $p < 0.05$, fold change ≥ 1.5 and with at least two unique peptides. Among the 277 proteins identified, 126 were significantly changed between Y-exo and O-exo: 71 were up-regulated and 55 were down-regulated with age. Among these, 48 (38.1%) and 45 (35.7%) proteins were expressed only in Y-exo and O-exo, respectively (Figure 8A). A volcano plot shows these differentially expressed proteins according to their fold changes and *p*-values (Figure 8B). A biological heat map of clusters from the two groups was constructed using normalized data to provide an overview of the distribution of the expressed exosome proteins. After unsupervised hierarchical clustering, the heat map illustrated an overall reproducibility as well as individual heterogeneity of protein expression profiles among different subjects within the Y-exo and O-exo (Figure 8C). The complement proteins were 10-folds higher in O-exo compared with that in Y-exo. The identified differential proteins *C4b-binding protein* (C4BP) α chain and β chain, CD59, plasma protease C1 inhibitor, complement C1q, complement factor I, complement factor H, and complement C3.

Next, we performed gene ontology (GO) enrichment analysis of the identified differentially expressed proteins to gain insight into the molecular functions and biological processes that might implicate ischemic outcome after serum exosome treatment. We found that differentially expressed proteins in Y-exo and O-exo were significantly enriched with GO categories linked to

protein processing regulation, humoral immune response, protein activation cascade, intracellular signal transduction, complement activation, cell recognition, protein processing and maturation regulation, acute inflammatory response regulation and phagocytic recognition and engulfment (Figure 8D).

We then verified the differential abundance of three selected complement proteins (CD46, C3a and C3b) using Western blotting (Figure 8E). Consistent with the trend found with the proteomics analysis, the western blot results showed similar alterations in an independent set of samples. The levels of CD46 proteins were significantly higher in Y-exo as compared with O-exo. Conversely, the relative intensities of C3a and C3b were higher in O-exo *vs.* Y-exo (Figure 8F). The level of C3b, but not C1q and CD11b, was increased in the ischemic brain after injection of O-exo. While C1q and CD11b, but not C3b, were decreased in the ischemic brain 3 days after administration of Y-exo (Figure 9). Correspondingly, the levels of CD68 and CD86 proteins were increased but CD46 and CD206 were reduced in the ischemic brain of aged rats 3 days after injection of O-exo. The levels of CD68 and CD86 were reduced in the ischemic brain of aged rats injected with Y-exo (Figure 10). Thus, the data suggest that higher levels of activated complement in O-exo may prime the microglial response after ischemic stroke, which results in an exacerbation of ischemic stroke effects in aged rats after treatment with O-exo.

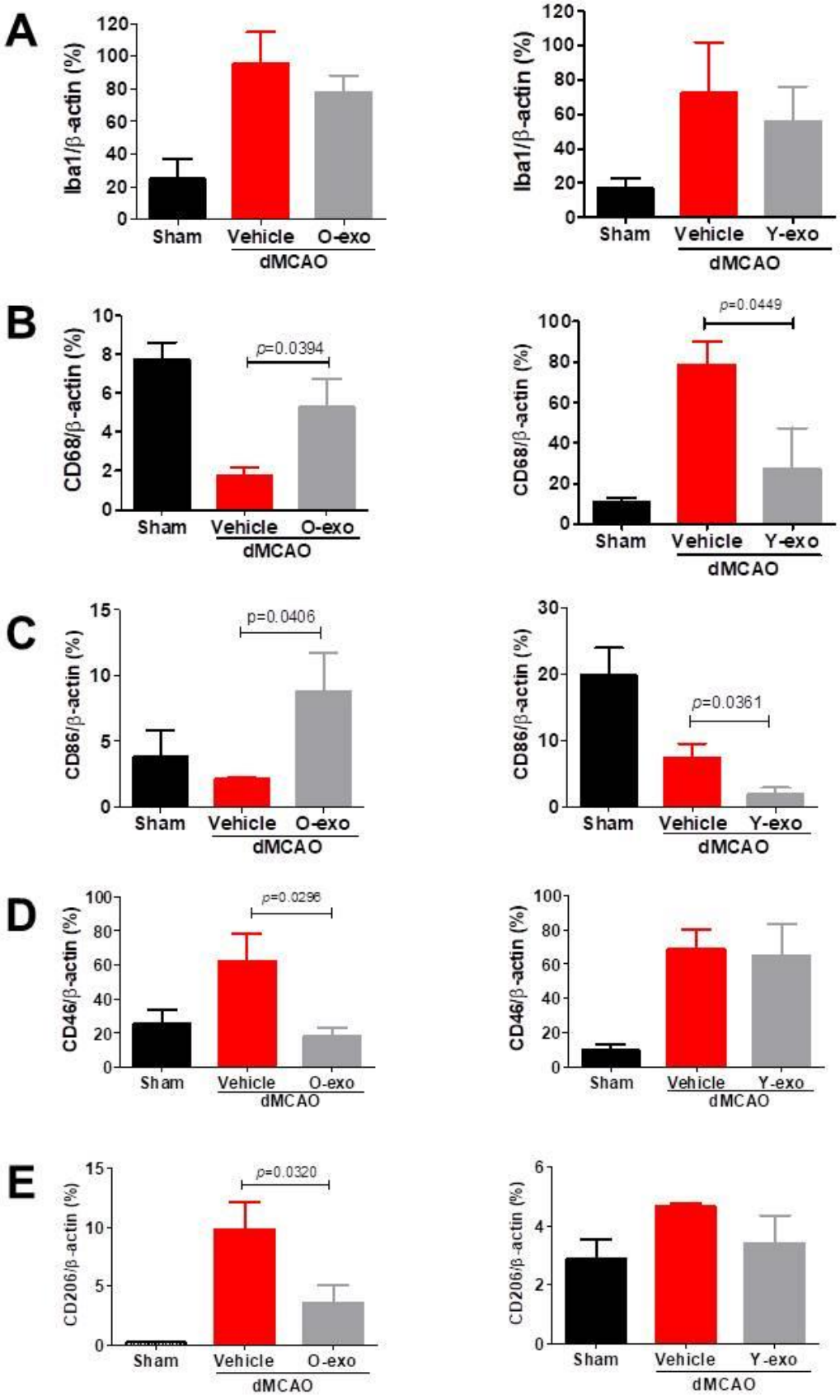
A
Iba1/β-actin (%)
120
100
80
60
40
20
0
Sham
Vehicle
O-exo
dMCAO
Iba1/β-actin (%)
120
100
80
60
40
20
0
Sham
Vehicle
Y-exo
dMCAO
B
CD68/β-actin (%)
10
8
6
4
2
0
p=0.0394
Sham
Vehicle
O-exo
dMCAO
CD68/β-actin (%)
100
80
60
40
20
0
p=0.0449
Sham
Vehicle
Y-exo
dMCAO
C
CD86/β-actin (%)
15
10
5
0
p=0.0406
Sham
Vehicle
O-exo
dMCAO
CD86/β-actin (%)
30
20
10
0
p=0.0361
Sham
Vehicle
Y-exo
dMCAO
D
CD46/β-actin (%)
100
80
60
40
20
0
p=0.0296
Sham
Vehicle
O-exo
dMCAO
CD46/β-actin (%)
100
80
60
40
20
0
Sham
Vehicle
Y-exo
dMCAO
E
CD206/β-actin (%)
15
10
5
0
p=0.0320
Sham
Vehicle
O-exo
dMCAO
CD206/β-actin (%)
6
4
2
0
Sham
Vehicle
Y-exo
dMCAO

Figure 9. Levels of complement protein (C1q and C3b) and C3 receptor (CD11b) in the normal cortex or ipsilateral cortex of ischemic brain after injection of Y-exo and O-exo.

(A-C) Vehicle, Y-exo or O-exo were intravenously injected into aged ischemic or sham-operated rats and protein was isolated from normal cortex (sham-operated aged rats) or ipsilateral cortex (aged ischemic rats) 3 days after ischemic stroke. Western blots were performed using antibodies as indicated. β-actin was used to protein loading control. Relative densities of C1q **(A)**, C3b **(B)** and CD11b **(C)** were determined. Data represent the mean ± SEM (N = 4–6 per group). Y-exo, serum exosomes from young rats; O-exo, serum exosomes from aged rats.

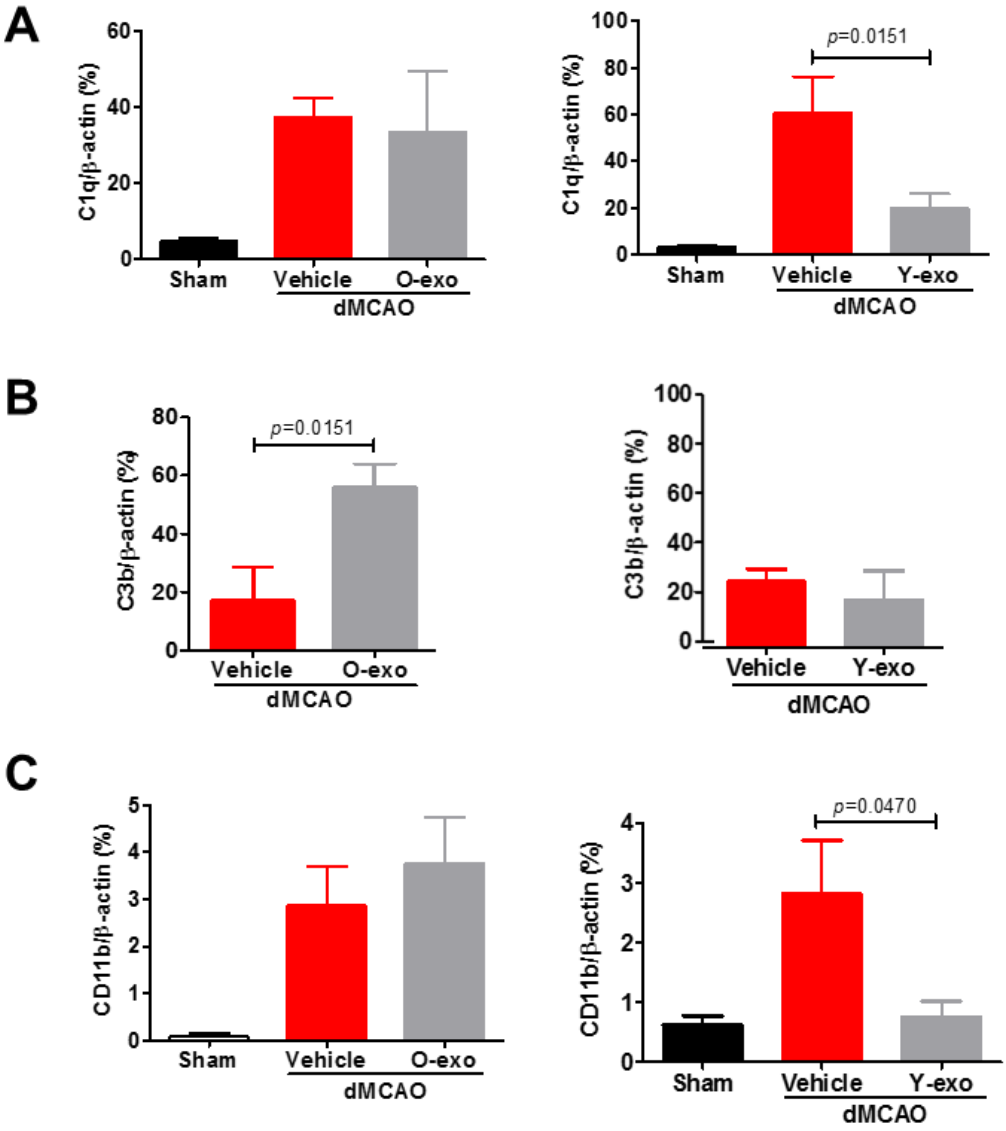
A
C1q/β-actin (%)
60
40
20
0
Sham
Vehicle
O-exo
dMCAO
C1q/β-actin (%)
100
80
60
40
20
0
p=0.0151
Sham
Vehicle
Y-exo
dMCAO
B
C3b/β-actin (%)
80
60
40
20
0
p=0.0151
Vehicle
O-exo
dMCAO
C3b/β-actin (%)
100
80
60
40
20
0
Vehicle
Y-exo
dMCAO
C
CD11b/β-actin (%)
5
4
3
2
1
0
Sham
Vehicle
O-exo
dMCAO
CD11b/β-actin (%)
4
3
2
1
0
p=0.0470
Sham
Vehicle
Y-exo
dMCAO

Figure 10. Expression levels of microglial protein in the normal cortex or ipsilateral cortex of ischemic brain after injection of Y-exo and O-exo.

(A-E) Vehicle, Y-exo or O-exo were intravenously injected into aged ischemic or sham-operated rats and protein was isolated from normal cortex (sham-operated aged rats) or ipsilateral cortex (aged ischemic rats) 3 days after ischemic stroke. Western blots were performed using antibodies against microglial protein markers. β-actin was used to protein loading control. Relative densities of Iba1 **(A)**, CD68 **(B)**, CD86 **(C)**, CD46 **(D)** and CD206 **(E)** were determined. Data represent the mean ± SEM (N = 4–-6 per group). Y-exo, serum exosomes from young rats; O-exo, serum exosomes from aged rats.

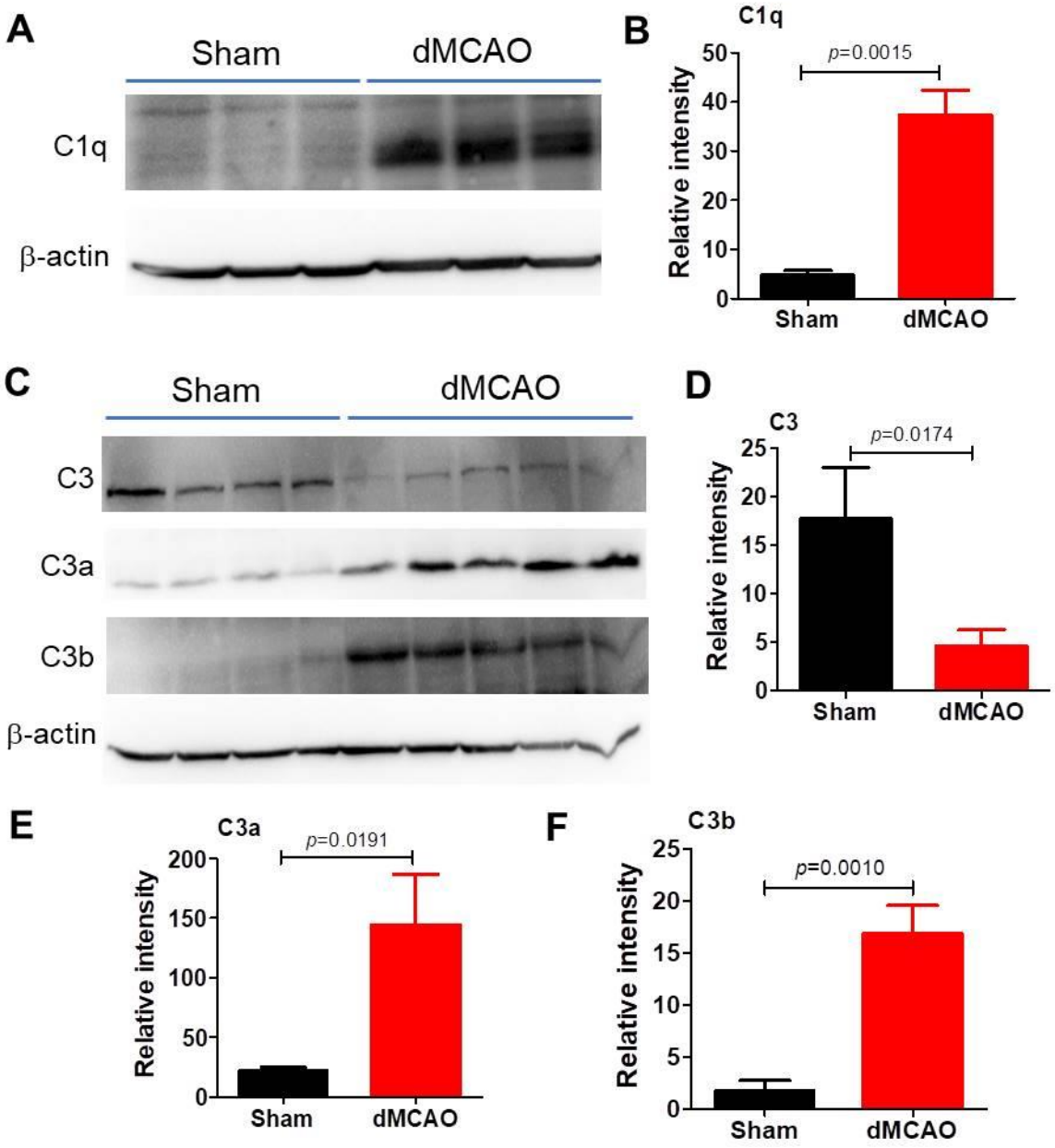
A
Sham
dMCAO
C1q
β-actin
B
C1q
p=0.0015
Relative intensity
50
40
30
20
10
0
Sham
dMCAO
C
Sham
dMCAO
C3
C3a
C3b
β-actin
D
C3
p=0.0174
Relative intensity
25
20
15
10
5
0
Sham
dMCAO
E
C3a
p=0.0191
Relative intensity
200
150
100
50
0
Sham
dMCAO
F
C3b
p=0.0010
Relative intensity
25
20
15
10
5
0
Sham
dMCAO
G
NeuN/C3/DAPI
10 μm
C3/PLP
10 μm
Iba1/C3aR/DAPI
10 μm

Figure 11. Focal ischemic stroke activates complement cascade in the brain.

(A) Western blots show that C1q is increased in the ipsilateral cortex after focal ischemia. β-actin was used as a protein loading control. **(B)** Relative density of C1q protein in sham-operated and ipsilateral cortex after ischemic stroke. **(C)** Western blots show the expression levels of C3, C3a and C3b in sham-operated and ischemic cortex. β-actin was used as a protein loading control. **(D–F)** Relative density of **(D)** C3, **(E)** C3a and **(F)** C3b proteins in sham-operated and ipsilateral cortex after ischemic stroke. **(G)** Double immunostaining shows that C3 is expressed in $NeuN^+$ cells and in PLP^+ myelin, and C3aR is expressed in $Iba1^+$ microglia. DAPI was used as a nuclear counterstain. Data represent the mean ± SEM (N = 6–9 per group).

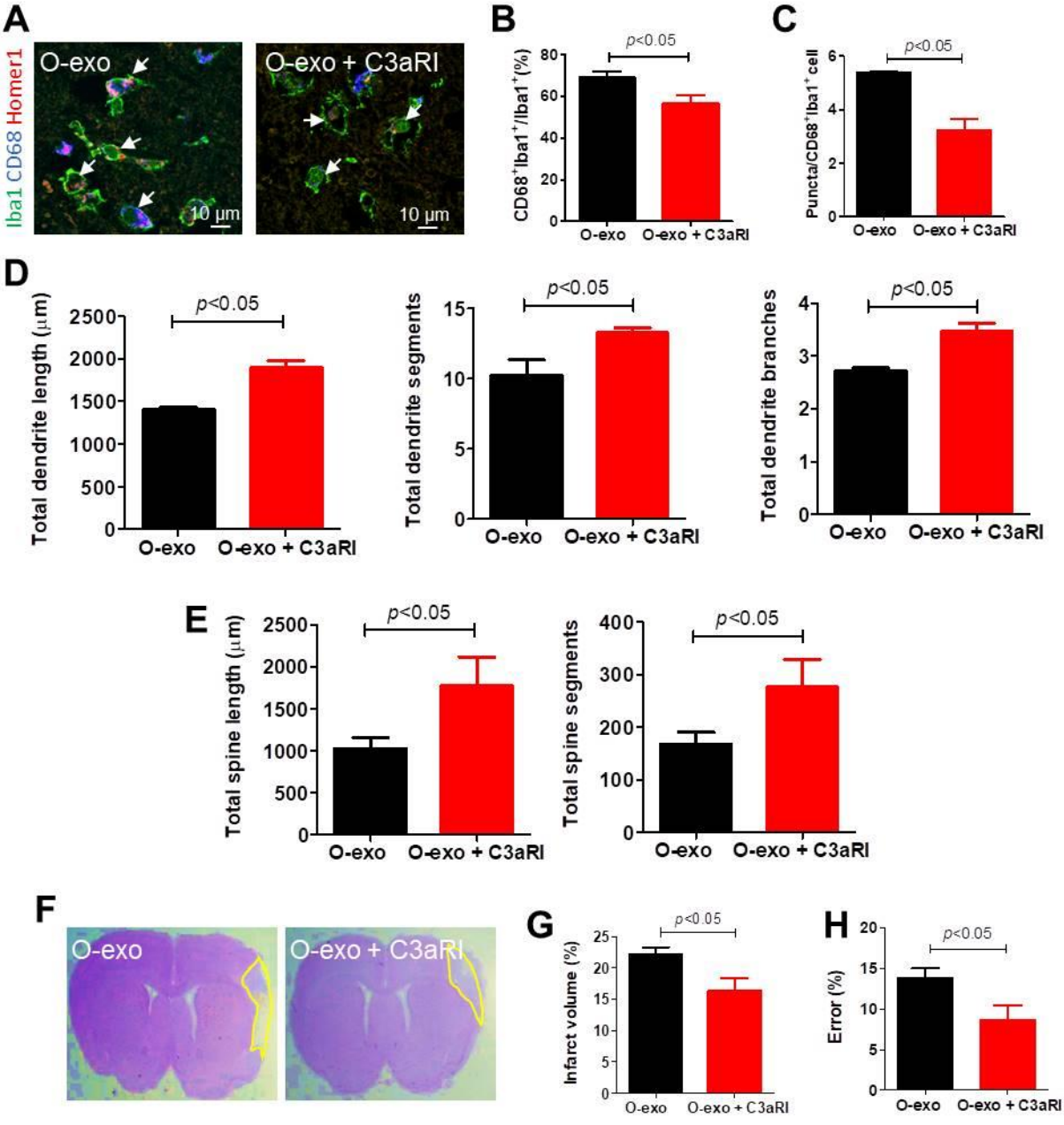
A
Iba1 CD68 Homer1
O-exo
O-exo + C3aRI
10 μm
10 μm
B
CD68+Iba1+/Iba1+(%)
p<0.05
O-exo
O-exo + C3aRI
C
Puncta/CD68+Iba1+ cell
p<0.05
O-exo
O-exo + C3aRI
D
Total dendrite length (μm)
p<0.05
O-exo
O-exo + C3aRI
Total dendrite segments
p<0.05
O-exo
O-exo + C3aRI
Total dendrite branches
p<0.05
O-exo
O-exo + C3aRI
E
Total spine length (μm)
p<0.05
O-exo
O-exo + C3aRI
Total spine segments
p<0.05
O-exo
O-exo + C3aRI
F
O-exo
O-exo + C3aRI
G
Infarct volume (%)
p<0.05
O-exo
O-exo + C3aRI
H
Error (%)
p<0.05
O-exo
O-exo + C3aRI

Figure 12. Inhibiting C3aR activity ameliorates O-exo–mediated detrimental effects in the aged ischemic brain.

(A) Confocal images showing Iba1 (green), CD68 (blue) and Homer1 (red) expression in the penumbra in aged ischemic rats treated with O-exo or a combination of O-exo and C3aR inhibitor (C3aRI). White arrows indicate $Iba1^{+}CD68^{+}$ $Homer1^{+}$ microglia. **(B)** Quantification of colocalized activated microglia using the marker CD68 with Iba1 in aged ischemic rats 3 days after injection of O-exo with and without C3aR inhibitor. **(C)** Quantification of $triple^{+}$ puncta per $Iba1^{+}$ cells in the aged ischemic brain after injection of O-exo with and without C3aR inhibitor. **(D, E)** Quantitative analyses of **(D)** total dendritic length, segments and branches and **(E)** total spine length and segments in the penumbra in aged ischemic rats 3 days after injection of O-exo with and without C3aR inhibition. (**F**) Representative CV-stained images showing infarct area in animals treated with O-exo with and without C3aR inhibitor. (**G**) Infarct volume in aged ischemic rats treated with O-exo with and without C3aR inhibitor. (**H**) Motor deficit was determined by the ladder rung walking test in aged ischemic rats treated with O-exo with and without C3aR inhibitor. Data represent the mean ± SEM. N = 7–12 rats per group. O-exo, serum exosomes from aged rats.

3.8 C3a receptor blockage reverses O-exo–mediated hyperactivation of microglial phagocytosis and deleterious stroke outcome

The complement pathway is activated after ischemic stroke and is implicated in promoting post-stroke pathology and leading to a worse outcome. We confirmed that C1q, C3a and C3b were increased in the ischemic brain by western blotting as compared with the sham-operated group (Figure 11A–F). To investigate the cellular localization of C3 and C3aR, double immunofluorescence staining was also performed on brain tissue obtained 72 h after ischemia. C3 protein was expressed on $NeuN^+$ and PLP^+ cells in the penumbra. $Iba1^+C3aR^+$ cells were also evident in the penumbra, confirming that microglia were the primary cell types for C3aR expression in the ischemic brain (Figure 11G).

As complement C3 acts on microglial C3aR to influence microglial phagocytosis of the synapse, we next sought to determine the functional effects of C3aR inhibitor (C3aRI; SB290157) on aged ischemic rats treated with O-exo. We found that the number of $CD68^+Iba1^+$ cells in the penumbra was reduced in aged ischemic rats treated with a combination of O-exo and C3aRI as compared with the group treated with O-exo only (Figure 12A and B). Consistently, the $Iba1^+CD68^+Homer1^+$ cells in the penumbra were also reduced in aged ischemic rats 72 h after O-exo + C3aRI treatment (Figure 12C), suggesting that phagocytic microglia were reduced after inhibiting C3aR activity.

Next, we quantified dendritic and synaptic numbers in the penumbra of aged ischemic rats. We found that total dendritic length, total dendritic branches and total dendritic segments within the

penumbra of the ipsilateral cortex were significantly increased at 72 h in aged ischemic rats treated with O-exo + C3aRI as compared with the group treated with O-exo only (Figure 12D). Similarly, the total spine length and total number of spine segments were also increased in the peri-infarct cortex in O-exo + C3aRI-treated rats 72 h after focal ischemia as compared with the group treated with O-exo only (Figure 12E). The data suggest that inhibiting C3aR activity attenuates synaptic loss after old serum exosome treatment.

We then investigated the role of inhibiting C3aR activity in functional outcomes in aged ischemic rats after injection of O-exo. Analysis of serial CV-stained coronal sections 72 h after ischemic stroke revealed a significantly decreased volume of subcortical infarction in aged rats treated with O-exo + C3aRI as compared with the group treated with O-exo only (Figure 12F and G). These findings indicate that C3aR inhibitor administration ameliorates O-exo–mediated brain damage. Post-stroke sensorimotor dysfunction was also evaluated using the ladder rung walking test. We found that motor deficits were significantly improved in aged ischemic rats treated with O-exo in combination with C3aRI, as compared with the group treated with O-exo only (Figure 12H). Taken together, these data suggest that pharmacologic inhibition of C3aR effectively protects against these deleterious outcomes of intravenous administration of O-exo after ischemic stroke in a complement-dependent process.

4. Conclusion

In summary, we have shown that pro-inflammatory mediators accumulate in blood exosomes with age, which prime microglia, making them prone to overreactions that exacerbate *synaptic loss* and motor deficits after ischemic stroke via microglial C3a receptors. While CD46 is increased in Y-exo, which could attenuate ischemic outcomes through blocking complement-microglia axis. Taken together, peripheral systemic inflammation can directly crosstalk with neuroinflammatory cells to influence stroke outcome in aged animals. Therefore, modulation of complement-dependent activation of microglial signaling may provide a therapeutic strategy for ischemic stroke.

CHAPTER 2

Peripheral Circulating Exosomal miRNAs Potentially Contribute to the Regulation of Molecular Signaling Networks in Aging

Abstract: People are living longer than ever. Consequently, they have a greater chance for developing a functional impairment or aging-related disease, such as a neurodegenerative disease, later in life. Thus, it is important to identify and understand mechanisms underlying aging as well as the potential for rejuvenation. Therefore, we used next-generation sequencing to identify differentially expressed microRNAs (miRNAs) in serum exosomes isolated from young (three-month-old) and old (22-month-old) rats and then used bioinformatics to explore candidate genes and aging-related pathways. We identified 2844 mRNAs and 68 miRNAs that were differentially expressed with age. TargetScan revealed that 19 of these miRNAs are predicated to target the 766 mRNAs. Pathways analysis revealed signaling components targeted by these miRNAs: mTOR, AMPK, eNOS, IGF, PTEN, p53, integrins, and growth hormone. In addition, the most frequently predicted target genes regulated by these miRNAs were EIF4EBP1, insulin receptor, PDK1, PTEN, paxillin, and IGF-1 receptor. These signaling pathways and target genes may play critical roles in regulating aging and lifespan, thereby validating our analysis. Understanding the causes of aging and the underlying mechanisms may lead to interventions that could reverse certain aging processes and slow development of aging-related diseases.

1. Introduction

Aging is a highly complex biological process that is often accompanied by a general decline in tissue function and an increased risk for aging-related diseases, such as cardiovascular disease, stroke, cancer, and neurodegenerative diseases. Indeed, as average lifespan continues to increase, aging-related functional decline, such as cognitive impairment, will likely become a health care priority (123). For example, the most common form of dementia is Alzheimer's disease (AD), but a large proportion of cognitive impairment cases in the aged population is not due to AD but rather to normal aging process. Thus, it is important to identify ways to maintain functional integrity during aging (162). Many theories have been proposed to explain why we age (163). Recently, we proposed a new theory positing that aging is the process of continuous impairment of microcirculation in the body (164). Indeed, compelling evidence indicates that systemic factors in the blood profoundly reverse aging-related impairments (23, 32, 124), which are influenced by specific rejuvenating or deteriorating factors, e.g., proteins, microRNAs (miRNAs), and mRNAs (165). Thus, many circulating factors have been identified as attractive biomarkers for tissue-specific diseases and aging (166, 167). However, the mechanisms underlying the contributions of blood-derived factors to aging remain unclear.

Research over the last two decades has demonstrated that cells mainly communicate by releasing extracellular vesicles (EV) that can act on nearby cells (paracrine signaling) or end up in circulating body fluids, with possible effects at distant sites (endocrine signaling) (168). Exosomes are small EVs (approximately 50–150 nm in diameter) of endosomal origin that

initially form as intraluminal vesicles inside late endosomal compartments. Indeed, exosomes contain many specific proteins, mRNAs, miRNAs, and long noncoding RNAs (125) and play a vital role in cell communication by transferring their cargo between source and target cells, which is also important in aging and aging-related disease (127). For example, injection of serum exosomes from young mice into old mice could alter the expression pattern of aging-associated molecules to mimic that of young mice (169). In addition, studies have documented that exosomes from brain cells can cross the blood-brain barrier (BBB) and serve as peripheral circulating biomarkers of cognitive impairment in AD (170-172), and blood exosomes can also cross the BBB to target brain cells and affect brain function (173-176). Thus, peripheral circulating exosomes have diagnostic and therapeutic potential. However, most studies have focused on establishing exosomal protein or miRNA profiles for comparing disease states and matched controls, and few studies have focused on characterizing proteins and miRNAs in peripheral circulating exosomes during normal aging (52). Therefore, it is critical to define the profiles for exosomal proteins and miRNAs that can be transferred from exosome to recipient cells. Importantly, it has been estimated that miRNAs regulate ~31% of all eukaryotic genes by promoting degradation of their mRNAs or inhibiting their translation (177, 178). Indeed, miRNA-mediated regulation governs metabolism, immunity, lifespan, cell proliferation, apoptosis, and development (179-181), as well as pathological processes such as cancer and cardiovascular and neurodegenerative disease (182-184). Therefore, among the exosomal cargo that is transferred to recipient cells, miRNAs likely have the greatest downstream impact on cell functions. To explore the role of circulating exosomes in aging processes, exosomal miRNAs must be more broadly characterized. In addition, recent evidence suggests that numerous signaling pathways regulate normal aging processes. However, research is lacking concerning

how aging affects co-expression profiles for exosomal miRNAs and mRNAs and how miRNA-mRNA regulatory networks systematically influence aging processes.

To address shortcomings in our knowledge of exosomal miRNA functions, we used next-generation sequencing to establish miRNA and mRNA profiles for circulating exosomes isolated from young and old rats. We also investigated the possible role of exosomal miRNAs in aging by analyzing the biological importance of the miRNA targets and in major signaling pathways associated with aging using bioinformatic tools including Gene Ontology (GO) enrichment, Kyoto Encyclopedia of Genes and Genomes (KEGG) enrichment and pathways, eukaryotic orthologous groups (KOG) function classification, and Ingenuity Pathway Analysis (IPA). Our findings may provide a basis for understanding the physiological consequences of aging-related changes in the makeup of circulating miRNAs and could lead to potential interventions for aging-related diseases.

2. Materials and Methods

2.1 Isolation of Serum Exosomes

Whole blood was collected from young (3-month-old) or old (22-month-old) rats (n = 6 per group) *via* cardiac puncture into BD Vacutainer® Plus Glass Serum blood collection tubes (Becton Dickinson, *NJ, USA).* Whole blood samples were allowed to clot by standing at room temperature for 30 min, and the clots were removed by centrifugation for 10 min at 1000× g at 4 °C. The isolated serum samples were aliquoted and stored at –80 °C.

Serum exosomes from young or old rats were isolated using the ExoQuick Exosome precipitation kit (System Biosciences, CA, USA). Briefly, serum (500 µL) was centrifuged at 3000× *g* for 15 min at 4 °C to eliminate cells and cell debris. The supernatant was transferred to a sterile micro-tube, and an appropriate volume of exosome precipitation solution from the kit was added, with incubation for 30 min at 4 °C. The mixture was then centrifuged at 1500× *g* for 30 min at 4 °C, and the exosome pellet was re-suspended in sterile phosphate-buffered saline at 4 °C.

2.2 Characterization of Serum Exosomes

Both the concentration and average size of the isolated serum exosomes were determined by nanoparticle-tracking analysis (NTA) using the Exosome Nanosight Analysis Service of System Biosciences (Palo Alto, CA, USA). The serum exosomes were also observed using transmission electron microscopy (TEM, *FEI Tecnai G2 Spirit BioTwin, OR, USA*) to determine morphology and the extent of dispersion, this analysis was performed at the Electron Microscopy Core Facility at the University of Texas Southwestern Medical Center, TX, USA. The enrichment of exosomes was determined by Western blotting using antibodies against exosomes components such as CD63 andCD9.

2.3 Western Blotting

Serum exosomes were lysed in RIPA buffer and the protein concentration was determined using the Quick Start Bradford protein assay (Pierce™ BCA Protein Assay kit, Thermo Fisher

Scientific, MA, USA). The lysates (10 µg) were electrophoresed through 8–12% SDS-PAGE gels, and the separated proteins were transferred to a nitrocellulose membrane. The membrane was incubated in blocking buffer (5% milk in Tris-buffered saline with 0.05% *w*/*v* Tween-20) for 1 h at room temperature and then incubated overnight at 4 °C with mouse antibody against rat CD63 (1:1000, BD Pharmingen, CA, USA) and CD9 (1:1000, BD Pharmingen). Immunopositivity was detected with a horseradish peroxidase (HRP)—conjugated secondary antibodies and the Pierce enhanced chemiluminescence (ECL) substrate (Thermo Fisher Scientific, MA, USA). The data were recorded and analyzed using the ChemiDoc Imaging System (Bio-Rad).

2.4 Isolation of Total RNA fromEexosomes and Next-Generation RNA Sequencing

Total RNA was isolated from serum exosomes using the SeraMir Exosome RNA Purification Column kit (System Biosciences, CA, USA). For each sample, 1 µL of the final RNA eluate was used for measurement of RNA concentration with the Agilent Bioanalyzer Small RNA Assay using the Bioanalyzer 2100 Expert instrument (Agilent Technologies, Santa Clara, CA, USA). Serum exosomal RNAs (N = 6 each group) were sent to the Exo-NGS™ (Exosomal RNA-Seq) services for next-generation RNA sequencing (System Biosciences, CA, USA) using small RNA libraries. Next-generation RNA sequencing was performed on an Illumina NextSeq instrument (Illumina, CA, USA) with 1 x 75 bp single-end reads at an approximate depth of 10–15 million reads per sample.

2.5 Data Processing

Raw data were analyzed using an integrated UCSC genome browser on the Banana Slug analytics platform (UCSC, CA, USA). Briefly, the exosome Small RNA-seq Analysis kit was initiated with a data quality check of each input sequence using FasQC (Wellcome Sanger Institute, UK) an open-source quality control tool for analyzing high-throughput sequence data. Following the quality-control step, the RNA-seq reads were processed to detect and remove unknown nucleotides at the ends of reads, trim sequencing adaptors, and filter reads for quality and length, using FastqMcf, which is part of the EA-utils package (ExpressionAnalysis, NC, USA) and PRINSEQ (http://prinseq.sourceforge.net/, USA). FastQC was then repeated to analyze the trimmed reads, thus allowing a before and after comparison. Sequence reads in the improved set were mapped to the reference genome using Bowtie, an ultrafast, memory-efficient short-read aligner. Expression analyses, including computation of read coverage and noncoding RNA abundance, were performed using the open-source software SAMtoolsand Picard (Github, CA, USA).

2.6 Bioinformatics Analysis

After data processing, expression statistics for the normalized reads were evaluated using analysis of variance to identify differentially expressed genes. Differentially expressed genes were selected if the fold changes (FC) in expression was > 1.5 with a *p*-value < 0.5. From the data set of miRNAs and mRNAs for which expression was significantly altered between serum exosomes isolated from young and old rats, the potential regulation of a mRNA by a particular

miRNA was predicted with TargetScan (http://www.targetscan.org/, MIT, MA, USA). The paired miRNAs and mRNAs were used for further analysis.

Hierarchical cluster analysis (HCA) is an algorithmic approach to identify groups with varying degrees of (dis)similarity in a data set represented by a (dis)similarity matrix. This analysis was carried out with the Pheatmap package (https://CRAN.R-project.org/package=pheatmap, Estonia). The volcano plot is a type of scatter-plot that can quickly identify changes in individual data in large data-sets composed of replicate data; ggplot2 package (http://ggplot2.org, New Zealand) was used for this purpose.

2.7 Gene Ontology (GO) and Pathway Enrichment Analysis

The biological function of each protein was annotated with Blastp (Blast2GO version 5, BioBam Bioinformatics, Spain) using the entire gene-expression database, and subsequent mapping was carried out with the GO database (www.geneontology.org/, Gene ontology resource, USA). To further understand the biological significance of differentially expressed exosome proteins, pathway analysis was carried out with the KEGG Orthology-Based Annotation System (http://kobas.cbi.pku.edu.cn, China). The association of proteins with different pathways was computed using the KEGG database (www.genome.jp/kegg, Japan). EuKaryotic Orthologous Groups (KOG) Analysis was based on the phylogenetic classification of proteins encoded in the complete genomes (www.ncbi.nlm.nih.gov/COG/, NCBI, MD, USA) project. IPA (QIAGEN, Germany) was used for additional functional annotation, including top canonical pathway, top

disease and function and molecular and cellular functions, prediction of upstream, regulator effectors, and miRNA–mRNA relationship and interaction network analysis.

2.8 Statistical Analysis

For the GO analysis, statistically significant alterations in functions of differentially expressed exosome proteins were assessed with Fisher's exact test in Blast2GO with an adjusted *p*-value (false discovery rate, FDR) of <0.05 and fold change > 1.5. The statistical significance of changes in pathways identified with IPA was assessed with the right-tailed Fisher's Exact test. A *p*-value of < 0.05 implies that the relationship of a set of targeted molecules and a process/pathway/transcription was randomly matched. A Z score of ≥ 2 or ≤ -2 indicated significant activation or significant inhibition, respectively. For all analysis, the difference was considered significant for $p < 0.05$.

3. Results

3.1 Characterization of Serum Exosomes

We first characterized the protein content of serum exosomes isolated from young and old rats using Western blotting. Serum exosomes from each of young and old rats were positive for the exosome markers, CD63 and CD9 (Figure 13A). Nanoparticle tracking analysis (NTA) (Figure 13B) verified a strong enrichment of particles in the range 40–120 nm, with mean size of 82 +/− 0.8 nm, supporting a multimodal size distribution of exosomes with a peak diameter of 70–120 nm, consistent with previous reports (148, 149). In addition, transmission electron microscopy

(TEM) was used to confirm that the purified particles were membrane bound, round and heterogeneous in size (40–120 nm) (Figure 13C).

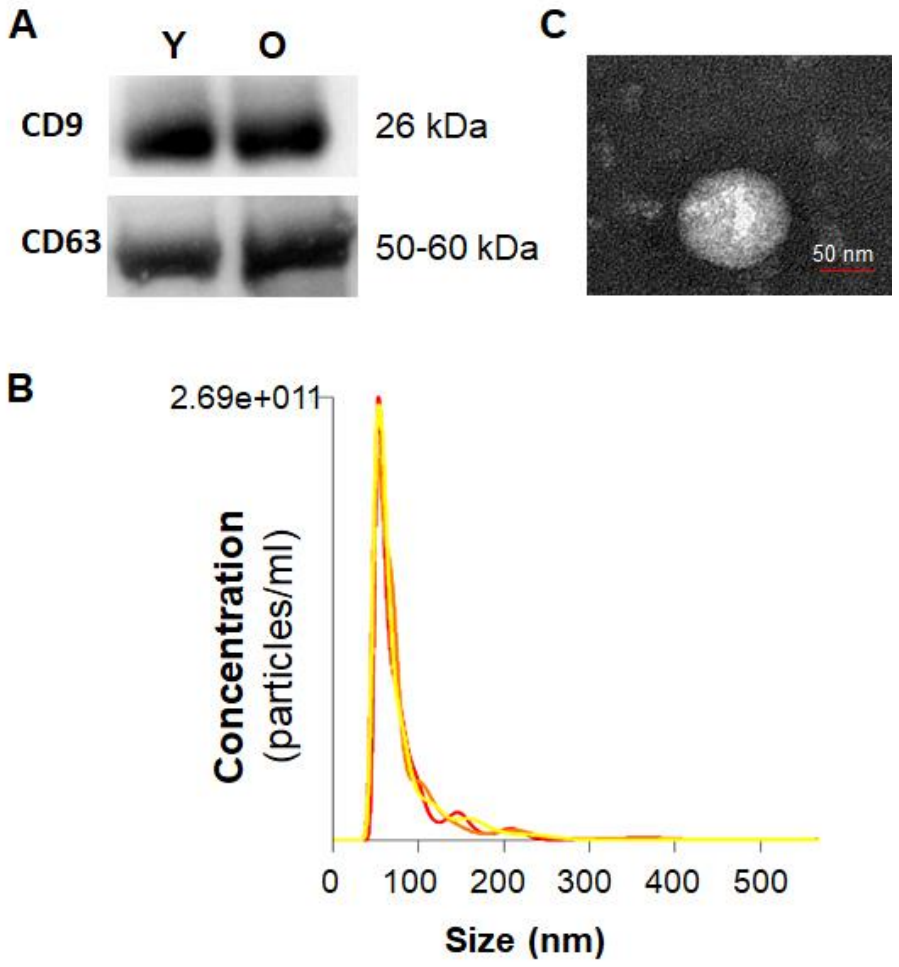

Figure 13. Characterization of serum exosomes.

(**A**) Western blotting for CD63 and CD9 in serum exosomes isolated from young and old rats. (**B**) Average overall size distribution of exosomes from serum of old rats using the Nanoparticle Tracking Analysis. (**C**) Representative transmission electron microscopy image showing the typical morphology and size range of exosomes from serum of old rat. Y, serum exosomes from young rats; O, serum exosomes from old rats.

3.2 Differentially Expressed RNAs in Serum Exosomes with Age

To determine whether aging affects the levels of serum exosomal RNAs, RNA profiles were determined by next-generation RNA Sequencing. After quality control and filtering, a total of 35117 RNAs, including mRNA, miRNAs and other type of RNAswere identified in exosomes from serum of young and old rats (Supplementary data). Following application of thresholds for significance, 2736 (17.9%) were down-regulated and 108 (7%) were up-regulated in serum exosomes from old rats ($p < 0.05$, >1.5-fold change; Figure 14A), among identified 15272 mRNA. In addition, 600 miRNAs were identified after quality control, among which 68 were relatively abundant in old rats, including 28 that were down-regulated and 40 that were up-regulated serum exosomes from old rats ($p < 0.05$, >1.5-fold change; Figure 14B). A volcano plot (Figure 14C) and cluster analysis (Figure 14D) revealed the overall distribution of differentially expressed mRNAs and miRNAs of serum exosomes with age after analysis with TargetScan.

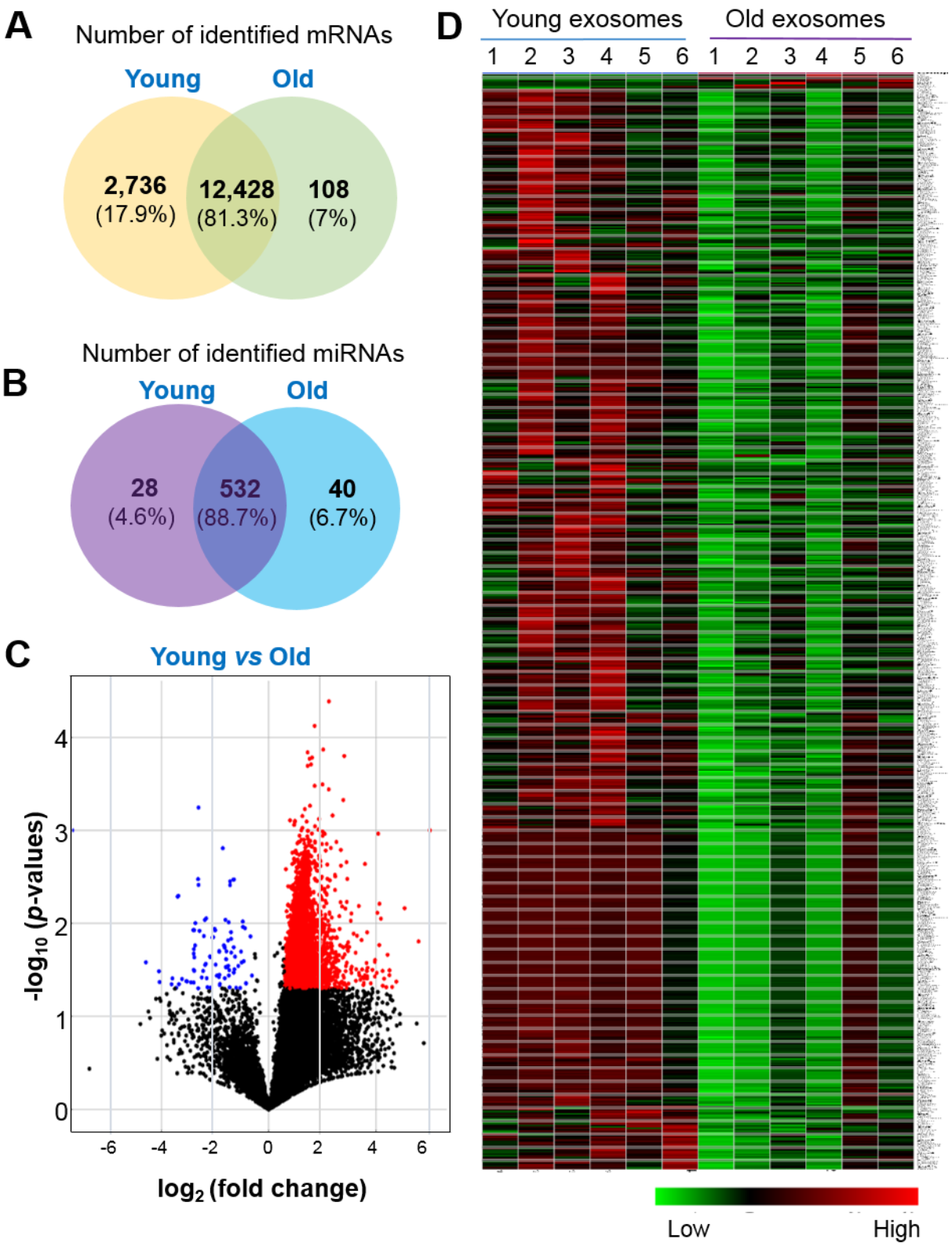
A
Number of identified mRNAs
Young
Old
2,736
(17.9%)
12,428
(81.3%)
108
(7%)
B
Number of identified miRNAs
Young
Old
28
(4.6%)
532
(88.7%)
40
(6.7%)
C
Young vs Old
-log10 (p-values)
log2 (fold change)
D
Young exosomes
Old exosomes
1 2 3 4 5 6 1 2 3 4 5 6
Low
High

Figure 14. Profiles for mRNAs and miRNAs of serum exosomes from young and old rats.

(**A-B**) Venn diagram of all differentially expressed mRNAs (**A**) and miRNAs (**B**) identified in serum exosomes. (**C**) Volcano plot for comparing the differentially expressed exosomal mRNAs and miRNAs in serum from young and old rats after analysis with TargetScan (fold change > 1.5 and $p < 0.05$). (**D**) Heatmap of the differentially expressed mRNAs and miRNAs in serum exosomes from young and old rats ($n = 6$ each group) after TargetScan (fold change > 1.5 and $p < 0.05$). Young, serum exosomes from young rats; Old, serum exosomes from old rats.

3.3 Identification of miRNA-Targeted mRNAs

MiRNAs regulate expression of specific genes via hybridization to mRNAs to promote their degradation in order to inhibit their translation or both (185). A volcano plot revealed the overall distribution of the exosomal miRNAs we identified in this study (Figure 15A). To study the possible functional roles of the differentially expressed miRNAs, their potential mRNA targets were analyzed with Targetscan. Among the 68 miRNAs, only 19 were associated with 766 of the 2844 mRNAs that were differentially expressed with age (Figure 15B), suggesting that these miRNAs contribute to the age-dependent regulation of specific mRNAs. Among them, 5 mRNAs were down-regulated and 14 were up-regulated in serum exosomes from old rats compared with those from young rats (Figure 15C). MiRNA-483-3p and miRNA-489-3p were detected only in exosomes from young rats, and miRNA-187-3p, miRNA-202-3p, miRNA-450b-5p, miRNA-501-3p, miRNA-511-5p, and miRNA-598-3p were detected only in exosomes from old rats (Table 2). Figure 15D presents results of a cluster analysis of differentially expressed miRNAs for each sample.

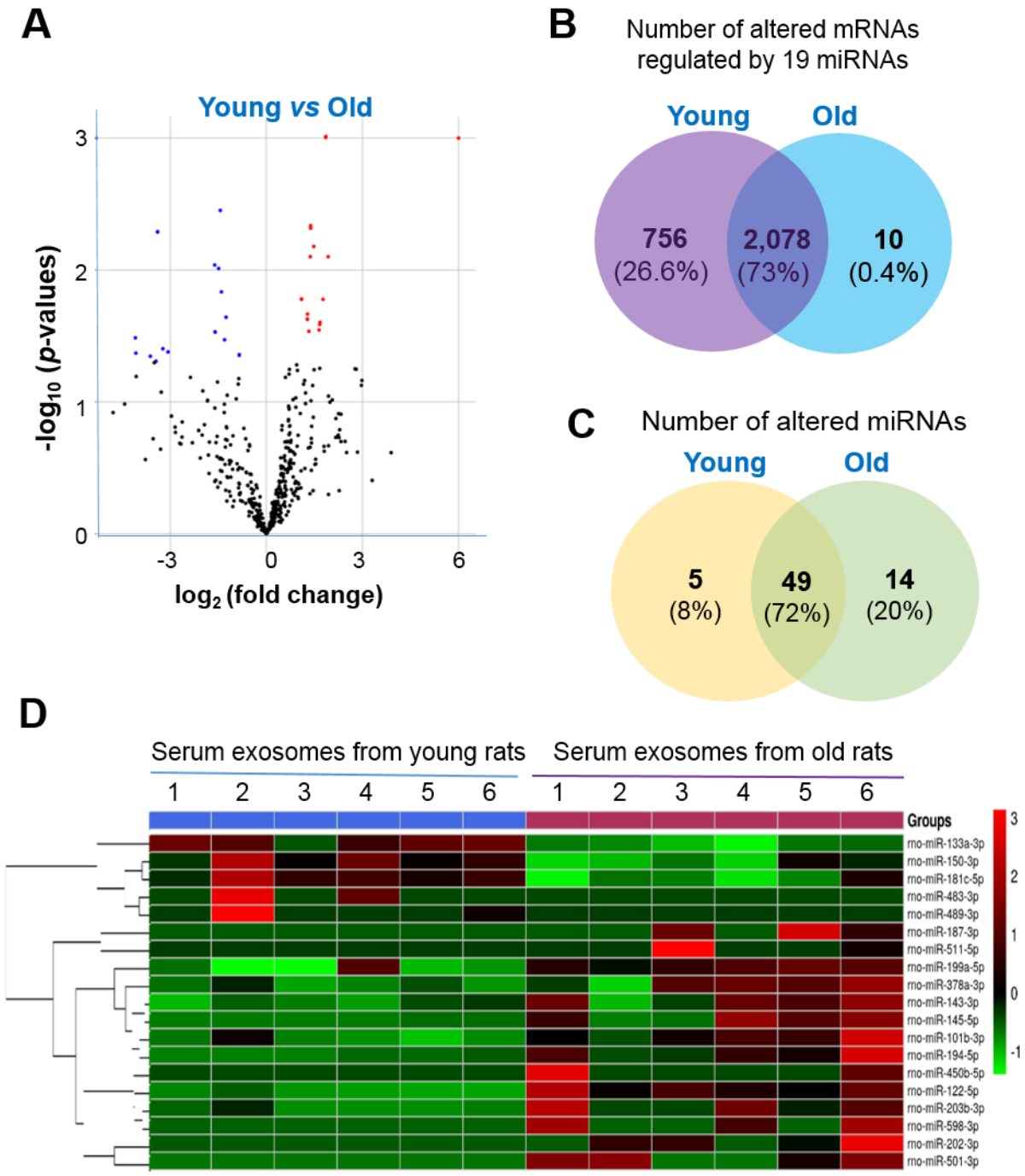
A
Young vs Old
-log10 (p-values)
log2 (fold change)
B
Number of altered mRNAs regulated by 19 miRNAs
Young
Old
756 (26.6%)
2,078 (73%)
10 (0.4%)
C
Number of altered miRNAs
Young
Old
5 (8%)
49 (72%)
14 (20%)
D
Serum exosomes from young rats
Serum exosomes from old rats
Groups
rno-miR-133a-3p
rno-miR-150-3p
rno-miR-181c-5p
rno-miR-483-3p
rno-miR-489-3p
rno-miR-187-3p
rno-miR-511-5p
rno-miR-199a-5p
rno-miR-378a-3p
rno-miR-143-3p
rno-miR-145-5p
rno-miR-101b-3p
rno-miR-194-5p
rno-miR-450b-5p
rno-miR-122-5p
rno-miR-203b-3p
rno-miR-598-3p
rno-miR-202-3p
rno-miR-501-3p

Figure 15. Profiles for differentially expressed miRNAs of serum exosomes from young and old rats.

(A) Volcano plot showing the differentially expressed miRNAs (fold change > 1.5 and $p < 0.05$). **(B)** Venn diagram showing the differentially expressed mRNAs. **(C)** Venn diagram of the differentially expressed miRNAs. **(D)** Heat map of hierarchical clustering of 19 miRNAs that were identified in serum exosomes from young and old rats ($n = 6$ each group).

Table 2. List of circulating miRNAs in exosome with age.

ID	*p*-Value	Fold Change	Expression Level (Old vs. Young)
rno-miR-101b-3p	0.0295919	3.0300921	Up
rno-miR-122-5p	0.005130112	10.50495019	Up
rno-miR-133a-3p	0.000973173	−3.631787956	Down
rno-miR-143-3p	0.033831212	2.469145377	Up
rno-miR-145-5p	0.032740298	17.04524832	Up
rno-miR-150-3p	0.016694482	−3.404719964	Down
rno-miR-181c-5p	0.006634803	−2.79454293	Down
rno-miR-187-3p	0.001	64	Up
rno-miR-194-5p	0.042745612	16.8112814	Up
rno-miR-199a-5p	0.009166599	3.06058214	Up
rno-miR-202-3p	0.001	64	Up
rno-miR-203b-3p	0.03954997	9.395112765	Up
rno-miR-378a-3p	0.043871243	1.797380304	Up
rno-miR-450b-5p	0.001	64	Up

rno-miR-483-3p	0.001	−64	Down
rno-miR-489-3p	0.001	−64	Down
rno-miR-501-3p	0.001	64	Up
rno-miR-511-5p	0.001	64	Up
rno-miR-598-3p	0.001	64	Up

3.4 GO Enrichment Analysis of miRNA-Targeted mRNAs

To gain a better understanding of the potential role of these exosomal miRNAs in aging, we used Blastp to carry out functional annotation and enrichment analysis of their target genes identified in the GO enrichment analysis. Functional annotation was categorized by biological process, cellular component and molecular function, and only the top 10 GO terms having the smallest *p*-value were considered. These categories represent the annotation of the functional enrichment of targeted genes, and a lower *p*-value represents a greater functional enrichment of a relative term. Notably, almost all the genes listed under these GO terms were downregulated in serum exosomes from old rats. This analysis revealed several enriched functional categories and target genes, including genes involved in the posttranslational modification of proteins, metabolic processes, cell communication, molecular function, and intracellular signal transduction (Figure 16A).

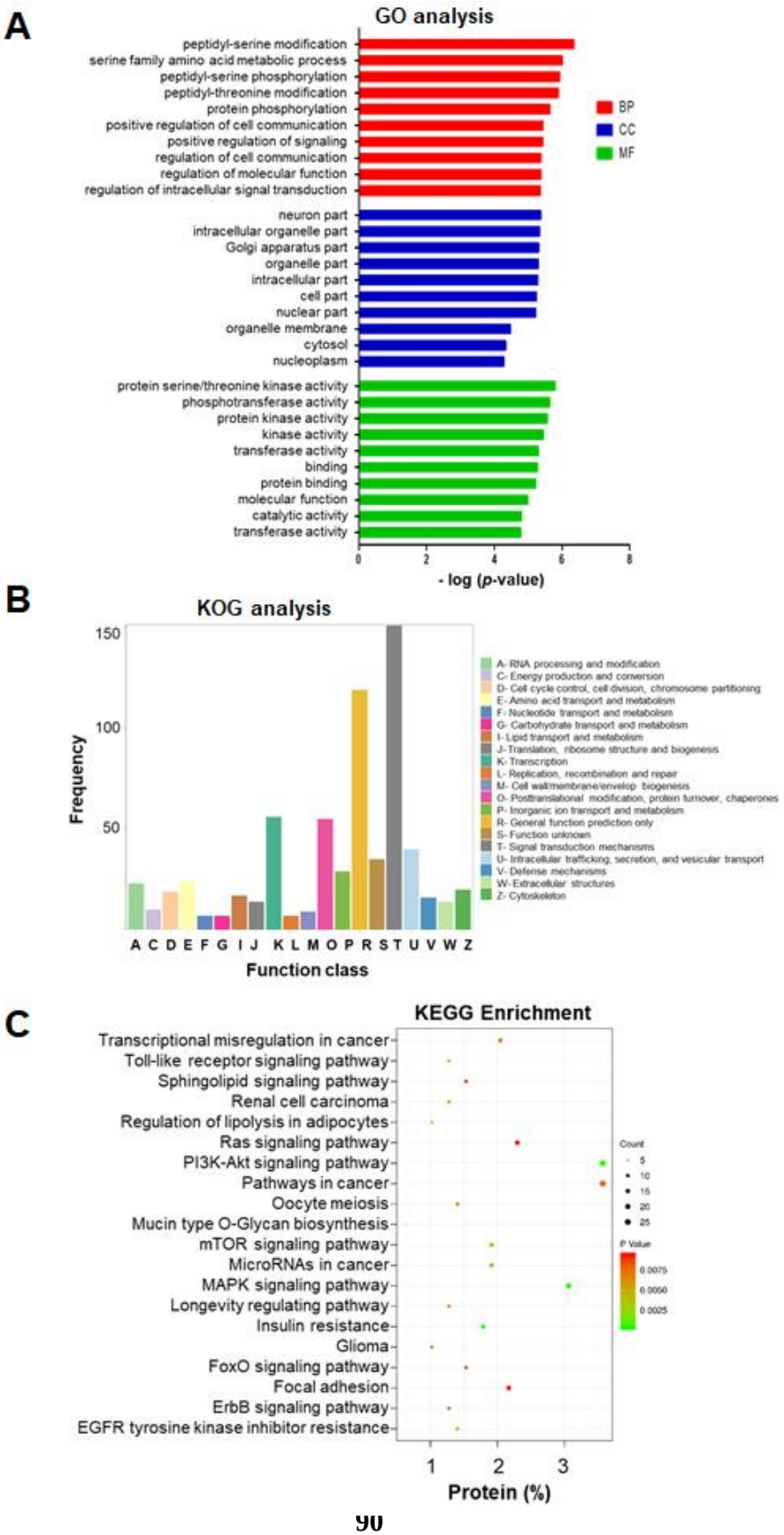
A
GO analysis
peptidyl-serine modification
serine family amino acid metabolic process
peptidyl-serine phosphorylation
peptidyl-threonine modification
protein phosphorylation
positive regulation of cell communication
positive regulation of signaling
regulation of cell communication
regulation of molecular function
regulation of intracellular signal transduction
neuron part
intracellular organelle part
Golgi apparatus part
organelle part
intracellular part
cell part
nuclear part
organelle membrane
cytosol
nucleoplasm
protein serine/threonine kinase activity
phosphotransferase activity
protein kinase activity
kinase activity
transferase activity
binding
protein binding
molecular function
catalytic activity
transferase activity
BP
CC
MF
0
2
4
6
8
- log (p-value)
B
KOG analysis
150
100
50
Frequency
A C D E F G I J K L M O P R S T U V W Z
Function class
A- RNA processing and modification
C- Energy production and conversion
D- Cell cycle control, cell division, chromosome partitioning
E- Amino acid transport and metabolism
F- Nucleotide transport and metabolism
G- Carbohydrate transport and metabolism
I- Lipid transport and metabolism
J- Translation, ribosome structure and biogenesis
K- Transcription
L- Replication, recombination and repair
M- Cell wall/membrane/envelop biogenesis
O- Posttranslational modification, protein turnover, chaperones
P- Inorganic ion transport and metabolism
R- General function prediction only
S- Function unknown
T- Signal transduction mechanisms
U- Intracellular trafficking, secretion, and vesicular transport
V- Defense mechanisms
W- Extracellular structures
Z- Cytoskeleton
C
KEGG Enrichment
Transcriptional misregulation in cancer
Toll-like receptor signaling pathway
Sphingolipid signaling pathway
Renal cell carcinoma
Regulation of lipolysis in adipocytes
Ras signaling pathway
PI3K-Akt signaling pathway
Pathways in cancer
Oocyte meiosis
Mucin type O-Glycan biosynthesis
mTOR signaling pathway
MicroRNAs in cancer
MAPK signaling pathway
Longevity regulating pathway
Insulin resistance
Glioma
FoxO signaling pathway
Focal adhesion
ErbB signaling pathway
EGFR tyrosine kinase inhibitor resistance
1
2
3
Protein (%)
Count
5
10
15
20
25
P Value
0.0075
0.0050
0.0025

Figure 16. Gene Ontology (GO) analysis, eukaryotic orthologous groups (KOG) functional classification, and Kyoto Encyclopedia of Genes and Genomes (KEGG) pathway analysis of target genes (mRNAs) regulated by the 19 miRNAs that were differentially expressed between young and old rats.

(**A**) GO annotation of predicted targets. The top 10 most enriched GO terms are listed in terms for biological process (BP), cellular component (CC), and molecular function (MF) based on *p*-values. (**B**) KOG functional classification of target genes. The vertical axis represents the frequency of target genes classified into the specific categories, and the horizontal axis represents the KOG functional classification. (**C**) The top 20 most common KEGG pathways of the differentially expressed mRNAs regulated by the 19 miRNAs. Fold change > 1.5 and $p < 0.05$. GO, gene ontology; KOG, eukaryotic orthologous groups; KEGG, Kyoto Encyclopedia of Genes and Genomes.

3.5 KOG and KEGG Enrichment and Analyses

KOG was used to functionally classify mRNAs (766) regulated by the 19 exosomal miRNAs that were differentially expressed between young and old rats. Among the resultant 25 KOG classifications, genes involved in "signal transduction mechanisms" were the ones most commonly targeted (151 genes), followed by "general function prediction only" (119 genes), "transcription" (56 genes), "posttranslational modification and protein turnover" (55 genes), and "intracellular function and secretion and vesicular transport "(40 genes) (Figure 16B).

KEGG is a comprehensive knowledge base for both functional interpretation and practical application of genomic information (186). KEGG pathway analysis identified 20 pathways that differed significantly ($p < 0.05$) between exosomes of young and old rats (Figure 16C). Among these pathways, the following were found to be involved in aging and lifespan: insulin resistance, mitogen-activated protein kinase (MAPK) signaling, PI3 kinase (PI3K)–Akt signaling, mammalian target of rapamycin (mTOR) signaling, toll-like receptor signaling, FoxO signaling, ErbB signaling, longevity-regulating signaling, and resistance to inhibitors o*f* epidermal growth-factor receptor (EGFR) tyrosine kinase (Figure 16C).

3.6 Analysis of Pathways and Interaction Networks

We then carried out IPA for molecular pathways associated with serum exosomal miRNAs during aging. The results showed that 163 IPA canonical pathways were predicted to be significantly related to the expression of serum exosomal miRNAs, based on $p < 0.05$. The top

22 most strongly aging-associated pathways targeted by miRNAs are shown in Figure 17A. Those discovered aging-related signaling pathways included insulin, integrin, ErbB, neuregulin, mTOR, opioid, telomerase, phosphatase and tensin homolog 10 (PTEN), insulin-like growth factor-1 (IGF-1), adenosine monophosphate-activated protein kinase (AMPK), growth hormone, endothelial nitric oxide synthase (eNOS), nitric oxide, fibroblast growth factor (FGF), cyclic adenosine monophosphate (cAMP), sphingosine, platelet-derived growth factor (PDGF), docosahexaenoic acid (DHA), triggering receptor expressed on myeloid cells 1 (TREM1), and p53, suggesting that miRNAs target multiple biological pathways that modulate aging.

Figure 17B presents the IPA network results, and Table 3 lists the miRNAs involved in the nine pathways. Similar to IPA results, the networks contained genes predicted to be involved in metabolism, growth hormone signaling, and oxidative stress. As shown in Figure 17B, each pathway was linked with several gene transcripts, and individual genes could be regulated by several miRNAs. This suggested that the serum exosomal miRNAs that regulate crosstalk between pathways differ among young and old rats. The most common proteins in the networks were eukaryotic translation initiation factor 4E binding protein 1 (EIF4EBP1), insulin receptor (INSR), phosphoinositide dependent protein kinase 1 (PDPK1), PTEN, paxillin (PXN), and insulin-like growth factor 1 receptor (IGF-1R) that were targeted by the most prominent miRNAs (Figure 18A). Overall, the results establish putative functions between miRNAs and their target mRNAs, molecular networks, and biological pathways that modulate the makeup of serum exosomal miRNAs in young versus old animals. Figure 18B shows one such example of miRNA-mediated regulation.

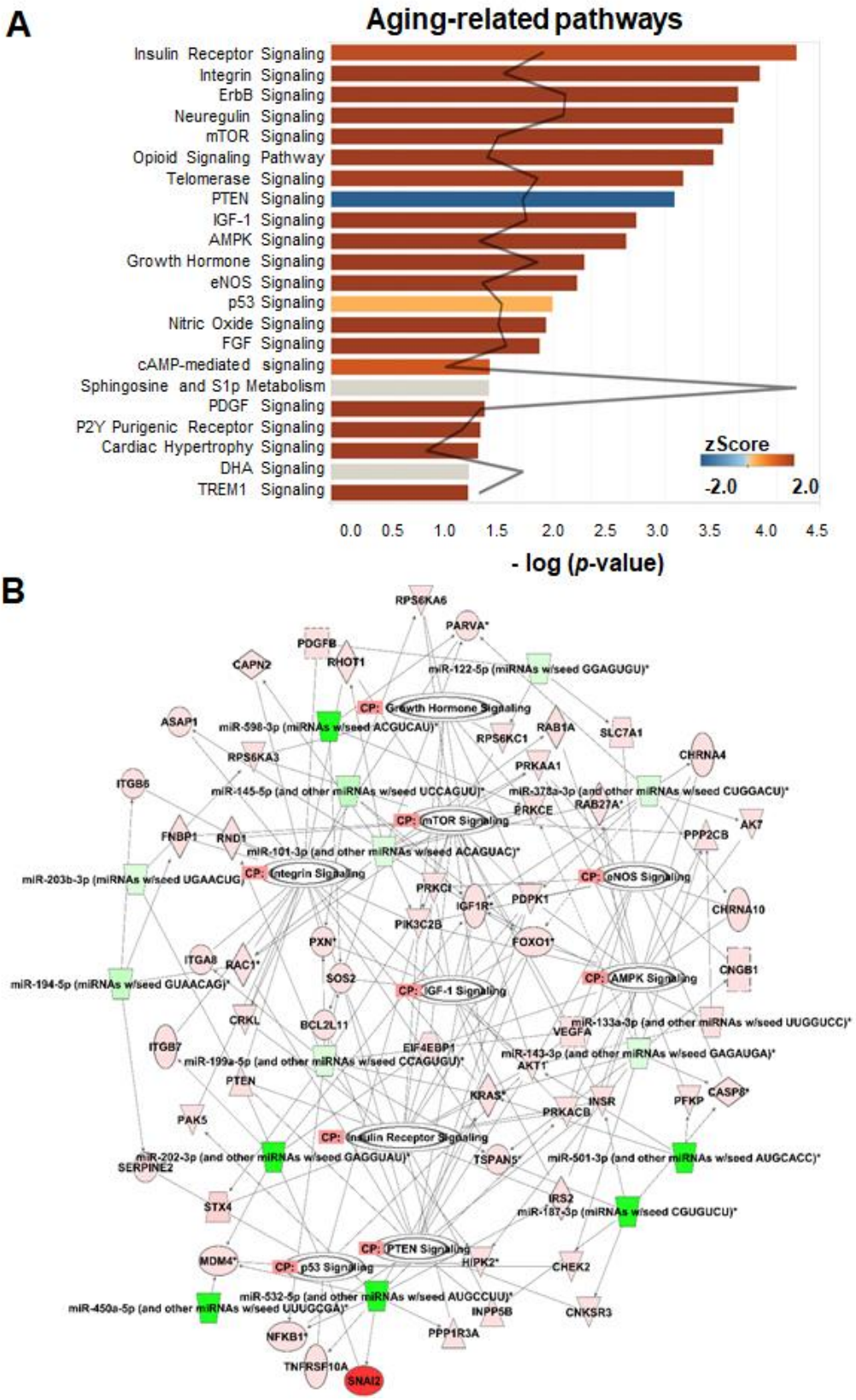
A
Aging-related pathways
Insulin Receptor Signaling
Integrin Signaling
ErbB Signaling
Neuregulin Signaling
mTOR Signaling
Opioid Signaling Pathway
Telomerase Signaling
PTEN Signaling
IGF-1 Signaling
AMPK Signaling
Growth Hormone Signaling
eNOS Signaling
p53 Signaling
Nitric Oxide Signaling
FGF Signaling
cAMP-mediated signaling
Sphingosine and S1p Metabolism
PDGF Signaling
P2Y Purigenic Receptor Signaling
Cardiac Hypertrophy Signaling
DHA Signaling
TREM1 Signaling
zScore
-2.0
2.0
0.0 0.5 1.0 1.5 2.0 2.5 3.0 3.5 4.0 4.5
- log (p-value)
B
RPS6KA6
PARVA*
PDGFB
CAPN2
RHOT1
miR-122-5p (miRNAs w/seed GGAGUGU)*
CP: Growth Hormone Signaling
ASAP1
miR-598-3p (miRNAs w/seed ACGUCAU)*
RPS6KC1
RAB1A
SLC7A1
CHRNA4
RPS6KA3
PRKAA1
ITGB6
miR-145-5p (and other miRNAs w/seed UCCAGUU)*
miR-378a-3p (and other miRNAs w/seed CUGGACU)*
PRKCE
RAB27A*
CP: mTOR Signaling
AK7
FNBP1
RND1
PPP2CB
miR-101-3p (and other miRNAs w/seed ACAGUAC)*
miR-203b-3p (miRNAs w/seed UGAACUG)
CP: Integrin Signaling
CP: eNOS Signaling
PRKCI
PDPK1
IGF1R*
CHRNA10
PIK3C2B
FOXO1*
PXN*
ITGA8
RAC1*
CNGB1
miR-194-5p (miRNAs w/seed GUAACAG)*
SOS2
CP: IGF-1 Signaling
CP: AMPK Signaling
CRKL
BCL2L11
miR-133a-3p (and other miRNAs w/seed UUGGUCC)*
VEGFA
ITGB7
EIF4EBP1
miR-199a-5p (and other miRNAs w/seed CCAGUGU)*
miR-143-3p (and other miRNAs w/seed GAGAUGA)*
AKT1*
PTEN
KRAS*
INSR
PFKP
CASP8*
PRKACB
PAK5
CP: Insulin Receptor Signaling
miR-202-3p (and other miRNAs w/seed GAGGUAU)*
TSPAN5*
miR-501-3p (and other miRNAs w/seed AUGCACC)*
SERPINE2
IRS2
STX4
miR-187-3p (miRNAs w/seed CGUGUCU)*
CP: PTEN Signaling
MDM4*
CP: p53 Signaling
HIPK2*
CHEK2
miR-532-5p (and other miRNAs w/seed AUGCCUU)*
miR-450a-5p (and other miRNAs w/seed UUUGCGA)*
INPP5B
CNKSR3
NFKB1*
PPP1R3A
TNFRSF10A
SNAI2

Figure 17. Ingenuity Pathway Analysis (IPA) of the differentially expressed miRNAs in serum exosomes from young and old rats.

(**A**) IPA showing the 22 most significant aging-related pathways involving mRNAs, whose expression is regulated by differentially expressed miRNAs in serum exosomes from young and old rats. Each Z score represents the upregulation or downregulation of gene expression based on young vs. old. The black curve denotes the ratio between the number of the differentially expressed target genes and the total number of genes in each of these pathways. (**B**) IPA-predicted network for the differentially expressed miRNAs showing predicted targets and their association with biological functions in aging-related signaling pathways governed by the following factors: growth hormone signaling, mammalian target of rapamycin (mTOR) signaling, endothelial nitric oxide synthase (eNOS) signaling, integrin signaling, insulin-like growth factor-1 (IGF-1) signaling, AMP-activated protein kinase (AMPK) signaling, insulin receptor signaling, p53 signaling, and phosphatase and tensin homolog 10 (PTEN) signaling.

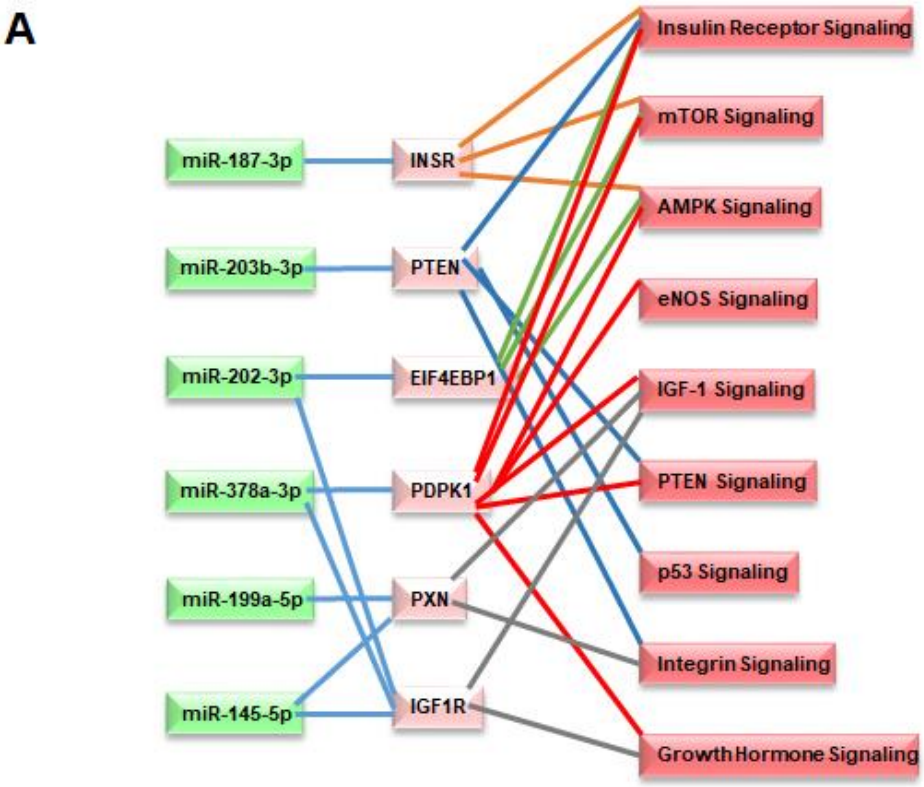
A
miR-187-3p
miR-203b-3p
miR-202-3p
miR-378a-3p
miR-199a-5p
miR-145-5p
INSR
PTEN
EIF4EBP1
PDPK1
PXN
IGF1R
Insulin Receptor Signaling
mTOR Signaling
AMPK Signaling
eNOS Signaling
IGF-1 Signaling
PTEN Signaling
p53 Signaling
Integrin Signaling
Growth Hormone Signaling

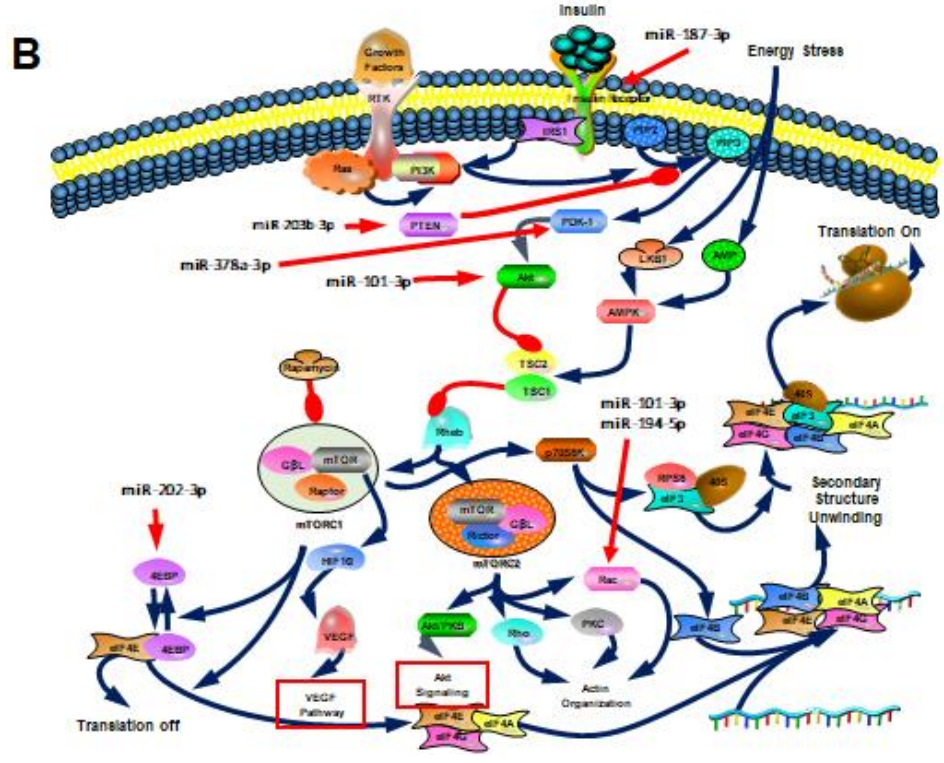
B
Insulin
miR-187-3p
Energy Stress
Growth Factors
RTK
IRS1
Ras
PI3K
miR-203b-3p
PTEN
PDK-1
miR-378a-3p
miR-101-3p
Akt
LKB1
AMP
AMPK
Translation On
TSC2
TSC1
Rheb
Rapamycin
mTOR
GβL
Raptor
mTORC1
mTORC2
p70S6K
miR-101-3p
miR-194-5p
miR-202-3p
4EBP1
eIF4E
HIF1α
VEGF
VEGF Pathway
Translation off
Rac
Rho
PKC
Akt Signaling
Actin Organization
Secondary Structure Unwinding
eIF4G
eIF4A
eIF3
40S
RPS6

Figure 18. The most common target genes and mTOR pathway regulated by the differentially expressed exosomal miRNAs.

(**A**) *EIF4EBP1*, *INSR*, *PDPK1*, *PTEN*, *PXN*, and *IGF-1R* are the most common network genes targeted by the prominent circulating exosomal miRNAs including miR-187-3p, miR-203b-3p, miR-202-3p, miR-378a-3p, miR-199a-5p, and miR-145-5p. (**B**) IPA networks showing the regulatory effects of the differentially expressed miRNAs from rat serum on mTOR signaling.

Table 3. IPA of genes targeted by 19 miRNAs that were altered with age.

Ingenuity Canonical Pathways	**−log (*p*-Value)**	**Related miRNA**	**Target Genes**	**Full Name**
Insulin receptor signaling	4.48	miR-378a-3p	*PDK1*	3-phosphoinositide-dependent protein kinase 1
		miR-187-3p	*INSR*	insulin receptor
		miR-202-3p	*4E-BP1*	Eukaryotic translation initiation factor 4E-binding protein 1
		miR-101b-3p	*AKT*	RAC-alpha serine/threonine-protein kinase
		miR-199a-5p	*STX4*	Syntaxin-4
		miR-203b-3p	*PTEN*	phosphatase and tensin homolog deleted on chromosome
mTOR signaling	3.77	miR-378a-3p	*PDK1*	3-phosphoinositide-dependent protein kinase 1
		miR-187-3p	*INSR*	insulin receptor
		miR-202-3p	*eIF4E-BP1*	Eukaryotic translation initiation factor 4E-

				binding protein 1
		miR-101b-3p	*AKT*	RAC-alpha serine/threonine-protein kinase
		miR-194-5p	*RAC*	Aryl-hydrocarbon-interacting protein-like 1
AMPK signaling	2.84	miR-378a-3p	*PDK1*	phosphoinositide-dependent kinase-1
		miR-187-3p	*INSR*	insulin receptor
		miR-202-3p	*eIF4E-BP1*	Eukaryotic translation initiation factor 4E-binding protein 1
		miR-101b-3p	*AKT*	RAC-alpha serine/threonine-protein kinase
eNOS signaling	2.37	miR-378a-3p	*PDK1*	phosphoinositide-dependent kinase-1
		miR-187-3p	*CASP8*	caspase-8
		miR-101b-3p	*AKT*	RAC-alpha serine/threonine-protein kinase
		miR-122-5p	*CAT1*	cationic amino acid transporter 1
		miR-143-3p	*CASP8*	caspase-8
IGF-1	2.94	miR-378a-	*PDK1, IGF-*	phosphoinositide-dependent kinase-1,

signaling		3p	*1R*	Insulin-like growth factor 1 receptor
		miR-202-3p	*IGF-1R*	Insulin-like growth factor 1 receptor
		miR-101b-3p	*AKT*	RAC-alpha serine/threonine-protein kinase
		miR-145-5p	*IGF-1R*, *PXN*	insulin-like growth factor 1 receptor, Paxillin
		miR-199a-5p	*PXN*	paxillin
PTEN signaling	3.31	miR-378a-3p	*PDK1*	phosphoinositide-dependent kinase-1
		miR-101b-3p	*BCL2L11*, *AKT*	bcl-2-like protein 11, RAC-alpha serine/threonine-protein kinase
		miR-203b-3p	*PTEN*	phosphatase and tensin homolog deleted on chromosome
		miR-532-5p	*NF-ƙB*	Nuclear factor NF-kappa-B
p53 signaling	2.13	miR-202-3p	*MDM4*	protein Mdm4
		miR-101b-3p	*AKT*	RAC-alpha serine/threonine-protein kinase
		miR-203b-	*PTEN*	phosphatase and tensin homolog deleted on

		3p		chromosome
		miR-532-5p	*MDM4*, *Slug*	Protein Mdm4, Zinc finger protein SNAI2
		miR-450b-5p	*MDM4*	Protein Mdm4
		miR-194-5p	*PAI-1*	Glia-derived nexin
		miR-199a-5p	*HIPK2*	Homeodomain-interacting protein kinase 2
		miR-143-3p	*HIPK2*, *Chk2*	Homeodomain-interacting protein kinase 2, Serine/threonine-protein kinase Chk2
Integrin signaling	4.13	miR-378a-3p	*PARVIN-α*	parvin alpha
		miR-101b-3p	*ASAP1*, *PARVIN-α*, *AKT*	arf-GAP with SH3 domain, ANK repeat and PH domain-containing protein 1, parvin alpha, RAC-alpha serine/threonine-protein kinase
		miR-145-5p	*PXN, CRKL*	Paxillin, Crk-like protein
		miR-122-5p	*PDGFβ*	Platelet-derived growth factor subunit B
		miR-203b-	*PTEN*	phosphatase and tensin homolog deleted on

		3p		chromosome
		miR-598-3p	*PARVIN-α*	parvin alpha
		miR-199a-5p	*PXN*	Paxillin
Growth hormone signaling	2.44	miR-378a-3p	*PDK1*	phosphoinositide-dependent kinase-1
		miR-202-3p	*IGF-1R*	Insulin-like growth factor 1 receptor
		miR-145-5p	*IGF-1R*	Insulin-like growth factor 1 receptor

4. Conclusion

Taken together, our findings suggest that changes in the makeup of circulating exosomal miRNAs with age not only can be considered as a potential predictor of animal age but also may contribute to aging via several key signaling pathways that regulate aging and lifespan. It will be important to identify and understand the mechanisms of rejuvenation and accelerated aging, because the findings concerning rejuvenation can potentially reverse deleterious processes of aging, whereas the findings concerning accelerated aging may pinpoint potential pathways for interventions that may slow the rate of aging and the incidence of aging-related disease. The challenge for the future will be to determine how these mediators map onto the different pathways and interact with each other, and to decipher how they contribute to the molecular mechanisms in aging.

DISCUSSION

1. Serum exosomes isolated from old rats affect the outcome of ischemic stroke

Aging is associated with immune dysregulation, with characteristics that include high circulating levels of pro-inflammatory mediators, which may result from repeated microbial infections or chronic inflammatory diseases. Age not only affects stroke incidence but also the outcome. elderly patients have higher mortality, morbidity and poorer functional recovery after ischemic stroke compared with younger patients (187). Our results showed that the infarct volume in 23-month-old rats was higher than 21-month-old ischemic rats, confirming that the elderly ischemic stroke individual had poorer functional outcome. These systemic inflammatory mediators in the blood are associated with age-related functional decline, such as cognitive decline, and chronic diseases (188), but the link to ischemic stroke outcome remains unexplored. Here, we found that pro-inflammatory mediators (Cq1, C3a and C3b) were increased with age, which could pass the BBB and prime microglia, leading to excessive microglial phagocytosis of synapses. The effect of O-exo on ischemic stroke outcome is highlighted by the findings that depletion of microglia or blockade of C3aR attenuated these more deleterious outcomes mediated by O-exo, along with reduced synaptic loss in the ischemic brain. In contrast, CD46 was much higher in Y-exo relative to O-exo, which could block the complement-triggered phagocytosis of microglia

(Figure 8). Our data may explain why elderly stroke patients have worsened functional outcomes than do younger stroke patients, which persist even after adjusting for stroke risk factors and other comorbidities.

In the ischemic brain, the penumbra is functionally impaired. Although it is potentially salvageable, it can be incorporated the developing infarct core if secondary damage signaling persists. We found that injection of O-exo increased the infarct volume, but Y-exo treatment could salvage much of the ischemic penumbra. The changes in histological outcomes corresponded to the level of motor deficits after ischemic stroke following serum exosome treatment. Spontaneous recovery of motor function after stroke is thought to be mediated primarily through the reorganization and rewiring of the surviving brain circuits. Dendrites and dendritic spines receive most of the excitatory synapses, which transmit normal and potentially abnormal and injurious synaptic signaling. Given that dendritic spine turnover underlies rewiring during normal development and plasticity, the structure and number of dendritic spines in the penumbra are likely to play a key role in mediating motor deficits that occur during and after stroke. We found that worsened motor deficits after O-exo treatment were accompanied by a reduced number of dendritic spines, whereas improved motor deficits after Y-exo administration were associated with increased neuroplasticity in the penumbra after ischemic stroke. Our findings suggest that the mechanism underlying motor deficits after serum exosome treatment may primarily result from changes in the structure of neurons in the surviving penumbra regions, particularly at the level of the dendritic spines. With increasing age, neuronal dendritic trees undergo progressive regression. Therefore, these changes in the dendritic spines are critical for recovery of sensory, motor and cognitive functions after ischemic stroke in aged animals.

Next, we explored the mechanism underlying the loss of these dendritic spines. We first investigated the microglial response in the penumbra after serum exosome treatment, as a major function of microglia is phagocytosis, in addition to the release of inflammatory cytokines. Indeed, acute ischemic strokes trigger an innate immune response, leading to severe inflammation, which plays a crucial role in the pathogenesis of *ischemic* brain injury. Stroke-induced pro-inflammatory signals activate resident immune cells (microglia), resulting in the production of pro-inflammatory cytokines and phagocytic activities, leading to secondary brain injury after stroke. It is worth noting that microglial activation has a dual role in that it has beneficial and detrimental effects on neurons. On the one hand, microglial activation is necessary for the removal of debris for tissue repair; on the other hand, high levels of pro-inflammatory and cytotoxic mediators contribute to secondary brain injury. We found that ischemic stroke mainly activated pro-inflammatory microglia in the penumbra during the early stage of a stroke. These pro-inflammatory microglia could be further primed after exposure to O-exo or could be attenuated after injection of Y-exo. In parallel, microglial phagocytosis of *synapses*, which was based on the colocalization of postsynaptic proteins with Iba-1 (microglial) and CD68 (lysosomal) markers, was increased in the penumbra after O-exo treatment but was reduced after Y-exo treatment. After microglial depletion, we found that the extent of O-exo–mediated synaptic loss in the penumbra was significantly reduced, in conjunction with improved motor deficits, after ischemic stroke. These data suggest that microglial phagocytosis of synapses in the penumbra during the early stage of stroke is “healthy” rather than detrimental and that O-exo treatment promotes microglial phagocytic activity to exacerbate the loss of synapses, which, in turn, affects synaptic plasticity and motor function.

We then examined the protein profile of serum exosomes to identify the trigger(s) of microglial activation. We demonstrated that complement opsonins (C1q) and anaphylatoxins (C3a and C3b) were increased in O-exo, whereas CD46 was increased in Y-exo. The complement system is essential for the activation of the innate immune response and plays a vital role in host defense and tissue homeostasis. In addition, complement signaling is also an important driver of inflammation, and thus inappropriate or uncontrolled activation of complement can cause systemic inflammation, tissue damage and disease (189). Studies have also documented that complement emerges as a masterful regulator of neural synaptic plasticity and complement activation plays a major role in brain injury after acute ischemic stroke. Ischemic stroke induces pathologic activation of complement, leading to the promotion of post-stroke pathology and worsened outcomes (190). Therefore, deterioration of functional outcomes could be due to excessive complement activation delivered by O-exo. Importantly, complement is critical for microglial activation and phagocytosis, as the C3aR expressed on microglia is essential for microglial activation. We found that inhibiting C3aR activity attenuated the worsened outcomes mediated by O-exo in aged rats after ischemic stroke. Therefore, the underlying mechanism is likely that O-exo carrying pro-inflammatory modulators, such as complement opsonins and anaphylatoxins, pass the BBB and trigger microglial activation via C3aR, which leads to neuronal and dendritic damage and, subsequently, worsened motor deficits after ischemic stroke. As CD46 has cofactor activity for inactivation of complement C3b and C4b (191), increased levels of CD46 in Y-exo can inhibit microglial activation and protect neurons from damage mediated by complement signaling in the ischemic brain.

Studies have documented that exosomes from brain cells are able to cross the BBB and can serve as biomarkers of cognitive impairment in Alzheimer's disease (170-172) and brain injury (192). Blood exosomes can also pass the BBB to target brain cells and have been used as a drug delivery vehicle (173-176). Therefore, exosomes can cross the BBB in a bi-directional manner. We found that circulating exosomes could pass the BBB of normal and ischemic brains and were taken up by recipient cells including neurons and microglia, indicating that blood exosomes could transport all the main biomolecules, including pro-inflammatory mediators, into the brain from distant target tissues.

2. The potential relationship between molecules in serum exosomes and aging signaling pathway

The past two decades have witnessed the use of heterochronic blood exchange techniques, including heterochronic parabiosis, heterochronic blood or plasma transfer, or heterochronic apheresis, as tools for studying the biology of aging. Indeed, heterochronic blood exchange from a young to an old animal resulted in rejuvenation, whereas accelerated aging in a young animal was observed after heterochronic blood exchange from an old animal (32). To explore the underlying mechanism, we used Exo-NGS analysis to compare the expression profiles for mRNAs and miRNAs in serum exosomes isolated from young and old rats. We Identified 68 miRNAs and 2,844 mRNAs in serum exosomes that were differentially expressed between young and old rats. In contrast to mRNAs, little is known about changes in miRNA abundance in the aging process. For this reason, we focused on circulating miRNAs, which serve as potential biomarkers and therapeutic targets for aging-related disease. To determine how these circulating

miRNA affect aging, it is important to identify the targets for each miRNA. Our data revealed that, of the 68 differentially expressed serum exosome miRNAs we identified, 19 were predicated to target 766 differentially expressed mRNAs based on TargetScan analysis. Among the 19 miRNAs, 14 were more abundant in exosomes from old rats than from young rats, and five were less abundant**.** These results are consistent with reports that the abundance of the majority of these 14 miRNAs including miR-150-3p, miR-378-3p, miR-199a-5p, miR-145-5p, miR-598-3p, miR-122-5p, miR-194-5p, miR-203a-3p, miR-202-3p, miR-145-5p, and miR-532-5p, was elevated in blood or tissue samples from older humans, mice and rats (172, 193-199). Our data also confirmed that miR-181a-5p and miR-133a-3p decreased with age (198, 200). These 14 miRNAs have been linked with aging, and the expression of some of them has been associated with cancer, longevity, inflammatory responses, and aging-related neurodegenerative and cardiac diseases (172, 194-204). Collectively, the abundance of the majority of our differentially expressed miRNAs has been previously reported to be altered with age, suggesting roles for these miRNAs in lifespan. Interestingly, downregulation of miR-181a-5p in serum exosomes from old rats correlates negatively with the expression of pro-inflammatory cytokines interleukin 6 (IL-6) and tumor necrosis factor alpha (TNFα) and correlates positively with that of the anti-inflammatory cytokines trandforming growth factor beta (TGFβ) and IL-10 in the serum of rhesus monkeys (200). Notably, the abundance of IL-6 and TNF-α has been correlated with aging (188). Therefore, certain exosomal miRNAs may contribute to aging by regulating systemic inflammation, and the makeup of these miRNAs may serve as a biological signature of aging.

We used Blastp and GO to functionally annotate miRNA-regulated genes and, identified biological processes that are altered by changes in exosomal miRNAs abundance changes with age. Among these processes, the most highly represented and enriched terms were protein posttranslational modification, metabolic process, cell communication, molecular function, and intracellular signal transduction, implying that these miRNAs may provide a significant link between aging and multiple biological processes through their regulation of target genes (205). KEGG pathway analysis revealed that the mRNAs targeted by these miRNA targets were enriched in known aging-related signaling pathways (206-208). The GO and KEGG analysis also revealed that most of the miRNA-targeted mRNAs are involved in signaling pathways and biological processes, that are critical for aging, suggesting that circulating miRNAs may help regulate the rate of aging and therefore are potential biomarkers for aging. Any individual miRNA may have the potential to act on numerous target genes, and therefore, multiple miRNAs have the potential to modulate numerous biological pathways. Hence, the impact of miRNAs on any particular pathway(s) can be assessed most effectively by examining any synergism between the miRNAs (209). To further investigate how any single miRNA-mRNA interaction regulates aging-related pathways, we performed IPA and found that the altered circulating miRNAs target the signaling pathways governed by insulin, integrin, mTOR, AMPK, PTEN, IGF-1, growth hormone, eNOS and p53, which are crucial pathways in aging and lifespan (206-208). For example, we found that miRNA-187-3p can regulate INSR mRNA and that miRNA-378a-3p andmiRNA-202-3p can regulate IGF-1R mRNA. Studies have documented an inverse correlation between cellular miRNA-187 levelss and glucose-stimulated insulin secretion (210) and that miRNA-378a may play a role in insulin resistant and the consequent of obesity (211). It is well documented that the insulin/IGF-1 pathway plays a critical role in aging and longevity

across a wide spectrum of species (212-214). Evidence includes that either reducing the level of circulating IGF-1 or reducing the expression of IGF-1R increases longevity (214); moreover, the loss of one allele of the *Igf-1* receptor increases the lifespan of mice by 33% (215). We also found that miR-187-3p, miR-202-3p, and miR-378a-3p regulate the mRNA levels of *INSR*, *EIF4EBP1* and *PDK1*, the genes for which are targeted by*)* mTOR *signaling* pathway. The mTOR pathway integrates both intracellular and extracellular signals and serves as a central regulator of cell metabolism, proliferation and survival, and it also controls lifespan by regulating translation through activation of p70S6K and inhibition of the translation repressor eIF4EBP (216). For example, knocking down three translational regulators, namely eIF4E, eIF4G, and eIF2B homologs, in *C. elegans* extends worm lifespan (217-219), and modulation of the translation of their mRNAs by a dominant-negative form of TOR extends lifespan (220). Recent studies have shown that the lifespan of different mouse strains can be extended significantly when mTOR inhibitor of rapamycin is administrated (221, 222). There is no clear explanation how a reduction in signaling via mTOR or insulin/IGF-1 affects lifespan. However, one potential explanation is that global mRNA translation is reduced after inhibiting either of these signaling pathways, which may reduce the burden and energetic demands associated with protein folding, repair, and degradation, thus maintaining better overall protein homeostasis (208). Our findings support this hypothesis.

In addition to the insulin/IGF-1 and mTOR pathways, many other signaling pathways, such as the PTEN pathway, also modulate lifespan (223). Indeed, PTEN has significant implications for extending human longevity through its antioxidant activity and contribution to the benefits of caloric restriction as well as its involvement DNA-damage reduction, inhibition of DNA

replication, and tumor suppression (224). We found that miR-203b-3p can target PTEN. Notably, signaling pathways, such as the insulin/IGF-1, mTOR and PTEN pathways, may individually regulate aging and lifespan. However, these signaling networks are not autonomous but connected through some specific mediators. For instance, mTOR has two complexes, namely mTOR complex 1 (mTORC1) and mTOR complex 2 (mTORC2) (216). mTORC1 is regulated by Akt, and mTORC2 is an Akt activator (225). PI3 kinase signaling activates mTORC2, which in turn activates a number of other kinases, including PKCα. Consistently, we found that the EIF4EBP1, INSR, PDPK1, PTEN, PXN, and IGF1R overlap and are regulated by at least two circulating miRNAs, and each of these pathways may play a unique role in aging (206-208).

FUTURE DIRECTION

Our data have documented that proinflammatory mediators in the O-exo play an important role in synaptic loss and motor deficits after stroke. In addition, our study also indicated that anaphylatoxins in serum exosomes could stimulate proinflammatory microglial activation via C3a receptor, leading to excessive phagocytosis of synapses after stroke, suggesting the role of O-exo in stroke outcome. Further research will focus on the molecular and cellular mechanisms underlying O-exo-mediated worsened outcome after ischemic stroke. Particularly, we will further investigate the role of miRNAs in Y-exo and O-exo in microglial activation and complement cascade, and their link to stroke outcome. The date generated from aged ischemic rat model will be verified in young rat ischemic model as well as female rat stroke model. In addition, we will also further understand the role of systemic inflammatory and peripheral immune response in age-related diseases, such as Alzheimer Disease. To determine whether systemic inflammatory exosomes with age can communicate with brain and contribute to age-related disease.

BIBLIOGRAPHY

1. Rosamond W, *et al.* (2008) Heart disease and stroke statistics--2008 update: a report from the American Heart Association Statistics Committee and Stroke Statistics Subcommittee. *Circulation* 117(4):e25-146.
2. Brott T & Bogousslavsky J (2000) Treatment of acute ischemic stroke. *N Engl J Med* 343(10):710-722.
3. Adams HP, Jr., *et al.* (2007) Guidelines for the early management of adults with ischemic stroke: a guideline from the American Heart Association/American Stroke Association Stroke Council, Clinical Cardiology Council, Cardiovascular Radiology and Intervention Council, and the Atherosclerotic Peripheral Vascular Disease and Quality of Care Outcomes in Research Interdisciplinary Working Groups: the American Academy of Neurology affirms the value of this guideline as an educational tool for neurologists. *Stroke; a journal of cerebral circulation* 38(5):1655-1711.
4. Traystman RJ (2003) Animal models of focal and global cerebral ischemia. *ILAR J* 44(2):85-95.
5. Megyesi JF, Vollrath B, Cook DA, & Findlay JM (2000) In vivo animal models of cerebral vasospasm: a review. *Neurosurgery* 46(2):448-460; discussion 460-441.

6. Ashwal S & Pearce WJ (2001) Animal models of neonatal stroke. *Curr Opin Pediatr* 13(6):506-516.

7. Alonso de Lecinana M, Diez-Tejedor E, Carceller F, & Roda JM (2001) Cerebral ischemia: from animal studies to clinical practice. Should the methods be reviewed? *Cerebrovasc Dis* 11 Suppl 1:20-30.

8. Harris NR & Rumbaut RE (2001) Age-related responses of the microcirculation to ischemia-reperfusion and inflammation. *Pathophysiology* 8(1):1-10.

9. Boehme AK, Esenwa C, & Elkind MS (2017) Stroke Risk Factors, Genetics, and Prevention. *Circ Res* 120(3):472-495.

10. Kidwell CS, Liebeskind DS, Starkman S, & Saver JL (2001) Trends in acute ischemic stroke trials through the 20th century. *Stroke; a journal of cerebral circulation* 32(6):1349-1359.

11. Suenaga J, *et al.* (2015) White matter injury and microglia/macrophage polarization are strongly linked with age-related long-term deficits in neurological function after stroke. *Experimental neurology* 272:109-119.

12. Lewis EM, Jr BJ, Freshwater L, Hoberman AM, & Christian MS (2002) Sexual maturation data for Crl Sprague-Dawley rats: criteria and confounding factors. *Drug & Chemical Toxicology* 25(4):437.

13. Adams N & Boice R (1983) A longitudinal study of dominance in an outdoor colony of domestic rats. *Journal of Comparative Psychology* 97(1):24-33.

14. Baker HJ, Lindsey JR, & Weisbroth SH (1979) Appendix 1–Selected Normative Data. *Laboratory Rat*:411-412.

15. Pass D & Freeth G (1993) The rat. *Anzccart News* 6:1-4.

16. O'Connor KJ & Graham C (2018) Longer, More Optimistic, Lives: Historic Optimism and Life Expectancy in the United States. *Working Papers*.

17. Sengupta P (2013) The Laboratory Rat: Relating Its Age With Human's. *Int J Prev Med* 4(6):624-630.

18. Quinn R (2005) Comparing rat's to human's age: How old is my rat in people years? *Nutrition* 21(6):775-777.

19. Ramirez-Lassepas M (1998) Stroke and the aging of the brain and the arteries. *Geriatrics* 53(Suppl 1):S44-48.

20. Arnold KG (1981) Cerebral blood flow in geriatrics--a review. *Age Ageing* 10(1):5-9.

21. Waskow C (2010) Generation of parabiotic mice for the study of DC and DC precursor circulation. *Methods Mol Biol* 595:413-428.

22. Kamran P, *et al.* (2013) Parabiosis in mice: a detailed protocol. *J Vis Exp* (80).

23. Loffredo FS, *et al.* (2013) Growth differentiation factor 11 is a circulating factor that reverses age-related cardiac hypertrophy. *Cell* 153(4):828-839.

24. Liu D, *et al.* (2018) Youthful systemic milieu alleviates renal ischemia-reperfusion injury in elderly mice. *Kidney Int* 94(2):268-279.

25. Finerty JC (1952) Parabiosis in physiological studies. *Physiol Rev* 32(3):277-302.

26. Weissman IL, Jerabek L, & Greenspan S (1984) Tolerance and the H-Y antigen: Requirement for male T cells, but not B cells, to induce tolerance in neonatal female mice. *Transplantation* 37(1):3-6.

27. Eggel A & Wyss-Coray T (2014) A revival of parabiosis in biomedical research. *Swiss Med Wkly* 144:w13914.

28. Hall CE, Hall O, & Nevis AH (1959) Prolongation of survival by parabiosis in strain 129 dystrophic mice. *Am J Physiol* 196(1):110-112.

29. Conboy MJ, Conboy IM, & Rando TA (2013) Heterochronic parabiosis: historical perspective and methodological considerations for studies of aging and longevity. *Aging Cell* 12(3):525-530.

30. McCay CM, Pope F, Lunsford W, Sperling G, & Sambhavaphol P (1957) Parabiosis between old and young rats. *Gerontologia* 1(1):7-17.

31. Ludwig FC & Elashoff RM (1972) Mortality in syngeneic rat parabionts of different chronological age. *Trans N Y Acad Sci* 34(7):582-587.

32. Conboy IM, *et al.* (2005) Rejuvenation of aged progenitor cells by exposure to a young systemic environment. *Nature* 433(7027):760-764.

33. Villeda SA, *et al.* (2011) The ageing systemic milieu negatively regulates neurogenesis and cognitive function. *Nature* 477(7362):90-94.

34. Britschgi M, *et al.* (2011) Modeling of pathological traits in Alzheimer's disease based on systemic extracellular signaling proteome. *Mol Cell Proteomics* 10(10):M111 008862.

35. Villeda SA, *et al.* (2014) Young blood reverses age-related impairments in cognitive function and synaptic plasticity in mice. *Nat Med* 20(6):659-663.

36. Castellano JM, *et al.* (2017) Human umbilical cord plasma proteins revitalize hippocampal function in aged mice. *Nature* 544(7651):488-492.

37. Katsimpardi L, *et al.* (2014) Vascular and neurogenic rejuvenation of the aging mouse brain by young systemic factors. *Science* 344(6184):630-634.

38. Smith LK, White CW, 3rd, & Villeda SA (2018) The systemic environment: at the interface of aging and adult neurogenesis. *Cell Tissue Res* 371(1):105-113.

39. Arraud N, *et al.* (2014) Extracellular vesicles from blood plasma: determination of their morphology, size, phenotype and concentration. *J Thromb Haemost* 12(5):614-627.

40. Turpin D, *et al.* (2016) Role of extracellular vesicles in autoimmune diseases. *Autoimmun Rev* 15(2):174-183.

41. Santiago-Dieppa DR, *et al.* (2014) Extracellular vesicles as a platform for 'liquid biopsy' in glioblastoma patients. *Expert Rev Mol Diagn* 14(7):819-825.

42. Colombo M, Raposo G, & Thery C (2014) Biogenesis, secretion, and intercellular interactions of exosomes and other extracellular vesicles. *Annu Rev Cell Dev Biol* 30:255-289.

43. Yanez-Mo M, *et al.* (2015) Biological properties of extracellular vesicles and their physiological functions. *J Extracell Vesicles* 4:27066.

44. Lotvall J, *et al.* (2014) Minimal experimental requirements for definition of extracellular vesicles and their functions: a position statement from the International Society for Extracellular Vesicles. *J Extracell Vesicles* 3:26913.

45. Liang Y, Ridzon D, Wong L, & Chen C (2007) Characterization of microRNA expression profiles in normal human tissues. *BMC Genomics* 8:166.

46. Bobrie A, Colombo M, Raposo G, & Thery C (2011) Exosome secretion: molecular mechanisms and roles in immune responses. *Traffic* 12(12):1659-1668.

47. Pusic AD & Kraig RP (2014) Youth and environmental enrichment generate serum exosomes containing miR-219 that promote CNS myelination. *Glia* 62(2):284-299.

48. Smith JA, *et al.* (2015) Extracellular vesicles and their synthetic analogues in aging and age-associated brain diseases. *Biogerontology* 16(2):147-185.

49. Gercel-Taylor C, Atay S, Tullis RH, Kesimer M, & Taylor DD (2012) Nanoparticle analysis of circulating cell-derived vesicles in ovarian cancer patients. *Anal Biochem* 428(1):44-53.

50. Rodriguez M, *et al.* (2014) Different exosome cargo from plasma/bronchoalveolar lavage in non-small-cell lung cancer. *Genes Chromosomes Cancer* 53(9):713-724.

51. King HW, Michael MZ, & Gleadle JM (2012) Hypoxic enhancement of exosome release by breast cancer cells. *BMC Cancer* 12:421.

52. Eitan E, *et al.* (2017) Age-Related Changes in Plasma Extracellular Vesicle Characteristics and Internalization by Leukocytes. *Sci Rep* 7(1):1342.

53. Bari R, *et al.* (2011) Tetraspanins regulate the protrusive activities of cell membrane. *Biochem Biophys Res Commun* 415(4):619-626.

54. Soo CY, *et al.* (2012) Nanoparticle tracking analysis monitors microvesicle and exosome secretion from immune cells. *Immunology* 136(2):192-197.

55. Chauhan SC, *et al.* (2006) Aberrant expression of MUC4 in ovarian carcinoma: diagnostic significance alone and in combination with MUC1 and MUC16 (CA125). *Mod Pathol* 19(10):1386-1394.

56. Kumari S, Devi Gt, Badana A, Dasari VR, & Malla RR (2015) CD151-A Striking Marker for Cancer Therapy. *Biomark Cancer* 7:7-11.

57. Baek R, Varming K, & Jorgensen MM (2016) Does smoking, age or gender affect the protein phenotype of extracellular vesicles in plasma? *Transfus Apher Sci* 55(1):44-52.

58. Janas AM, Sapon K, Janas T, Stowell MH, & Janas T (2016) Exosomes and other extracellular vesicles in neural cells and neurodegenerative diseases. *Biochim Biophys Acta* 1858(6):1139-1151.

59. Ambros V (2001) microRNAs: tiny regulators with great potential. *Cell* 107(7):823-826.

60. Hunter MP, *et al.* (2008) Detection of microRNA expression in human peripheral blood microvesicles. *PLoS One* 3(11):e3694.

61. Balaj L, *et al.* (2011) Tumour microvesicles contain retrotransposon elements and amplified oncogene sequences. *Nat Commun* 2:180.

62. Valadi H, *et al.* (2007) Exosome-mediated transfer of mRNAs and microRNAs is a novel mechanism of genetic exchange between cells. *Nat Cell Biol* 9(6):654-659.

63. Wang K, Zhang S, Weber J, Baxter D, & Galas DJ (2010) Export of microRNAs and microRNA-protective protein by mammalian cells. *Nucleic Acids Res* 38(20):7248-7259.

64. Sheinerman KS & Umansky SR (2013) Circulating cell-free microRNA as biomarkers for screening, diagnosis and monitoring of neurodegenerative diseases and other neurologic pathologies. *Front Cell Neurosci* 7:150.

65. Olivieri F, Rippo MR, Procopio AD, & Fazioli F (2013) Circulating inflamma-miRs in aging and age-related diseases. *Front Genet* 4:121.

66. Olivieri F, *et al.* (2013) MicroRNAs linking inflamm-aging, cellular senescence and cancer. *Ageing Res Rev* 12(4):1056-1068.

67. Berdasco M & Esteller M (2012) Hot topics in epigenetic mechanisms of aging: 2011. *Aging Cell* 11(2):181-186.

68. Cipollone F, *et al.* (2011) A unique microRNA signature associated with plaque instability in humans. *Stroke; a journal of cerebral circulation* 42(9):2556-2563.

69. Dharap A, Bowen K, Place R, Li LC, & Vemuganti R (2009) Transient focal ischemia induces extensive temporal changes in rat cerebral microRNAome. *Journal of cerebral*

blood flow and metabolism : official journal of the International Society of Cerebral Blood Flow and Metabolism 29(4):675-687.

70. Jeyaseelan K, Lim KY, & Armugam A (2008) MicroRNA expression in the blood and brain of rats subjected to transient focal ischemia by middle cerebral artery occlusion. *Stroke* 39(3):959-966.

71. Tan KS, *et al.* (2009) Expression profile of MicroRNAs in young stroke patients. *PloS one* 4(11):e7689.

72. Guo D, *et al.* (2013) Alteration in abundance and compartmentalization of inflammation-related miRNAs in plasma after intracerebral hemorrhage. *Stroke; a journal of cerebral circulation* 44(6):1739-1742.

73. Chen X, *et al.* (2008) Characterization of microRNAs in serum: a novel class of biomarkers for diagnosis of cancer and other diseases. *Cell Res* 18(10):997-1006.

74. Fichtlscherer S, *et al.* (2010) Circulating microRNAs in patients with coronary artery disease. *Circulation research* 107(5):677-684.

75. Li T, *et al.* (2011) Identification of miR-130a, miR-27b and miR-210 as serum biomarkers for atherosclerosis obliterans. *Clinica chimica acta; international journal of clinical chemistry* 412(1-2):66-70.

76. Selvamani A, Williams MH, Miranda RC, & Sohrabji F (2014) Circulating miRNA profiles provide a biomarker for severity of stroke outcomes associated with age and sex in a rat model. *Clin Sci (Lond)* 127(2):77-89.

77. Candelario-Jalil E (2009) Injury and repair mechanisms in ischemic stroke: considerations for the development of novel neurotherapeutics. *Curr Opin Investig Drugs* 10(7):644-654.

78. Mehta SL, Manhas N, & Raghubir R (2007) Molecular targets in cerebral ischemia for developing novel therapeutics. *Brain Res Rev* 54(1):34-66.

79. Xing C, Arai K, Lo EH, & Hommel M (2012) Pathophysiologic cascades in ischemic stroke. *Int J Stroke* 7(5):378-385.

80. Dirnagl U (2004) Inflammation in stroke: the good, the bad, and the unknown. *Ernst Schering Res Found Workshop* (47):87-99.

81. Shichita T, Ito M, & Yoshimura A (2014) Post-ischemic inflammation regulates neural damage and protection. *Front Cell Neurosci* 8:319.

82. Shi K, *et al.* (2019) Global brain inflammation in stroke. *Lancet Neurol* 18(11):1058-1066.

83. Dirnagl U, Iadecola C, & Moskowitz MA (1999) Pathobiology of ischaemic stroke: an integrated view. *Trends Neurosci* 22(9):391-397.

84. Gauberti M, Fournier AP, Docagne F, Vivien D, & Martinez de Lizarrondo S (2018) Molecular Magnetic Resonance Imaging of Endothelial Activation in the Central Nervous System. *Theranostics* 8(5):1195-1212.

85. Neumann J, *et al.* (2015) Very-late-antigen-4 (VLA-4)-mediated brain invasion by neutrophils leads to interactions with microglia, increased ischemic injury and impaired behavior in experimental stroke. *Acta Neuropathol* 129(2):259-277.

86. Gan Y, *et al.* (2014) Ischemic neurons recruit natural killer cells that accelerate brain infarction. *Proc. Natl. Acad. Sci. U. S. A.* 111(7):2704-2709.

87. De Meyer SF, *et al.* (2016) Thromboinflammation in Stroke Brain Damage. *Stroke* 47(4):1165-1172.

88. Smirkin A, *et al.* (2010) Iba1(+)/NG2(+) macrophage-like cells expressing a variety of neuroprotective factors ameliorate ischemic damage of the brain. *J Cereb Blood Flow Metab* 30(3):603-615.

89. Iadecola C & Anrather J (2011) The immunology of stroke: from mechanisms to translation. *Nat Med* 17(7):796-808.

90. Wake H, Moorhouse AJ, Jinno S, Kohsaka S, & Nabekura J (2009) Resting microglia directly monitor the functional state of synapses in vivo and determine the fate of ischemic terminals. *J Neurosci* 29(13):3974-3980.

91. Ekdahl CT, Kokaia Z, & Lindvall O (2009) Brain inflammation and adult neurogenesis: the dual role of microglia. *Neuroscience* 158(3):1021-1029.

92. Battista D, Ferrari CC, Gage FH, & Pitossi FJ (2006) Neurogenic niche modulation by activated microglia: transforming growth factor beta increases neurogenesis in the adult dentate gyrus. *Eur J Neurosci* 23(1):83-93.

93. Banati RB, Gehrmann J, Schubert P, & Kreutzberg GW (1993) Cytotoxicity of microglia. *Glia* 7(1):111-118.

94. Kettenmann H, Hanisch UK, Noda M, & Verkhratsky A (2011) Physiology of microglia. *Physiol Rev* 91(2):461-553.

95. Ransohoff RM & Cardona AE (2010) The myeloid cells of the central nervous system parenchyma. *Nature* 468(7321):253-262.

96. Ransohoff RM & Perry VH (2009) Microglial physiology: unique stimuli, specialized responses. *Annu Rev Immunol* 27:119-145.

97. Polazzi E & Monti B (2010) Microglia and neuroprotection: from in vitro studies to therapeutic applications. *Prog Neurobiol* 92(3):293-315.

98. Merson TD, Binder MD, & Kilpatrick TJ (2010) Role of cytokines as mediators and regulators of microglial activity in inflammatory demyelination of the CNS. *Neuromolecular Med* 12(2):99-132.

99. Fu R, Shen Q, Xu P, Luo JJ, & Tang Y (2014) Phagocytosis of microglia in the central nervous system diseases. *Mol Neurobiol* 49(3):1422-1434.

100. Veerhuis R, Nielsen HM, & Tenner AJ (2011) Complement in the brain. *Mol Immunol* 48(14):1592-1603.

101. Lucin KM & Wyss-Coray T (2009) Immune activation in brain aging and neurodegeneration: too much or too little? *Neuron* 64(1):110-122.

102. Shin YJ, *et al.* (2011) Osteopontin: correlation with phagocytosis by brain macrophages in a rat model of stroke. *Glia* 59(3):413-423.

103. Neumann J, *et al.* (2008) Microglia cells protect neurons by direct engulfment of invading neutrophil granulocytes: a new mechanism of CNS immune privilege. *J Neurosci* 28(23):5965-5975.

104. Kato H, Kogure K, Liu XH, Araki T, & Itoyama Y (1996) Progressive expression of immunomolecules on activated microglia and invading leukocytes following focal cerebral ischemia in the rat. *Brain Res* 734(1-2):203-212.

105. Schilling M, *et al.* (2005) Predominant phagocytic activity of resident microglia over hematogenous macrophages following transient focal cerebral ischemia: an investigation using green fluorescent protein transgenic bone marrow chimeric mice. *Exp Neurol* 196(2):290-297.

106. Brown GC & Neher JJ (2014) Microglial phagocytosis of live neurons. *Nat Rev Neurosci* 15(4):209-216.

107. Sierra A, Abiega O, Shahraz A, & Neumann H (2013) Janus-faced microglia: beneficial and detrimental consequences of microglial phagocytosis. *Front Cell Neurosci* 7:6.

108. Neher JJ, *et al.* (2011) Inhibition of microglial phagocytosis is sufficient to prevent inflammatory neuronal death. *J Immunol* 186(8):4973-4983.

109. Neher JJ, *et al.* (2013) Phagocytosis executes delayed neuronal death after focal brain ischemia. *Proc. Natl. Acad. Sci. U. S. A.* 110(43):E4098-4107.

110. Cunningham CL, Martinez-Cerdeno V, & Noctor SC (2013) Microglia regulate the number of neural precursor cells in the developing cerebral cortex. *J Neurosci* 33(10):4216-4233.

111. Schafer DP, *et al.* (2012) Microglia sculpt postnatal neural circuits in an activity and complement-dependent manner. *Neuron* 74(4):691-705.

112. Linnartz B, Kopatz J, Tenner AJ, & Neumann H (2012) Sialic acid on the neuronal glycocalyx prevents complement C1 binding and complement receptor-3-mediated removal by microglia. *J Neurosci* 32(3):946-952.

113. Cramer SC (2008) Repairing the human brain after stroke: I. Mechanisms of spontaneous recovery. *Ann Neurol* 63(3):272-287.

114. Murphy TH & Corbett D (2009) Plasticity during stroke recovery: from synapse to behaviour. *Nat Rev Neurosci* 10(12):861-872.

115. Winship IR & Murphy TH (2009) Remapping the somatosensory cortex after stroke: insight from imaging the synapse to network. *Neuroscientist* 15(5):507-524.

116. Schabitz WR, *et al.* (2004) Effect of brain-derived neurotrophic factor treatment and forced arm use on functional motor recovery after small cortical ischemia. *Stroke* 35(4):992-997.

117. Brown CE, Aminoltejari K, Erb H, Winship IR, & Murphy TH (2009) In vivo voltage-sensitive dye imaging in adult mice reveals that somatosensory maps lost to stroke are replaced over weeks by new structural and functional circuits with prolonged modes of activation within both the peri-infarct zone and distant sites. *J Neurosci* 29(6):1719-1734.

118. Brown CE, Li P, Boyd JD, Delaney KR, & Murphy TH (2007) Extensive turnover of dendritic spines and vascular remodeling in cortical tissues recovering from stroke. *J Neurosci* 27(15):4101-4109.

119. Hattiangady B, Rao MS, Shetty GA, & Shetty AK (2005) Brain-derived neurotrophic factor, phosphorylated cyclic AMP response element binding protein and neuropeptide Y decline as early as middle age in the dentate gyrus and CA1 and CA3 subfields of the hippocampus. *Exp Neurol* 195(2):353-371.

120. Carmichael ST (2006) Cellular and molecular mechanisms of neural repair after stroke: making waves. *Ann Neurol* 59(5):735-742.

121. Carmichael ST & Chesselet MF (2002) Synchronous neuronal activity is a signal for axonal sprouting after cortical lesions in the adult. *J Neurosci* 22(14):6062-6070.

122. Lee JK, Kim JE, Sivula M, & Strittmatter SM (2004) Nogo receptor antagonism promotes stroke recovery by enhancing axonal plasticity. *J Neurosci* 24(27):6209-6217.

123. Tinetti ME, Speechley M, & Ginter SF (1988) Risk factors for falls among elderly persons living in the community. *N Engl J Med* 319(26):1701-1707.

124. Brack AS, *et al.* (2007) Increased Wnt signaling during aging alters muscle stem cell fate and increases fibrosis. *Science* 317(5839):807-810.

125. Zomer A, *et al.* (2010) Exosomes: Fit to deliver small RNA. *Commun Integr Biol* 3(5):447-450.

126. Wolf P (1967) The nature and significance of platelet products in human plasma. *Br J Haematol* 13(3):269-288.

127. Zhang Y, *et al.* (2017) Hypothalamic stem cells control ageing speed partly through exosomal miRNAs. *Nature* 548(7665):52-57.

128. Dorn GW, 2nd (2011) MicroRNAs in cardiac disease. *Transl Res* 157(4):226-235.

129. Cortez MA, *et al.* (2011) MicroRNAs in body fluids--the mix of hormones and biomarkers. *Nat Rev Clin Oncol* 8(8):467-477.

130. Ruckh JM, *et al.* (2012) Rejuvenation of regeneration in the aging central nervous system. *Cell Stem Cell* 10(1):96-103.

131. Xin H, *et al.* (2013) Systemic administration of exosomes released from mesenchymal stromal cells promote functional recovery and neurovascular plasticity after stroke in rats. *J Cereb Blood Flow Metab* 33(11):1711-1715.

132. Xin H, *et al.* (2017) MicroRNA cluster miR-17-92 Cluster in Exosomes Enhance Neuroplasticity and Functional Recovery After Stroke in Rats. *Stroke* 48(3):747-753.

133. Won SJ, *et al.* (2006) Influence of age on the response to fibroblast growth factor-2 treatment in a rat model of stroke. *Brain Res* 1123(1):237-244.

134. Pan M, *et al.* (2017) Aging Systemic Milieu Impairs Outcome after Ischemic Stroke in Rats. *Aging Dis* 8(5):519-530.

135. Tureyen K, Vemuganti R, Sailor KA, & Dempsey RJ (2004) Infarct volume quantification in mouse focal cerebral ischemia: a comparison of triphenyltetrazolium chloride and cresyl violet staining techniques. *J Neurosci Methods* 139(2):203-207.

136. Swanson RA, *et al.* (1990) A semiautomated method for measuring brain infarct volume. *J Cereb Blood Flow Metab* 10(2):290-293.

137. Risher WC, Ustunkaya T, Singh Alvarado J, & Eroglu C (2014) Rapid Golgi analysis method for efficient and unbiased classification of dendritic spines. *PLoS One* 9(9):e107591.

138. Bayram-Weston Z, Olsen E, Harrison DJ, Dunnett SB, & Brooks SP (2016) Optimising Golgi-Cox staining for use with perfusion-fixed brain tissue validated in the zQ175 mouse model of Huntington's disease. *J Neurosci Methods* 265:81-88.

139. Paxinos G & Watson C (2014) *Paxino's and Watson's The rat brain in stereotaxic coordinates* (Elsevier/AP, Academic Press is an imprint of Elsevier, Amsterdam ; Boston) Seventh edition. Ed p 1 volume (unpaged).

140. Papadopoulos CM, *et al.* (2006) Dendritic plasticity in the adult rat following middle cerebral artery occlusion and Nogo-a neutralization. *Cereb Cortex* 16(4):529-536.

141. Wang X, Mao X, Xie L, Greenberg DA, & Jin K (2009) Involvement of Notch1 signaling in neurogenesis in the subventricular zone of normal and ischemic rat brain in vivo. *J Cereb Blood Flow Metab* 29(10):1644-1654.

142. Jin K, *et al.* (2001) Neurogenesis in dentate subgranular zone and rostral subventricular zone after focal cerebral ischemia in the rat. *Proc Natl Acad Sci U S A* 98(8):4710-4715.

143. Ames RS, *et al.* (2001) Identification of a selective nonpeptide antagonist of the anaphylatoxin C3a receptor that demonstrates antiinflammatory activity in animal models. *Journal of Immunology* 166(10):6341-6348.

144. Lian H, *et al.* (2016) Astrocyte-Microglia Cross Talk through Complement Activation Modulates Amyloid Pathology in Mouse Models of Alzheimer's Disease. *Journal of Neuroscience* 36(2):577-589.

145. Spangenberg EE, *et al.* (2016) Eliminating microglia in Alzheimer's mice prevents neuronal loss without modulating amyloid-beta pathology. *Brain* 139:1265-1281.

146. Schaar KL, Brenneman MM, & Savitz SI (2010) Functional assessments in the rodent stroke model. *Exp Transl Stroke Med* 2(1):13.

147. Metz GA & Whishaw IQ (2002) Cortical and subcortical lesions impair skilled walking in the ladder rung walking test: a new task to evaluate fore- and hindlimb stepping, placing, and co-ordination. *J Neurosci Methods* 115(2):169-179.

148. Cossetti C, *et al.* (2014) Extracellular vesicles from neural stem cells transfer IFN-gamma via Ifngr1 to activate Stat1 signaling in target cells. *Mol Cell* 56(2):193-204.

149. Dragovic RA, *et al.* (2011) Sizing and phenotyping of cellular vesicles using Nanoparticle Tracking Analysis. *Nanomedicine* 7(6):780-788.

150. Carson MJ, Doose JM, Melchior B, Schmid CD, & Ploix CC (2006) CNS immune privilege: hiding in plain sight. *Immunol Rev* 213:48-65.

151. Jickling GC & Sharp FR (2015) Improving the translation of animal ischemic stroke studies to humans. *Metab Brain Dis* 30(2):461-467.

152. Rosen CL, Dinapoli VA, Nagamine T, & Crocco T (2005) Influence of age on stroke outcome following transient focal ischemia. *J Neurosurg* 103(4):687-694.

153. Herson PS & Traystman RJ (2014) Animal models of stroke: translational potential at present and in 2050. *Future Neurol* 9(5):541-551.

154. Chen RL, Balami JS, Esiri MM, Chen LK, & Buchan AM (2010) Ischemic stroke in the elderly: an overview of evidence. *Nat Rev Neurol* 6(5):256-265.

155. Hossmann KA (1994) Viability thresholds and the penumbra of focal ischemia. *Ann Neurol* 36(4):557-565.

156. Ramos-Cabrer P, Campos F, Sobrino T, & Castillo J (2011) Targeting the ischemic penumbra. *Stroke* 42(1 Suppl):S7-11.

157. Hering H & Sheng M (2001) Dendritic spines: structure, dynamics and regulation. *Nat Rev Neurosci* 2(12):880-888.

158. Waisman A, Ginhoux F, Greter M, & Bruttger J (2015) Homeostasis of Microglia in the Adult Brain: Review of Novel Microglia Depletion Systems. *Trends Immunol* 36(10):625-636.

159. Elmore MR, *et al.* (2014) Colony-stimulating factor 1 receptor signaling is necessary for microglia viability, unmasking a microglia progenitor cell in the adult brain. *Neuron* 82(2):380-397.

160. Elmore MR, Lee RJ, West BL, & Green KN (2015) Characterizing newly repopulated microglia in the adult mouse: impacts on animal behavior, cell morphology, and neuroinflammation. *PLoS One* 10(4):e0122912.

161. Rice RA, *et al.* (2017) Microglial repopulation resolves inflammation and promotes brain recovery after injury. *Glia* 65(6):931-944.

162. Hebert LE, Scherr PA, Bienias JL, Bennett DA, & Evans DA (2003) Alzheimer disease in the US population: prevalence estimates using the 2000 census. *Arch Neurol* 60(8):1119-1122.

163. Jin K (2010) Modern Biological Theories of Aging. *Aging Dis* 1(2):72-74.

164. Jin K (2019) A Microcirculatory Theory of Aging. *Aging Dis* 10(3):676-683.

165. Zhang H, Cherian R, & Jin K (2019) Systemic milieu and age-related deterioration. *Geroscience* 41(3):275-284.

166. Sebastiani P, *et al.* (2017) Biomarker signatures of aging. *Aging Cell* 16(2):329-338.

167. Xia X, Chen W, McDermott J, & Han JJ (2017) Molecular and phenotypic biomarkers of aging. *F1000Res* 6:860.

168. Urbanelli L, *et al.* (2013) Signaling pathways in exosomes biogenesis, secretion and fate. *Genes (Basel)* 4(2):152-170.

169. Lee BR, Kim JH, Choi ES, Cho JH, & Kim E (2018) Effect of young exosomes injected in aged mice. *Int J Nanomedicine* 13:5335-5345.

170. Pulliam L, Sun B, Mustapic M, Chawla S, & Kapogiannis D (2019) Plasma neuronal exosomes serve as biomarkers of cognitive impairment in HIV infection and Alzheimer's disease. *J Neurovirol*.

171. Sun B, Dalvi P, Abadjian L, Tang N, & Pulliam L (2017) Blood neuron-derived exosomes as biomarkers of cognitive impairment in HIV. *AIDS* 31(14):F9-F17.

172. Rani A, *et al.* (2017) miRNA in Circulating Microvesicles as Biomarkers for Age-Related Cognitive Decline. *Front Aging Neurosci* 9:323.

173. Alvarez-Erviti L, *et al.* (2011) Delivery of siRNA to the mouse brain by systemic injection of targeted exosomes. *Nat Biotechnol* 29(4):341-345.

174. Matsumoto J, Stewart T, Banks WA, & Zhang J (2017) The Transport Mechanism of Extracellular Vesicles at the Blood-Brain Barrier. *Curr Pharm Des* 23(40):6206-6214.

175. Yang T, *et al.* (2015) Exosome delivered anticancer drugs across the blood-brain barrier for brain cancer therapy in Danio rerio. *Pharm Res* 32(6):2003-2014.

176. Qu M, *et al.* (2018) Dopamine-loaded blood exosomes targeted to brain for better treatment of Parkinson's disease. *J Control Release* 287:156-166.

177. Lewis BP, Shih IH, Jones-Rhoades MW, Bartel DP, & Burge CB (2003) Prediction of mammalian microRNA targets. *Cell* 115(7):787-798.

178. Bartel DP (2009) MicroRNAs: target recognition and regulatory functions. *Cell* 136(2):215-233.

179. Tan CL, *et al.* (2013) MicroRNA-128 governs neuronal excitability and motor behavior in mice. *Science* 342(6163):1254-1258.

180. Pedersen ME, *et al.* (2013) An epidermal microRNA regulates neuronal migration through control of the cellular glycosylation state. *Science* 341(6152):1404-1408.

181. Gomez GG, *et al.* (2014) Suppression of microRNA-9 by mutant EGFR signaling upregulates FOXP1 to enhance glioblastoma tumorigenicity. *Cancer Res* 74(5):1429-1439.

182. Mushtaq G, *et al.* (2016) miRNAs as Circulating Biomarkers for Alzheimer's Disease and Parkinson's Disease. *Med Chem* 12(3):217-225.

183. Schwarzenbach H, Nishida N, Calin GA, & Pantel K (2014) Clinical relevance of circulating cell-free microRNAs in cancer. *Nat Rev Clin Oncol* 11(3):145-156.

184. Sheinerman KS, Tsivinsky VG, Abdullah L, Crawford F, & Umansky SR (2013) Plasma microRNA biomarkers for detection of mild cognitive impairment: biomarker validation study. *Aging (Albany NY)* 5(12):925-938.

185. Feng LB, *et al.* (2015) MicroRNA involvement in mechanism of endogenous protection induced by fastigial nucleus stimulation based on deep sequencing and bioinformatics. *BMC Med Genomics* 8:79.

186. Kanehisa M, Furumichi M, Tanabe M, Sato Y, & Morishima K (2017) KEGG: new perspectives on genomes, pathways, diseases and drugs. *Nucleic Acids Res* 45(D1):D353-D361.

187. Roy-O'Reilly M & McCullough LD (2018) Age and Sex Are Critical Factors in Ischemic Stroke Pathology. *Endocrinology* 159(8):3120-3131.

188. Chung HY, *et al.* (2019) Redefining Chronic Inflammation in Aging and Age-Related Diseases: Proposal of the Senoinflammation Concept. *Aging Dis* 10(2):367-382.

189. Morgan BP & Harris CL (2015) Complement, a target for therapy in inflammatory and degenerative diseases. *Nat Rev Drug Discov* 14(12):857-877.

190. Alawieh A, Langley EF, & Tomlinson S (2018) Targeted complement inhibition salvages stressed neurons and inhibits neuroinflammation after stroke in mice. *Sci Transl Med* 10(441).

191. Riley-Vargas RC, Gill DB, Kemper C, Liszewski MK, & Atkinson JP (2004) CD46: expanding beyond complement regulation. *Trends Immunol* 25(9):496-503.

192. Gill J, *et al.* (2018) Higher exosomal tau, amyloid-beta 42 and IL-10 are associated with mild TBIs and chronic symptoms in military personnel. *Brain Inj* 32(10):1277-1284.

193. Hatse S, *et al.* (2014) Circulating MicroRNAs as easy-to-measure aging biomarkers in older breast cancer patients: correlation with chronological age but not with fitness/frailty status. *PLoS One* 9(10):e110644.

194. Xiao H, Huang R, Diao M, Li L, & Cui X (2018) Integrative analysis of microRNA and mRNA expression profiles in fetal rat model with anorectal malformation. *PeerJ* 6:e5774.

195. Kim JH, *et al.* (2017) Reverse Expression of Aging-Associated Molecules through Transfection of miRNAs to Aged Mice. *Mol Ther Nucleic Acids* 6:106-115.

196. Lee BP, *et al.* (2017) MicroRNAs miR-203-3p, miR-664-3p and miR-708-5p are associated with median strain lifespan in mice. *Sci Rep* 7:44620.

197. Zhao Y, *et al.* (2013) Decrease of miR-202-3p expression, a novel tumor suppressor, in gastric cancer. *PLoS One* 8(7):e69756.

198. Dluzen DF, *et al.* (2018) Extracellular RNA profiles with human age. *Aging Cell* 17(4):e12785.

199. Tsai HP, Huang SF, Li CF, Chien HT, & Chen SC (2018) Differential microRNA expression in breast cancer with different onset age. *PLoS One* 13(1):e0191195.

200. Noren Hooten N, *et al.* (2013) Age-related changes in microRNA levels in serum. *Aging (Albany NY)* 5(10):725-740.

201. Noren Hooten N, *et al.* (2010) microRNA expression patterns reveal differential expression of target genes with age. *PLoS One* 5(5):e10724.

202. Inukai S, de Lencastre A, Turner M, & Slack F (2012) Novel microRNAs differentially expressed during aging in the mouse brain. *PLoS One* 7(7):e40028.

203. Hara N, *et al.* (2017) Serum microRNA miR-501-3p as a potential biomarker related to the progression of Alzheimer's disease. *Acta Neuropathol Commun* 5(1):10.

204. Kovanda A, *et al.* (2018) Differential expression of microRNAs and other small RNAs in muscle tissue of patients with ALS and healthy age-matched controls. *Sci Rep* 8(1):5609.

205. Lafferty-Whyte K, Cairney CJ, Jamieson NB, Oien KA, & Keith WN (2009) Pathway analysis of senescence-associated miRNA targets reveals common processes to different senescence induction mechanisms. *Biochim Biophys Acta* 1792(4):341-352.

206. Carlson ME, Silva HS, & Conboy IM (2008) Aging of signal transduction pathways, and pathology. *Exp Cell Res* 314(9):1951-1961.

207. Newgard CB & Pessin JE (2014) Recent progress in metabolic signaling pathways regulating aging and life span. *J Gerontol A Biol Sci Med Sci* 69 Suppl 1:S21-27.

208. Pan H & Finkel T (2017) Key proteins and pathways that regulate lifespan. *J Biol Chem* 292(16):6452-6460.

209. Dharap A & Vemuganti R (2010) Ischemic pre-conditioning alters cerebral microRNAs that are upstream to neuroprotective signaling pathways. *J Neurochem* 113(6):1685-1691.

210. Locke JM, da Silva Xavier G, Dawe HR, Rutter GA, & Harries LW (2014) Increased expression of miR-187 in human islets from individuals with type 2 diabetes is associated with reduced glucose-stimulated insulin secretion. *Diabetologia* 57(1):122-128.

211. Jones A, *et al.* (2017) miRNA Signatures of Insulin Resistance in Obesity. *Obesity (Silver Spring)* 25(10):1734-1744.

212. Tatar M, Bartke A, & Antebi A (2003) The endocrine regulation of aging by insulin-like signals. *Science* 299(5611):1346-1351.

213. Markowska AL, Mooney M, & Sonntag WE (1998) Insulin-like growth factor-1 ameliorates age-related behavioral deficits. *Neuroscience* 87(3):559-569.

214. Vijg J & Campisi J (2008) Puzzles, promises and a cure for ageing. *Nature* 454(7208):1065-1071.

215. Holzenberger M, *et al.* (2003) IGF-1 receptor regulates lifespan and resistance to oxidative stress in mice. *Nature* 421(6919):182-187.

216. Kennedy BK & Lamming DW (2016) The Mechanistic Target of Rapamycin: The Grand ConducTOR of Metabolism and Aging. *Cell Metab* 23(6):990-1003.

217. Henderson ST, Bonafe M, & Johnson TE (2006) daf-16 protects the nematode Caenorhabditis elegans during food deprivation. *J Gerontol A Biol Sci Med Sci* 61(5):444-460.

218. Hansen M, *et al.* (2007) Lifespan extension by conditions that inhibit translation in Caenorhabditis elegans. *Aging Cell* 6(1):95-110.

219. Syntichaki P, Troulinaki K, & Tavernarakis N (2007) eIF4E function in somatic cells modulates ageing in Caenorhabditis elegans. *Nature* 445(7130):922-926.

220. Kapahi P, *et al.* (2004) Regulation of lifespan in Drosophila by modulation of genes in the TOR signaling pathway. *Curr. Biol.* 14(10):885-890.

221. Harrison DE, *et al.* (2009) Rapamycin fed late in life extends lifespan in genetically heterogeneous mice. *Nature* 460(7253):392-395.

222. Miller RA, *et al.* (2014) Rapamycin-mediated lifespan increase in mice is dose and sex dependent and metabolically distinct from dietary restriction. *Aging Cell* 13(3):468-477.

223. Greer EL & Brunet A (2008) Signaling networks in aging. *J Cell Sci* 121(Pt 4):407-412.

224. Tait IS, Li Y, & Lu J (2013) PTEN, Longevity and Age-Related Diseases. *Biomedicines* 1(1):17-48.

225. Iwanami A, Cloughesy TF, & Mischel PS (2009) Striking the balance between PTEN and PDK1: it all depends on the cell context. *Genes Dev* 23(15):1699-1704.